ROTATIONAL VELOCITIES IN LARGE SCALE STRUCTURE

By

JAMES H. COONEY

A DISSERTATION PRESENTED TO THE GRADUATE SCHOOL
OF THE UNIVERSITY OF FLORIDA IN PARTIAL FULFILLMENT
OF THE REQUIREMENTS FOR THE DEGREE OF
DOCTOR OF PHILOSOPHY

UNIVERSITY OF FLORIDA

2004

For my parents

Digitized by the Internet Archive
in 2011 with funding from
University of Florida, George A. Smathers Libraries with support from LYRASIS and the Sloan Foundation

http://www.archive.org/details/rotationalveloci00coon

ACKNOWLEDGMENTS

First, I wish to thank my advisor, Dr. Jim Fry, without whose wisdom and patience this dissertation would never have been completed. This project was his idea from the start and his assistance along the way has proved invaluable. I also wish to thank my dissertation committee members, Drs. Steve Detweiler, Bernard Whiting, Peter Hirschfeld, Art Hebard, and Fred Hamman.

Thanks go to my parents, Peter and Adele Cooney, and my brother Dan for their support over the years in every way that I needed it. My gratitude also goes to my friends in the department, including Kevin McCarthy, David Red, and Brian Thorndyke, for sharing in the fun, and my SMCM chums, affetionately known as The Herd, for many years of great times.

TABLE OF CONTENTS

page

ACKNOWLEDGMENTS iii

LIST OF TABLES vi

LIST OF FIGURES vii

ABSTRACT ix

CHAPTER

1 INTRODUCTION 1

1.1 Overview 1
1.2 Motivation and Outline 3

2 FOUNDATIONS 5

2.1 Gravitational Instability 5
2.2 Statistics 12
2.3 Small-Scale Considerations 15

3 VELOCITY MODES IN PERTURBATION THEORY 19

3.1 First Order Solutions 19
3.2 Second Order Solutions in Real Space 20
3.3 Second Order Solutions in Fourier Space 22
3.4 Third Order Solutions in Real Space 26
3.5 Evolution of Vorticity 30

4 THE CMB AND THE SUNYAEV-ZELDOVICH EFFECT 32

4.1 Introduction 32
4.2 Anisotropies in the CMB 34
4.3 Primary Anisotropies 34
4.4 Secondary Anisotropies 36
4.5 Thermal and Non-Thermal Sunyaev-Zeldovich Effects 40
4.6 Kinetic Sunyaev-Zeldovich Effect 41

5 KINETIC SZ ANGULAR POWER SPECTRUM INGREDIENTS 42

5.1 Introduction 42
5.2 Linear Power Spectrum 42

5.3 Nonlinear Power Spectrum 44
5.4 Angular Power Spectrum Machinery 49
5.5 Ostriker-Vishniac Angular Power Spectrum 57
5.6 Nonlinear Angular Power Spectrum 58

6 SZ POWER SPECTRUM INCLUDING ROTATIONAL MODES 63

6.1 Introduction 63
6.2 First-Order Results 63
6.3 Non-Linear Results 64

7 CONCLUSION 84

APPENDIX

A CONSERVATION OF ANGULAR MOMENTUM IN AN EXPANDING UNIVERSE 86

B SPHERICAL COLLAPSE AND THE DERIVATION OF δ_C 88

C PHYSICAL CONSTANTS AND COSMOLOGICAL PARAMETERS . . 93

D CODE FOR CALCULATING ANGULAR SZ SPECTRUM 94

REFERENCE LIST 105

BIOGRAPHICAL SKETCH 110

LIST OF TABLES

Table page

5–1 Linear Power Spectrum Parameters 43

C–1 Physical Constants and Cosmological Parameters 93

LIST OF FIGURES

Figure page

4–1 Cosmic Blackbody 33

4–2 WMAP Angular Power Spectrum 37

4–3 Assorted Angular Power Spectrum Data 38

5–1 Input Linear Power Spectrum 45

5–2 $\sigma(M)$ vs. M 48

5–3 Bias Parameter Versus Mass 50

5–4 Power Spectra for NFW Halo Profile 51

5–5 Power Spectra for Moore Halo Profile 52

5–6 Power Spectra for Mixed Halo Profile 53

5–7 Breakdown of Non-linear Power Spectrum 54

5–8 Distance vs. Redshift 56

5–9 Ostriker-Vishniac Angular Power Spectrum 59

5–10 Nonlinear Angular Power Spectrum 61

5–11 Kinetic and Thermal SZ Effects 62

6–1 C_ℓ's for First Order Rotational Velocities 65

6–2 Moore Profile Mapping 67

6–3 NFW Profile Mapping 68

6–4 Moore Collapse Transforms 74

6–5 Moore Collapse Fit 75

6–6 NFW Collapse Transforms 76

6–7 NFW Collapse Fit 77

6–8 Comparison of Density-Density Power Spectra 79

6–9 Different Halo Profiles and the Density-Density Power Spectrum . . . 80

6–10 Angular Spectrum Due to Rotational Mode 81
6–11 Angular Spectrum Due to Rotational Mode Comparison 82
6–12 Linear and Nonlinear Rotational Mode Contributions 83
B–1 Radius and Time in Spherical Collapse 89
B–2 Densities in Spherical Collapse 92

Abstract of Dissertation Presented to the Graduate School
of the University of Florida in Partial Fulfillment of the
Requirements for the Degree of Doctor of Philosophy

ROTATIONAL VELOCITIES IN LARGE SCALE STRUCTURE

By

James H. Cooney

August 2004

Chair: James N. Fry
Major Department: Physics

In perturbation theory studies of the large-scale structure of the universe, it is common procedure to ignore the effects of an initial rotational velocity field. This has been justified by the fact that in the linear regime, rotational velocities decay with the expansion of the universe, a simple result of conservation of angular momentum. In this dissertation, we explore the consequences of retaining this mode, based on the assumption that gravitational collapse should lead to the return of appreciable rotational velocities. We extend the classical perturbation theory to include rotational modes up to the quasi-linear third order and find that these modes contribute in a non-trivial manner. We then include these modes in the non-linear regime, incorporating them into the halo model. We study a specific application of non-linear collapse, the calculation of the kinetic Sunyaev-Zeldovich effect, with the inclusion of rotational velocity modes. We find that these modes do not contribute significantly at any angular scale available to modern observation.

CHAPTER 1
INTRODUCTION

1.1 Overview

Cosmology, the study of the nature and evolution of the universe as a whole, has emerged in the last one hundred years as a mature science. Though cosmology encompasses a great many fields of study, we will primarily be interested in what is called large-scale structure, the study of the general distribution of matter and energy in the universe. To understand this distribution today, we must first understand what processes underlie its evolution.

The first part of the twentieth century was marked by a great number of advancements in the physical sciences, not the least of which was Albert Einstein's development of the theory of relativity. This is a theory in which time and space are no longer absolute, and the physics of Newton and his followers no longer applies. One of the strangest predictions of the theory was that the universe may not be static, that is, that the universe as a whole may be expanding or contracting. If it were expanding, then at some point in the past, everything must have been much closer together, a tiny speck that expanded into everything in the universe today. This state of affairs became known as the big bang. Einstein himself held this possibility in distaste, and when it was shown that a static universe was, in fact, necessarily unstable, he added another term into his equations, the cosmological constant, to allow for a stable universe. Not long after, the astronomer Edwin Hubble made the discovery that galaxies far away from our own are receding from us, in fact the farther away they are, the faster they are receding. The only conclusion to be drawn was that the universe is expanding. So the distribution of matter and energy in the universe is first influenced by the general expansion of the universe.

The other process which is believed to play a major role in shaping today's universe is gravity. It is believed that tiny irregularities early in the universe grew, as the universe expanded, by gravitational attraction. A volume with a slightly higher density than the surrounding region would grow by gravitational accretion until it had gathered enough to form the stars and galaxies we see today. In actuality, however, what we see is but a tiny fraction of all that is out there. The universe is dominated by mysterious "dark matter" and even more mysterious "dark energy." Dark matter is matter that we cannot see, but it is influenced by gravity in the same way as normal matter. One of the primary goals of cosmology today is to determine the nature of dark matter. Dark energy is even less well understood, but its presence is implied by a number of current intriguing observational and theoretical findings. It is believed responsible for the fact that the rate of expansion of the universe seems to be increasing. Curiously, it can be seen as a realization of the very cosmological constant that Einstein called his greatest blunder.

With these two ingredients we are in a position to describe the evolution of both fluctuations in the density field of the universe and fluctuations in the peculiar velocity, the quantity of central interest in this dissertation. The peculiar velocity is simply the velocity of some cosmological object with the velocity due to the expansion of the universe factored out.

One way to get a handle on the nature of the distribution of matter and energy today, as well as far into the past, is to look at fluctuations of the temperature of the cosmic microwave background (CMB). The CMB is a steady stream of microwave light that reaches us after a journey of more than 13 billion years. The light comes from a period of time called recombination, just a few hundred thousand years after the big bang, so it is able to indirectly give us information about the state of the universe at that time. It also contains information about the universe of the more recent past and present because some of it has interacted with galaxies and clusters

of galaxies on its way to us. The peculiar velocities of these foreground objects cause distinct fluctuations in the temperature of the CMB, a process known as the kinetic Sunyaev-Zeldovich (kSZ) effect. The particular goal of this dissertation is to determine the role rotational peculiar velocities play in this effect. It is hoped that near-future astronomical missions can provide observations of these fluctuations to verify the predictions made by the powerful theoretical framework.

1.2 Motivation and Outline

The initial conditions for formation of large-scale structure are imprinted at the time of the decoupling of matter from radiation. The peculiar velocity field of matter at that time can be decomposed into two modes. The first, called the longitudinal mode, is a purely radial velocity. The other, called the rotational mode, is, as the name suggests, a pure rotation. In most cosmological applications it has been common procedure to disregard the rotational mode of the peculiar velocity because it is seen to decay as the universe expands, a simple consequence of the conservation of angular momentum. While this is indeed true, conservation of angular momentum demands the return of appreciable rotational velocities upon gravitational collapse of cosmological objects. This means that for applications where nonlinear (large density fluctuations) scales are important, the rotational velocities may make important contributions. One application where this may be important is in the aforementioned kSZ effect, where photons from the CMB are scattered by moving, collapsed, foreground objects. It is hoped that the next generation of CMB anisotropy observations will be able to see this effect.

The basic model for understanding the evolution of densities and velocities, the gravitational instability picture, will be discussed in chapter 2. Chapter 3 will explore the perturbation theory approach with the rotational velocity modes included. In chapter 4 we will introduce the physics of the CMB and its anisotropies. Chapter 5 will discuss the ingredients that go into a calculation of the expected angular

power spectrum of CMB temperature fluctuations and then show the results for the quasi-linear and nonlinear regimes, both without inclusion of rotational velocity effects. In chapter 6 we will build a model which includes rotational velocity effects and calculate the expected angular spectrum with this inclusion. Chapter 7 will contain concluding remarks.

CHAPTER 2
FOUNDATIONS

2.1 Gravitational Instability

One of the great cosmological puzzles of the last half century has been explaining the nature and evolution of inhomogeneities in today's universe. Einstein's cosmological principle makes the claim that on the largest scales the universe is homogeneous and isotropic, and this assumption is strongly supported by numerous observations.[1] On smaller scales, however, the universe is clearly quite inhomogeneous, as matter is clustered into stars, galaxies, clusters of galaxies, and beyond, with structure extending to the great walls and voids seen on scales of a few percent of the observable universe.

The leading picture for understanding the growth of these inhomogeneities from the early universe to today is known quite broadly as the gravitational instability model. The basic assumption of this model is that gravitation alone is responsible for the growth of inhomogeneities from their seeds in the early universe to their present state. The exact origin of these seeds is still something of an open question, but it is fairly well accepted today that they are inflationary amplifications of quantum zero-point fluctuations.[2] Quite generally, perturbations can be of two orthogonal modes, adiabatic or isocurvature, or a linear combination of the two. Adiabatic perturbations are those where volume elements are uniformly contracted or expanded, causing equal changes to the number densities of matter and radiation. This obviously causes perturbations in the energy densities, and, in fact, affects the energy density of matter differently than that of radiation. The orthogonal mode, consisting of isocurvature perturbations, describes entropy density fluctuations where the

energy densities remain smooth. Number density fluctuations in one species are balanced by those of the others. At times well earlier than the era of matter-radiation equivalence, both modes are distinct and take on important roles. At and after the matter-radiation equivalence era, we are principally interested in sub-horizon sized fluctuations, and sub-horizon sized isocurvature perturbations become adiabatic as pressure differences lead to actual density fluctuations. Thus beginning at the era of equivalence we can effectively treat all perturbations as adiabatic and use Newtonian fluid dynamics to follow their evolution.

The use of Newtonian mechanics in place of general relativity in describing the evolution of density fluctuations is justified so long as the characteristic size of the perturbations is small compared to the horizon size and the magnitude of the density perturbations is not large, thus ensuring nonrelativistic gravitational potentials. To find the equations that govern such evolution we begin by writing down the basic equations for an ideal, pressureless fluid. The first is the continuity equation, expressing conservation of mass.

$$\left(\frac{\partial \rho}{\partial t}\right)_r + \nabla_r \cdot (\rho \boldsymbol{u}) = 0, \tag{2.1}$$

or

$$\left[\left(\frac{\partial}{\partial t}\right)_r + \boldsymbol{u} \cdot \nabla_r\right] \rho = -\rho \nabla_r \cdot \boldsymbol{u}. \tag{2.2}$$

Here ρ is the density, $\boldsymbol{r}$ is the proper distance, and $\boldsymbol{u}$ its time derivative. We can also write down the Euler equation, expressing conservation of momentum,

$$\frac{d\boldsymbol{u}}{dt} = \left(\frac{\partial \boldsymbol{u}}{\partial t}\right)_r + \boldsymbol{u} \cdot \nabla_r \boldsymbol{u} = -\frac{\nabla_r p}{\rho} - \nabla_r \Phi. \tag{2.3}$$

Here p refers to pressure, which we will set to zero for the remainder of this discussion. When density contrasts become large, as in the collapse of a cluster of material, pressure again becomes important, but at that point the perturbative approach we are now exploring fails. The Φ in the above equation is the gravitational potential.

The final necessary fluid flow equation is the Poisson equation

$$\nabla_r^2 \Phi = 4\pi G\rho, \tag{2.4}$$

where G is Newton's gravitational constant. Now we wish to introduce a change of variables to "co-moving" coordinates, $\boldsymbol{x} = \boldsymbol{r}/a(t)$. $a(t)$ is just the cosmological scale factor, as it appears in the most general possible line element for a homogeneous, isotropic, expanding universe, the Robertson-Walker line element[3]

$$ds^2 = -c^2dt^2 + a^2(t)\left[\frac{dx^2}{(1-kx^2)} + x^2 d\Omega^2\right]. \tag{2.5}$$

The change of variables to co-moving coordinates is essentially a "subtracting out" of the effects of the expansion of the universe. With this definition of $\boldsymbol{x}$ we find

$$\begin{aligned} \boldsymbol{u} = \dot{\boldsymbol{r}} &= \dot{a}\boldsymbol{x} + \dot{\boldsymbol{x}}a \\ &= H\boldsymbol{r} + \boldsymbol{v}, \end{aligned} \tag{2.6}$$

where $H = \dot{a}/a$. H is known as the Hubble constant, which is a function of time. It is normally expressed as $H = 100h\text{km} \cdot \text{s}^{-1}\text{Mpc}^{-1}$, with the present value of the dimensionless constant being $h = 0.71 \pm 0.04$.[4] The velocity in these coordinates, $\boldsymbol{v}$, is called the peculiar velocity, and is just the velocity of the material in excess of its expansion velocity. It is the "perturbation" to the background smooth expansion.

Before continuing our look at the fluid flow equations, we should pause to take a closer look at the behavior of $a(t)$ and its time derivatives. To begin we express the pressureless Euler equation in terms of the new co-moving coordinates, noting that in the unperturbed case, $d\boldsymbol{x}/dt = 0$, and that the solution for Φ_0 in the unperturbed Poisson equation is $\Phi_0 = (2/3)\pi G\rho_0 r^2$. This gives us

$$\frac{d^2}{dt^2}(a\boldsymbol{x}) = -\frac{\nabla}{a}\frac{2}{3}\pi G\rho_0 a^2 x^2, \tag{2.7}$$

which leaves, (as $\nabla(x^2) = 2\boldsymbol{x}$),

$$\ddot{a} = -\frac{4}{3}\pi G\rho_0 a. \tag{2.8}$$

Here the ∇ refers to differentiation with respect to $\boldsymbol{x}$. We now have the behavior of $\ddot{a}$, which we will need later in this discussion. We gain further information by integrating the above equation once over time. This gives

$$\left(\frac{\dot{a}}{a}\right)^2 = \frac{8}{3}\pi G\rho_0 + \frac{C}{a^2}. \tag{2.9}$$

The constant of integration, C, is seen to be proportional to the k in the Robertson-Walker metric, which is a measure of the overall curvature of the universe. The most recent findings[4] suggest that the universe is flat, so we set $C = k = 0$ and ignore the contribution of curvature to the overall energy density of the universe for the remainder of the discussion.

Now, back to the discussion of the fluid flow equations. Since we are interested in examining the evolution of the density fluctuations, we write the density as $\rho = \rho_0[1+\delta]$. Our goal then is to determine the evolution of δ and $\boldsymbol{v}$. ρ_0 is the mean density, which satisfies $\rho_0 \propto a(t)^{-3}$ and therefore has a time evolution $\dot{\rho_0} = -3\rho_0 H$. Finally, we note the identity that for any function f under this change of coordinates

$$\left(\frac{\partial f}{\partial t}\right)_r = \left(\frac{\partial f}{\partial t}\right)_x - \frac{\dot{a}}{a}\boldsymbol{x}\cdot\nabla f \quad \text{where} \quad \nabla \equiv \frac{\nabla_r}{a}. \tag{2.10}$$

Now we are in a position to rewrite the fluid flow equations in terms of the co-moving variables and the perturbations, δ and $\boldsymbol{v}$. The continuity equation now looks like

$$\left(\frac{\partial}{\partial t} - \frac{\dot{a}}{a}\boldsymbol{x}\cdot\nabla\right)\rho_0[1+\delta] + \frac{\rho_0}{a}\nabla\cdot[(1+\delta)(\dot{a}\boldsymbol{x}+\boldsymbol{v})] = 0, \tag{2.11}$$

which simplifies to

$$\dot{\delta} + \frac{1}{a}\nabla\cdot[(1+\delta)\boldsymbol{v}] = 0. \tag{2.12}$$

Poisson's equation is now

$$\frac{1}{a^2}\nabla^2\Phi = 4\pi G\rho_0(1+\delta). \tag{2.13}$$

To remove the unperturbed part we write

$$\Phi = \phi + \frac{2}{3}\pi G\rho_0 a^2 x^2, \tag{2.14}$$

where the second term on the right hand side is the solution to the unperturbed Poisson's equation, as above. Using this for Φ we have

$$\nabla^2\phi = 4\pi G\rho_0 a^2\delta. \tag{2.15}$$

At this point we should note that in the above discussion we have assumed the density to consist only of mass density. This is certainly not at all the case, as fully seventy percent of the universe's energy density is contained in a mysterious "dark energy" or cosmological constant that provides a negative pressure and is thought to be fueling the acceleration of the expansion of the universe. As the name suggests, however, the contribution to the energy density from the cosmological constant is smooth and does not influence the evolution of density fluctuations; thus the terms involving the cosmological constant that belong in the full fluid flow equations cancel when we reduce to the perturbation evolution equations.

Finally, we look at the Euler equation under the change of coordinates. With the pressure term and the cosmological constant term left out we have

$$\left(\frac{\partial}{\partial t} - \frac{\dot{a}}{a}\boldsymbol{x}\cdot\nabla\right)(\dot{a}\boldsymbol{x}+\boldsymbol{v}) + \frac{1}{a}(\dot{a}\boldsymbol{x}+\boldsymbol{v})\cdot\nabla(\dot{a}\boldsymbol{x}+\boldsymbol{v}) = -\frac{1}{a}\nabla\phi - \frac{1}{a}\frac{4}{3}\pi G\rho_0 a^2\boldsymbol{x}. \tag{2.16}$$

Using the result of equation [2.8] for the second time derivative of $a(t)$, this simplifies to

$$\frac{\partial\boldsymbol{v}}{\partial t} + \frac{\dot{a}}{a}\boldsymbol{v} + \frac{1}{a}(\boldsymbol{v}\cdot\nabla)\boldsymbol{v} = -\frac{1}{a}\nabla\phi. \tag{2.17}$$

This equation, along with eqns.[2.12] and [2.15] describe the evolution of δ and $\boldsymbol{v}$. By combining equations [2.12] and [2.17] we can write one second order differential equation for the evolution of the density contrast.

$$\frac{\partial^2\delta}{\partial t^2} + 2\frac{\dot{a}}{a}\frac{\partial\delta}{\partial t} - 4\pi G\rho_0\delta = 4\pi G\rho_0\delta^2 + \frac{1}{a^2}\nabla\phi\cdot\nabla\delta + \frac{1}{a^2}\nabla_i\nabla_j[(1+\delta)v^iv^j]. \quad (2.18)$$

This equation is written so that the left hand side has only terms of first order in the perturbed quantities, while the right hand side has the higher order terms. Assuming the perturbations are small (i.e. $\delta \ll 1$) we can, to good approximation, set the right hand side equal to zero. When δ approaches unity, the above equation can be used to generate contributions to second order or higher. Analyses of these terms fall under the heading of "weakly non-linear" calculations and have been often explored.[5–8] At $\delta > 1$ perturbation theory breaks down and different methodologies must be pursued.

In order to solve for the first order behavior of δ we need to go back and look at the time dependence of $a(t)$. Equation [2.9] provides a differential equation for $a(t)$ which we can solve, noting again that $\rho_0 \propto a^{-3}$. The solution is $a(t) \propto t^{2/3}$, so that $\dot{a}/a \equiv H = 2/3t$. Our differential equation for δ is now, to first order,

$$\frac{\partial^2\delta}{\partial t^2} + \frac{4}{3t}\frac{\partial\delta}{\partial t} - \frac{2}{3t^2}\delta = 0. \quad (2.19)$$

The two solutions are $\delta \propto t^{2/3}$, the growing mode, and $\delta \propto t^{-1}$, the decaying mode. We will take a closer look at these solutions in the next chapter, as well as solutions to higher order in perturbation theory.

With these solutions in hand we can now begin to look at the behavior of the quantity of central interest in this dissertation, the peculiar velocity. We begin by noting that by observation we can write the general solution to the linearized version

of equation [2.12] (ignoring the $\nabla \cdot (\delta \boldsymbol{v})$ term) as

$$\boldsymbol{v}(\boldsymbol{x}, t) = -a \nabla \nabla^{-2} \dot{\delta}(\boldsymbol{x}, t) + \frac{\boldsymbol{F}(\boldsymbol{x})}{a}, \tag{2.20}$$

where $\boldsymbol{F}$ is an arbitrary function which satisfies $\nabla \cdot \boldsymbol{F} = 0$. We will pursue the higher order terms in the next chapter. Here the ∇^{-2} operator simply refers to the solution of the Poisson equation, $\nabla^{-2}\delta = \phi / 4\pi G \rho_0 a^2$. It is the second term in this expression for the velocity which will be of central importance for the majority of this dissertation. We can see that it decays as a^{-1}, and thus is typically (and often justifiably, for the large scales we are dealing with in the perturbation theory regime) ignored. The decay of this term is expected as a result of simple conservation of angular momentum in an expanding universe. Length grows by a factor of $a(t)$, so the product of length and rotational velocity should remain constant. See Appendix A for a more rigorous derivation of conservation of angular momentum in an expanding universe. Of course, when objects collapse, on small scales, the same conservation of momentum demands the return of appreciable rotational velocities.

We can write this solution more explicitly by writing $\delta(\boldsymbol{x}, t) \propto D(t)$ where D could be either the growing or decaying time dependence, and defining $f \equiv (a/D)(dD/da)$. If we only retain the growing mode for D, and we can ignore the relativistic background, as we already have, then f can be approximated by a simple function of Ω, $f(\Omega) = \Omega^{0.6}$.[1] Additionally, the Poisson equation is familiar from, among many physical applications, electromagnetism, and its solution is

$$\phi = -\rho_0 G a^2 \int d^3x' \frac{\delta(\boldsymbol{x}')}{|\boldsymbol{x}' - \boldsymbol{x}|}. \tag{2.21}$$

So, ignoring the divergence-free part of the velocity for now we can write

$$\boldsymbol{v} = \frac{Haf}{4\pi} \nabla \int d^3x' \delta(\boldsymbol{x}') \frac{1}{|\boldsymbol{x}' - \boldsymbol{x}|}. \tag{2.22}$$

We see that without the rotational term the velocity is a potential flow. This fact is used to great advantage in many applications, including a powerful method of reconstructing the three dimensional velocity field from redshift measurements, known as POTENT.[9,10]

Finally we note that the velocity is sometimes written in terms of the peculiar gravitational acceleration, defined by $\boldsymbol{g} \equiv -\nabla\phi/a$. We can then write

$$\boldsymbol{v} = -\frac{Hf\boldsymbol{g}}{4\pi G\rho_0}. \tag{2.23}$$

The disregard of the rotational term means that the peculiar velocity and acceleration are parallel.

2.2 Statistics

Now that we have some idea of how density fluctuations and peculiar velocities should act (at least on large scales, for now) we need to be able to compare these predictions to observations or to N-body simulation results. Of course it is not the density or velocity fluctuations at any one point that are of primary interest, but the statistical distributions of said quatities. The distributions of such quantities are defined by their moments. For a one dimensional variable, say x, with a distribution $f(x)$ the moments are defined by

$$\langle x^n \rangle = \int dx f(x) x^n. \tag{2.24}$$

This is easily generalized to fields, and the first few moments of the density, $\rho(\boldsymbol{x})$, are written

$$\langle \rho(\boldsymbol{x}) \rangle = \rho_0, \tag{2.25}$$

$$\langle \rho(\boldsymbol{x}_1)\rho(\boldsymbol{x}_2) \rangle = {\rho_0}^2(1 + \xi_{12}), \tag{2.26}$$

$$\langle \rho(\boldsymbol{x}_1)\rho(\boldsymbol{x}_2)\rho(\boldsymbol{x}_3) \rangle = {\rho_0}^3(1 + \xi_{12} + \xi_{13} + \xi_{23} + \zeta_{123}). \tag{2.27}$$

Here ξ is the irreducible two-point correlation function and ζ the irreducible three point correlation function. Of course this hierarchy can be continued, but the two and three point functions and their Fourier transforms are the most commonly used. The two point correlation function, ξ, is also seen to be the second moment of the density perturbation δ,

$$\xi_{12} = \frac{\langle \rho_1 \rho_2 \rangle - {\rho_0}^2}{{\rho_0}^2} = \frac{\langle (\rho_1 - \rho_0)(\rho_2 - \rho_0) \rangle}{{\rho_0}^2} = \langle \delta_1 \delta_2 \rangle, \tag{2.28}$$

where the subscripts 1 and 2 indicate a function of $\boldsymbol{x}_1$ or $\boldsymbol{x}_2$ respectively. In the second line we have used the fact that $\langle \delta_1 \rangle = \langle \delta_2 \rangle = (\langle \rho_{1,2} \rangle - \rho_0)/\rho_0 = 0$, by equation [2.25].

The physical meaning of ξ is easily appreciated when we look at its definition in terms of a discrete quantity, such as the number counts of galaxies. Assuming no bias between mass distribution and galaxy distribution, we can write the probability of finding a galaxy, which we assume to be a point-like object as far as the scales we are interested in are concerned, in an arbitrary infinitesimal volume as $dP = \rho(\boldsymbol{x})dV$. Then the probability of finding one galaxy in each of two different volumes is

$$dP = \langle \rho(\boldsymbol{x}_1)\rho(\boldsymbol{x}_2) \rangle dV_1 dV_2 = {\rho_0}^2 [1 + \xi(\boldsymbol{x}_{12})] dV_1 dV_2. \tag{2.29}$$

We can see then that ξ, as its name suggests, is simply the correlation between the two galaxies. That is, if ξ is positive for some $\boldsymbol{x}_{12}$ then galaxies are clustered at that length scale. Given one galaxy there is a greater chance of finding another at that distance than would be found by chance, as determined by the average density of the universe. Having said that we assumed no bias between mass distribution and galaxy distribution, we must at least acknowledge that such a bias may exist. At large scales there appears to be no bias, so the two correlation functions are equivalent, but on small scales a significant bias may exist. This is the likely source

of differences between correlation functions calculated from observations and those from N-body simulations and analytical calculations.[11]

It is often useful to examine density fluctuations and their associated statistics in Fourier space. In fact, the second moment of the transform of the density perturbation, the power spectrum, is much more often calculated than ξ itself. We define the Fourier transformed density fluctuation

$$\tilde{\delta}(\boldsymbol{k}) = \int d^3x \delta(\boldsymbol{x}) e^{i\boldsymbol{k}\cdot\boldsymbol{x}}, \tag{2.30}$$

then the power spectrum is defined by

$$\langle \tilde{\delta}(\boldsymbol{k}_1)\tilde{\delta}(\boldsymbol{k}_2)\rangle = [(2\pi)^3\delta_D(\boldsymbol{k}_1+\boldsymbol{k}_2)]P(k), \tag{2.31}$$

where $P(k)$ is the power spectrum and δ_D is the Dirac delta function. Here k is the magnitude of either wave vector (as the Delta function ensures they are equal.) Isotropy demands that the power spectrum is a function of magnitude only. With these definitions, the power spectrum can be written in terms of the two point correlation function like

$$P(k) = \int d^3x \xi(x) j_0(kx), \tag{2.32}$$

where $j_0(kx) = \sin(kx)/kx$ is the zeroth spherical Bessel function. The same procedure can be undertaken for the higher moments.[5,12]

Finally, we wish to examine the moments of the peculiar velocity field. As we already have a relationship between the peculiar velocity and the density fluctuations, it is straightforward to find the moments of the (irrotational) velocity field in terms of the correlation functions. For example,

$$\begin{aligned}\langle v^2\rangle &= \frac{1}{V}\int d^3x \left(\frac{Haf}{4\pi}\right)^2 \left[\int d^3x' \delta(\boldsymbol{x}')\nabla\frac{1}{|\boldsymbol{x}'-\boldsymbol{x}|}\right]\cdot\left[\int d^3x'' \delta(\boldsymbol{x}'')\nabla\frac{1}{|\boldsymbol{x}''-\boldsymbol{x}|}\right] \\ &= \frac{(Haf)^2}{4\pi}\int d^3y \xi(y)/y. \end{aligned} \tag{2.33}$$

gives the second moment of the peculiar velocity in terms of the two point correlation function. Many authors will instead calculate moments of a variable proportional to the velocity divergence, $\theta \equiv (1/\dot{a})\nabla \cdot \boldsymbol{v}$. This procedure obviously loses its utility if the rotational, or divergence-free, mode of the velocity is kept. Many examples can be found in the literature.[8,12,13] Another interesting set of moments to calculate are those of the difference between the velocity of two galaxies. For example the first moment of one component of the density weighted pair velocity is

$$\langle v_{12}^i \rangle_\rho = \frac{\langle (1+\delta_1)(1+\delta_2)(v_1 - v_2)^i \rangle}{\langle (1+\delta_1)(1+\delta_2) \rangle}, \tag{2.34}$$

where the subscripts refer to functions of $\boldsymbol{x}_1$ or $\boldsymbol{x}_2$.

One reason these are interesting is that they can be easier to calculate from actual data, due to difficulties in determining distances to galaxies independent of redshift.[13]

2.3 Small-Scale Considerations

The previous perturbative analysis works well as long as the density perturbations are small. ($\delta < 1.$) When δ becomes large we enter the non-linear regime and different analytic methods are required. This non-linear regime represents objects which have collapsed, which we can recognize as galaxies or clusters of galaxies with their associated dark matter halos. We typically do not speak of individual stars as collapsed objects in this sense, as much more complicated physics contributes at those scales. There are two main ingredients in the description of non-linear density perturbations. First one must know something about the distribution of sizes of the collapsed objects. This has traditionally been accomplished using a method known as the Press-Schechter approximation,[14] which has been improved upon since its original derivation.[15,16] To understand the Press-Schechter approach, we first remember that the density contrast, δ, is a Gaussian random field, or at least is assumed to be in this derivation, and we define its standard deviation, $\sigma \equiv \langle \delta^2 \rangle^{1/2}$.

We can then write the probability that the density contrast in some randomly placed window exceeds a critical density for collapse, δ_c, as

$$P = \frac{1}{\sigma(2\pi)^{1/2}} \int_{\delta_c}^{\infty} d\delta e^{-\delta^2/2\sigma^2} \tag{2.35}$$

where σ is a function of the window size, or of the contained mass, M. This can also be viewed as the fraction of perturbations within the window whose mean density exceeds δ_c. Press and Schechter themselves realized that this would only take into account the mass contained in the overdense regions of the universe, and since the mass in the under dense regions will eventually accrete onto the collapsed objects, they simply multiplied their result by a factor of two. Now, to find the number density of collapsed objects in the range dM (actually, it is typical to write the result in terms of logarithmic interval $d\ln M$) we differentiate the above probability and multiply by the inverse of the volume, ρ_0/M, (which is simply the number density of collapsed objects of that size if all mass were contained in objects of that size.) This gives us the result

$$\frac{dn}{d\ln M} = \left(\frac{2}{\pi}\right)^{1/2} \frac{\rho_0}{M} \frac{d\ln\sigma^{-1}}{d\ln M} \nu e^{-\nu^2/2}, \tag{2.36}$$

where $\nu \equiv \delta_c/\sigma$. The value of the critical density contrast for collapse is $\delta_c = 1.686$. (See Appendix B for a derivation and discussion of this result.)

Though the Press-Schechter mass function has been the standard model used since its inception, it seems to predict too many low mass halos, whereas N-body simulations and astronomical data suggest that the low mass objects are more strongly clustered and thus should properly be classified as higher mass objects. There have been many recent efforts to improve upon the Press-Schechter formalism, including an analytical attempt, based on the Zeldovich approximation[15] (using an ellipsoidal collapse model instead of the spherical collapse used by Press-Schechter), and fits to N-body data.[16] Sheth and Tormen,[16] find a mass function, valid for N-body

simulations of a variety of cold dark matter cosmologies, given by

$$\frac{dn}{d\ln M} = \frac{\rho_0}{M}\frac{d\ln\sigma^{-1}}{d\ln M} 2A\left(1+\frac{1}{\nu'^{2q}}\right)\left(\frac{\nu'^2}{2\pi}\right)^{1/2} e^{-\nu'^2/2}, \tag{2.37}$$

where $\nu' = \alpha^{-1/2}\nu, \alpha = 0.707, q = 0.3$, and $A = 0.322$. Note that the values $\alpha = 1, q = 0, A = 1/2$ reproduce the Press-Schechter function.

The second ingredient in describing non-linear perturbations is a knowledge of the shape and nature of the objects that have collapsed. This has been possible only through the analysis of N-body simulations, where (possibly) universal profiles of collapsed objects have been extracted. The first successful universal profile for dark matter halos was presented by Navarro, Frenk, and White (hereafter NFW) in 1997.[17] Their study of N-body results led to the suggestion of a universal density profile of the form

$$\frac{\rho(r)}{\rho_c} = \frac{\delta_a}{(r/r_s)(1+r/r_s)^2}, \tag{2.38}$$

where $\rho_c = 3H^2/8\pi G$ is the critical density for closure of the universe, δ_a is a characteristic density, and r_s is a scale radius which is different for each individual cluster. (The scale radius is found by N-body simulations to be a rough function of cluster mass, a fact we will use in chapters 5 and 6.) More recent results of numerical simulations, performed by Moore and collaborators, with higher resolution have indicated that the universal profile may instead be[18]

$$\frac{\rho(r)}{\rho_c} = \frac{\delta_a}{(r/r_s)^{1.5}[1+(r/r_s)^{1.5}]}. \tag{2.39}$$

As we have often made mention of the results of N-body simulations, it would be appropriate at this point to make a few remarks regarding them. Because exact solutions to non-linear equations of motion are difficult to come by, we are led to try to use computer simulation to gain insight. These N-body simulations approximate the continuous density field by a set of discrete particles. The simulations simply

calculate the gravitational force on each particle due to all the other particles, accelerate and move the particles appropriately by a small amount, then iterate the procedure. Of course this procedure quickly becomes intractable when the number of particles becomes large, so many methods have been developed to shorten the calculations. Typically, as in the most popularly used codes, called particle-particle-particle-mesh, or P^3M codes, exact forces are only calculated for particles close by, with the remaining particles binned onto a grid.[19]

The use of discrete particles to represent an essentially continuous density creates its own problems. The most serious of these arises when particles pass close to one another and scatter at wide angles. Since each particle actually represents a huge number of smaller particles spaced far apart, such collisions should not take place. In order to correct for this, forces are "softened" over appropriately small length scales. This effect, along with the complicated physics that arises out of the collisions that do take place, such as shock heating and radiative cooling, significantly limits the resolution of N-body simulations.

One of the key ingredients in determining the outcome of the simulations is the selection of the initial conditions. These conditions depend on the cosmology which one is trying to simulate, but typically the particle positions are distributed in a Guassian fashion and the initial velocities are projected onto the growing, radial, mode.

CHAPTER 3
VELOCITY MODES IN PERTURBATION THEORY

3.1 First Order Solutions

In this chapter we wish to systematically include rotational velocity terms in the structure of perturbation theory. We begin by rewriting the equations for the evolution of δ and $\boldsymbol{v}$ from the last chapter. Equation [2.12] is written with the first order terms on the left and the second order source term on the right,

$$\dot{\delta} + \frac{1}{a}\nabla \cdot \boldsymbol{v} = -\frac{1}{a}\nabla \cdot (\delta \boldsymbol{v}). \tag{3.1}$$

We also remember equation [2.17], which we divide by the scale factor a,

$$\frac{\partial}{\partial t}\left(\frac{\boldsymbol{v}}{a}\right) + \frac{\boldsymbol{v}}{a}\frac{4}{3t} + \frac{2}{3t^2}\nabla\nabla^{-2}\delta = -\left(\frac{\boldsymbol{v}}{a}\cdot\nabla\right)\frac{\boldsymbol{v}}{a}, \tag{3.2}$$

where we have used the fact that $a \propto t^{2/3}$ and eqns. [2.9] and [2.15]. As we saw, the first order solution for δ is

$$\delta_1 = A(\boldsymbol{x})t^{2/3} + B(\boldsymbol{x})t^{-1}, \tag{3.3}$$

where A and B are arbitrary functions of position which represent the density perturbations at some initial time. Here and in the rest of the chapter we adopt the notation used by Hwang.[20,21] The first order solution for $\boldsymbol{v}$ is obtained by setting the right hand side of equation [3.1] equal to zero and putting in the above solution for δ. We thus have

$$\begin{aligned} \frac{\boldsymbol{v}_1}{a} &= -\nabla\nabla^{-2}(\dot{\delta_1}) + \frac{\boldsymbol{F}(\boldsymbol{x})}{a^2} \\ &= \nabla\nabla^{-2}\left[-\frac{2}{3}At^{-1/3} + Bt^{-2}\right] + \boldsymbol{C}t^{-4/3}, \end{aligned} \tag{3.4}$$

where $\nabla \cdot \boldsymbol{F} = \nabla \cdot \boldsymbol{C} = 0$. The last term is the rotational mode. For algebraic ease we will set $B = 0$ as this is the decaying mode in the first order solution for δ. The function A then is the density perturbation at some initial time, $A(\boldsymbol{x}) \equiv \delta(\boldsymbol{x}, t_0) \equiv \delta_0(\boldsymbol{x})$. The vector $\boldsymbol{C}$ is the initial rotational velocity, $\boldsymbol{C}(\boldsymbol{x}) \equiv \boldsymbol{v}_0^t(\boldsymbol{x})$. As A and $\boldsymbol{C}$ describe initial conditions, they are typically taken to be random variables with Gaussian distribution.

3.2 Second Order Solutions in Real Space

In order to find second order solutions for δ we plug the first order solution into the right hand side of equation [3.1],

$$\dot{\delta}_2 + \frac{1}{a}\nabla \cdot \boldsymbol{v}_2 = -\frac{1}{a}\nabla \cdot (\boldsymbol{v}_1 \delta_1). \tag{3.5}$$

We then have

$$\begin{aligned} \dot{\delta}_2 + \frac{1}{a}\nabla \cdot \boldsymbol{v}_2 &= -\frac{1}{a}\nabla \cdot \left(At^{2/3} \left[\nabla\nabla^{-2}(-\frac{2}{3}At^{-1/3}) + \boldsymbol{C}t^{-4/3} \right] \right) \\ &= \frac{2}{3}E_1 t^{1/3} + E_2 t^{-2/3}, \end{aligned} \tag{3.6}$$

where

$$E_1 = \nabla \cdot (A\nabla\nabla^{-2}A) \quad \text{and} \quad E_2 = -\nabla \cdot (\boldsymbol{C}A) = -\boldsymbol{C} \cdot \nabla A. \tag{3.7}$$

Doing the same with equation [3.2] we have

$$\begin{aligned} &\frac{\partial}{\partial t}(\frac{\boldsymbol{v}_2}{a}) + \frac{\boldsymbol{v}_2}{a}\frac{4}{3t} + \frac{2}{3t^2}\nabla\nabla^{-2}\delta_2 \\ &\quad = -\left(\left[(-\nabla\nabla^{-2}\frac{2}{3}At^{-1/3}) + \boldsymbol{C}t^{-4/3} \right] \cdot \nabla \right) \left(-\nabla\nabla^{-2}\frac{2}{3}At^{-1/3} + \boldsymbol{C}t^{-4/3} \right) \\ &\quad = \frac{4}{9}t^{-2/3}\boldsymbol{F}_1 + \frac{2}{3}t^{-5/3}\boldsymbol{F}_2 + t^{-8/3}\boldsymbol{F}_3, \end{aligned} \tag{3.8}$$

where

$$\begin{aligned} \boldsymbol{F}_1 &= -(\nabla\nabla^{-2}A)\cdot\nabla(\nabla\nabla^{-2}A) \\ &= -\frac{1}{2}\nabla(\nabla\nabla^{-2}A\cdot\nabla\nabla^{-2}A) \qquad (3.9) \\ \boldsymbol{F}_2 &= (\nabla\nabla^{-2}A\cdot\nabla)\boldsymbol{C}+\boldsymbol{C}\cdot\nabla(\nabla\nabla^{-2}A) \qquad (3.10) \\ \boldsymbol{F}_3 &= -(\boldsymbol{C}\cdot\nabla)\boldsymbol{C}. \qquad (3.11) \end{aligned}$$

Taking the divergence of equation [3.8] and inserting equation [3.6], we obtain one second order differential equation for δ_2,

$$\begin{aligned} &\ddot{\delta}_2+\frac{4}{3}t^{-1}\dot{\delta}_2-\frac{2}{3}t^{-2}\delta_2 \\ &\quad-\left[t^{-2/3}(\frac{10}{9}E_1-\frac{4}{9}\nabla\cdot\boldsymbol{F}_1)+t^{-5/3}(\frac{2}{3}E_2-\frac{2}{3}\nabla\cdot\boldsymbol{F}_2)-t^{-8/3}(\nabla\cdot\boldsymbol{F}_3)\right] \\ &\quad=0, \qquad (3.12) \end{aligned}$$

which admits a solution of the form

$$\delta_2 = Ht^{-2/3}+It^{1/3}+Jt^{4/3}, \qquad (3.13)$$

where H, I and J are arbitrary functions of position. Plugging this in and matching powers of t, we obtain the result

$$\delta_2=\frac{1}{7}(5E_1-2\nabla\cdot\boldsymbol{F}_1)t^{4/3}+\frac{3}{2}(-E_2+\nabla\cdot\boldsymbol{F}_2)t^{1/3}+(\frac{9}{4}\nabla\cdot\boldsymbol{F}_3)t^{-2/3}. \qquad (3.14)$$

The first term is still the dominant one, and has no contribution from rotational modes. We will revisit this term in a moment, when we look at its Fourier counterpart. The second term describes the mixing of the rotational and longitudinal modes. An important feature is the fact that this mode does not decay with time buts actually grows, meaning that even an initially small rotational component will have an impact on the future longitudinal mode.The third term is due to the purely rotational mode, and it decays.

Putting this solution back into equation [3.6], we see that the solution for the second order velocity looks like

$$\begin{aligned}\frac{\boldsymbol{v}_2}{a} &= \nabla\nabla^{-2}\left[\frac{1}{7}(-2E_1+\frac{8}{3}\nabla\cdot\boldsymbol{F}_1)t^{1/3}+(\frac{3}{2}E_2-\frac{1}{2}\nabla\cdot\boldsymbol{F}_2)t^{-2/3}+(\frac{3}{2}\nabla\cdot\boldsymbol{F}_3)t^{-5/3}\right] \\ &+ \quad \text{divergence-free part.}\end{aligned} \tag{3.15}$$

To find the divergence free part, we look at the curl of equation [3.8] and note that $\nabla\times\boldsymbol{F}_1=0$. This implies

$$\frac{\partial}{\partial t}\left(\frac{\boldsymbol{v}_2^t}{a}\right)+\frac{\boldsymbol{v}_2^t}{a}\frac{4}{3}t^{-1}=\frac{2}{3}t^{-5/3}\boldsymbol{F}_2^t+t^{-8/3}\boldsymbol{F}_2^t, \tag{3.16}$$

where the superscript t indicates the transverse (or divergence-free) part, which is defined by $F^t_{n\alpha}=(\delta^\beta_\alpha-\nabla_\alpha\nabla^{-2}\nabla^\beta)F_{n\beta}$.[21] Here and for all that follows, α,β represent spatial indices and thus run from 1 to 3. Equation [3.16] admits a solution of the form

$$\frac{\boldsymbol{v}_2^t}{a}=\boldsymbol{L}t^{-2/3}+\boldsymbol{M}t^{-5/3}, \tag{3.17}$$

where $\boldsymbol{L}$ and $\boldsymbol{M}$ are arbitrary functions of position with the caveat that $\nabla\cdot\boldsymbol{L}=\nabla\cdot\boldsymbol{M}=0$. When $\boldsymbol{L}$ and $\boldsymbol{M}$ are solved for and inserted into the total solution we have

$$\begin{aligned}\frac{\boldsymbol{v}_2}{a} &= \nabla\nabla^{-2}\left[\frac{1}{7}(-2E_1+\frac{8}{3}\nabla\cdot\boldsymbol{F}_1)t^{1/3}+(\frac{3}{2}E_2-\frac{1}{2}\nabla\cdot\boldsymbol{F}_2)t^{-2/3}+(\frac{3}{2}\nabla\cdot\boldsymbol{F}_3)t^{-5/3}\right] \\ &+\boldsymbol{F}_2^t t^{-2/3}-3\boldsymbol{F}_3^t t^{-5/3}.\end{aligned} \tag{3.18}$$

We note that to second order the velocity still has only one growing mode, which is still purely longitudinal. It does, however, have several terms constant in time, one of which is a potential flow which is coupled to the initial rotational mode and one which is a pure rotation, coupled to the initial longitudinal mode.

3.3 Second Order Solutions in Fourier Space

It is often convenient to work in Fourier space. (One reason for this, among many others, is that spatial derivatives become products with the wave-vector.) We

define the Fourier transform in the normal way, i.e.,

$$\tilde{\delta}(\boldsymbol{k},t) = \int d^3x\delta(\boldsymbol{x},t)e^{-i\boldsymbol{k}\cdot\boldsymbol{x}}, \tag{3.19}$$

$$\delta(\boldsymbol{x},t) = \int \frac{d^3k}{(2\pi)^3}\tilde{\delta}(\boldsymbol{k},t)e^{i\boldsymbol{k}\cdot\boldsymbol{x}}. \tag{3.20}$$

To first order then, disregarding the decaying density term, we can write $\tilde{\delta}_1 = \tilde{A}t^{2/3}$, and

$$\frac{\tilde{v}_1}{a} = i\frac{2}{3}\frac{\boldsymbol{k}}{k^2}\tilde{A}t^{-1/3} + \tilde{\boldsymbol{C}}t^{-4/3}. \tag{3.21}$$

To transform the second order density, we look at each of the terms in equation [3.14] in order. The first term contains E_1 and the divergence of $\boldsymbol{F}_1$, which can be written

$$E_1 = \nabla\cdot(A\nabla\nabla^{-2}A) = (\nabla A)\cdot(\nabla\nabla^{-2}A) + A^2 \tag{3.22}$$

$$\begin{aligned}\nabla\cdot\boldsymbol{F}_1 &= -\frac{1}{2}\nabla\cdot\nabla[(\nabla\nabla^{-2}A)\cdot\nabla\nabla^{-2}A] \\ &= -\nabla_\alpha\nabla_\beta(\nabla^{-2}A)\nabla^\alpha\nabla^\beta\nabla^{-2}A - \nabla_\beta\nabla^{-2}A\nabla^\beta A.\end{aligned} \tag{3.23}$$

The first term of equation [3.14] can therefore be written

$$\delta_{2a} = t^{4/3}\left[\frac{5}{7}A^2 + (\nabla A)\cdot(\nabla\nabla^{-2}A) + \frac{2}{7}(\nabla_\alpha\nabla_\beta(\nabla^{-2}A)\nabla^\alpha\nabla^\beta\nabla^{-2}A)\right], \tag{3.24}$$

which is a well known result.[13,22,23] In Fourier space, products become convolutions, as defined by

$$\widetilde{F_1(\boldsymbol{x})\cdots F_n(\boldsymbol{x})} = \int \frac{d^3k_1}{(2\pi)^3}\cdots\frac{d^3k_n}{(2\pi)^3}\delta_D(\Sigma\boldsymbol{k}_i - \boldsymbol{k})\tilde{F}_1(\boldsymbol{k}_1)\cdots\tilde{F}_n(\boldsymbol{k}_n), \tag{3.25}$$

where a quantity with a tilde denotes its Fourier transform and δ_D indicates the Dirac delta function.

So we have

$$\tilde{\delta}_{2a} = t^{4/3}\int \frac{d^3k_1}{(2\pi)^3}\frac{d^3k_2}{(2\pi)^3}[(2\pi)^3\delta_D(\boldsymbol{k}_1+\boldsymbol{k}_2-\boldsymbol{k})]\tilde{A}(\boldsymbol{k}_1)\tilde{A}(\boldsymbol{k}_2)\left[\frac{5}{7} + \frac{\boldsymbol{k}_1\cdot\boldsymbol{k}_2}{k_2^2} + \frac{2}{7}\frac{(\boldsymbol{k}_1\cdot\boldsymbol{k}_2)^2}{k_1^2k_2^2}\right]. \tag{3.26}$$

The second term contains E_2 and the divergence of $\boldsymbol{F}_2$, so we write

$$E_2 = -C_\alpha \nabla^\alpha A \tag{3.27}$$

$$\begin{aligned} \nabla \cdot \boldsymbol{F}_2 &= \nabla \cdot [(\nabla \nabla^{-2} A \cdot \nabla)\boldsymbol{C} + \boldsymbol{C} \cdot \nabla(\nabla \nabla^{-2} A)] \\ &= (\nabla^\beta C^\alpha)\nabla_\alpha \nabla_\beta \nabla^{-2} A + (\nabla_\alpha C^\beta)(\nabla_\beta \nabla^\alpha \nabla^{-2} A) + C^\beta \nabla_\beta A. \end{aligned} \tag{3.28}$$

Thus

$$\delta_{2b} = t^{1/3}\left[\frac{5}{2} C_\alpha \nabla^\alpha A + (\nabla_\alpha \nabla_\beta \nabla^{-2} A)(\nabla^\beta C^\alpha + \nabla^\alpha C^\beta)\right], \tag{3.29}$$

and

$$\tilde{\delta}_{2b} = t^{1/3} \int \frac{d^3k_1}{(2\pi)^3}\frac{d^3k_2}{(2\pi)^3}[(2\pi)^3 \delta_D(\boldsymbol{k}_1 + \boldsymbol{k}_2 - \boldsymbol{k})]\left[i\frac{5}{2}\tilde{\boldsymbol{C}}_1 \cdot \boldsymbol{k}_2 \tilde{A}_2 + i2\tilde{A}_1 \frac{\boldsymbol{k}_1 \cdot \boldsymbol{k}_2}{k_1^2}\boldsymbol{k}_1 \cdot \tilde{\boldsymbol{C}}_2\right], \tag{3.30}$$

where the subscipts on $\tilde{A}$ and $\tilde{\boldsymbol{C}}$ refer to functions of $\boldsymbol{k}_1$ or $\boldsymbol{k}_2$. The third term contains only the divergence of $\boldsymbol{F}_3$, which is

$$\nabla \cdot \boldsymbol{F}_3 = -\nabla_\alpha C^\beta \nabla_\beta C^\alpha. \tag{3.31}$$

Thus

$$\delta_{2c} = t^{-2/3}\left(-\frac{9}{4}\nabla_\alpha C^\beta \nabla_\beta C^\alpha\right), \tag{3.32}$$

and

$$\tilde{\delta}_{2c} = t^{-2/3} \int \frac{d^3k_1}{(2\pi)^3}\frac{d^3k_2}{(2\pi)^3}[(2\pi)^3 \delta_D(\boldsymbol{k}_1 + \boldsymbol{k}_2 - \boldsymbol{k})]\frac{9}{4}(\boldsymbol{k}_1 \cdot \boldsymbol{C}_2)(\boldsymbol{k}_2 \cdot \boldsymbol{C}_1). \tag{3.33}$$

The final result for the Fourier transform of the second order density is of course just the sum of these terms,

$$\tilde{\delta}_2 = \tilde{\delta}_{2a} + \tilde{\delta}_{2b} + \tilde{\delta}_{2c}. \tag{3.34}$$

The Fourier transform of the second order velocity is found in similar fashion. Looking at each of the four terms in equation [3.18] in order, we have, for the first

term

$$\left(\frac{\boldsymbol{v}_2}{a}\right)_a = \nabla\nabla^{-2}\left[t^{1/3}\frac{1}{7}(-2E_1+\frac{8}{3}\nabla\cdot\boldsymbol{F}_1)\right]$$
$$= -\nabla\nabla^{-2}t^{1/3}\left[\frac{2}{7}A^2+\frac{2}{3}(\nabla A)\cdot(\nabla\nabla^{-2}A)\right.$$
$$\left.+\frac{8}{21}\nabla_\alpha\nabla_\beta(\nabla^{-2}A)\nabla^\alpha\nabla^\beta(\nabla^{-2}A)\right]. \quad (3.35)$$

Its Fourier transform is then

$$\left(\frac{\tilde{\boldsymbol{v}}_2}{a}\right)_a = -\frac{\boldsymbol{k}}{k^2}t^{1/3}\int\frac{d^3k_1}{(2\pi)^3}\frac{d^3k_2}{(2\pi)^3}[(2\pi)^3\delta_D(\boldsymbol{k}_1+\boldsymbol{k}_2-\boldsymbol{k})]\tilde{A}_1\tilde{A}_2$$
$$\times\left[\frac{2}{7}+\frac{2}{3}\frac{\boldsymbol{k}_1\cdot\boldsymbol{k}_2}{k_2^2}+\frac{8}{21}\frac{(\boldsymbol{k}_1\cdot\boldsymbol{k}_2)^2}{k_1^2k_2^2}\right]. \quad (3.36)$$

This is the full solution when the rotational mode is ignored and is well known in the literature.[1,5,7,22] The second term is

$$\left(\frac{\boldsymbol{v}_2}{a}\right)_b = \nabla\nabla^{-2}\left[t^{-2/3}(\frac{3}{2}E_2-\frac{1}{2}\nabla\cdot\boldsymbol{F}_2)\right]$$
$$= -\nabla\nabla^{-2}t^{-2/3}\left[2C_\alpha\nabla^\alpha A+\frac{1}{2}\nabla_\alpha\nabla_\beta\nabla^{-2}A(\nabla^\beta C^\alpha+\nabla^\alpha C^\beta)\right], \quad (3.37)$$

whose Fourier transform is

$$\left(\frac{\tilde{\boldsymbol{v}}_2}{a}\right)_b = -t^{-2/3}\frac{\boldsymbol{k}}{k^2}\int\frac{d^3k_1}{(2\pi)^3}\frac{d^3k_2}{(2\pi)^3}[(2\pi)^3\delta_D(\boldsymbol{k}_1+\boldsymbol{k}_2-\boldsymbol{k})]$$
$$\times\left[i2\tilde{\boldsymbol{C}}_1\cdot\boldsymbol{k}_2\tilde{A}_2+i\tilde{A}_1\frac{\boldsymbol{k}_1\cdot\boldsymbol{k}_2}{k_1^2}\boldsymbol{k}_1\cdot\tilde{\boldsymbol{C}}_2\right]. \quad (3.38)$$

The third term is

$$\left(\frac{\boldsymbol{v}_2}{a}\right)_c = \nabla\nabla^{-2}t^{-5/3}\left(\frac{3}{2}\nabla\cdot\boldsymbol{F}_3\right)$$
$$= \nabla\nabla^{-2}t^{-5/3}\left(\frac{3}{2}\nabla_\alpha C^\beta\nabla_\beta C^\alpha\right), \quad (3.39)$$

whose transform is

$$\left(\frac{\tilde{\boldsymbol{v}}_2}{a}\right)_c = -t^{-5/3}\frac{\boldsymbol{k}}{k^2}\int \frac{d^3k_1}{(2\pi)^3}\frac{d^3k_2}{(2\pi)^3}[(2\pi)^3\delta_D(\boldsymbol{k}_1+\boldsymbol{k}_2-\boldsymbol{k})]\left[\frac{3}{2}(\boldsymbol{k}_1\cdot\tilde{\boldsymbol{C}}_2)(\boldsymbol{k}_2\cdot\tilde{\boldsymbol{C}}_1)\right]. \tag{3.40}$$

The final term is the divergence free part,

$$\left(\frac{\boldsymbol{v}_2}{a}\right)_d = \boldsymbol{F}_2^t t^{-2/3} - 3\boldsymbol{F}_3^t t^{-5/3}. \tag{3.41}$$

Using the previous definitions, we can write this term in component notation as

$$\begin{aligned}\left(\frac{\boldsymbol{v}_2}{a}\right)_{d\alpha} &= t^{-2/3}\left[\nabla_\beta\nabla^{-2}A\nabla^\beta C^\alpha + C^\beta\nabla_\beta\nabla^\alpha\nabla^{-2}A\right.\\ &\quad \left.-\nabla_\alpha\nabla^{-2}\nabla^\beta(\nabla_\gamma\nabla^{-2}A\nabla^\gamma C^\beta) - \nabla_\beta\nabla^{-2}\nabla^\beta(C^\gamma\nabla_\gamma\nabla^\beta\nabla^{-2}A)\right]\\ &\quad -3t^{-5/3}[C_\gamma\nabla^\gamma C_\alpha - \nabla_\alpha\nabla^{-2}\nabla^\beta(C_\gamma\nabla^\gamma C_\beta)].\end{aligned} \tag{3.42}$$

The Fourier transform of this term is

$$\begin{aligned}\left(\frac{\tilde{\boldsymbol{v}}_2}{a}\right)_d &= t^{-2/3}\int \frac{d^3k_1}{(2\pi)^3}\frac{d^3k_2}{(2\pi)^3}[(2\pi)^3\delta_D(\boldsymbol{k}_1+\boldsymbol{k}_2-\boldsymbol{k})]\\ &\quad\times\left[\frac{\boldsymbol{k}_1\cdot\boldsymbol{k}_2}{k_1^2}\tilde{\boldsymbol{C}}_2 + \tilde{A}_2\frac{\tilde{\boldsymbol{C}}_1\cdot\boldsymbol{k}_2}{k_2^2}\boldsymbol{k}_2 - \hat{k}\cdot\left(\frac{\boldsymbol{k}_1\cdot\boldsymbol{k}_2}{k_1^2}\tilde{\boldsymbol{C}}_2 + \tilde{A}_2\frac{\tilde{\boldsymbol{C}}_1\cdot\boldsymbol{k}_2}{k_2^2}\boldsymbol{k}_2\right)\right]\\ &\quad -3t^{-5/3}\int \frac{d^3k_1}{(2\pi)^3}\frac{d^3k_2}{(2\pi)^3}[(2\pi)^3\delta_D(\boldsymbol{k}_1+\boldsymbol{k}_2-\boldsymbol{k})]\\ &\quad\times\left[(\tilde{\boldsymbol{C}}_1\cdot\boldsymbol{k}_2)\tilde{\boldsymbol{C}}_2 - \hat{k}\cdot(\tilde{\boldsymbol{C}}_1\cdot\boldsymbol{k}_2)\tilde{\boldsymbol{C}}_2\right].\end{aligned} \tag{3.43}$$

Written in this form it is easy to see that this contribution is purely perpendicular to the wave-vector $\boldsymbol{k}$.

3.4 Third Order Solutions in Real Space

Solutions to third order can be obtained in much the same way as second order solutions. They are necessary in order to calculate quantities which are sometimes of interest, such as the four-point function or its Fourier analog, the trispectrum.[12,24]

To third order, equation [3.1] becomes

$$\begin{aligned}
\dot{\delta}_3 + \nabla \cdot \frac{\boldsymbol{v}_3}{a} &= -\nabla \cdot \left(\frac{\boldsymbol{v}_1}{a}\delta_2\right) - \nabla \cdot \left(\frac{\boldsymbol{v}_2}{a}\delta_1\right) \\
&= -\nabla \cdot \left[\left\{ \left(\frac{9}{4}\nabla \cdot \boldsymbol{F}_3\right) t^{-2/3} + \frac{3}{2}(-E_2 + \nabla \cdot \boldsymbol{F}_2)t^{1/3} \right.\right. \\
&\quad \left.\left. + \frac{1}{7}(5E_1 - 2\nabla \cdot \boldsymbol{F}_1)t^{4/3} \right\} \left\{ \nabla\nabla^{-2}(-\frac{2}{3}At^{-1/3}) + \boldsymbol{C}t^{-4/3} \right\} \right] \\
&\quad -\nabla \cdot \left[(At^{2/3}) \left\{ \nabla\nabla^{-2}(t^{1/3}\frac{1}{7}(-2E_1 + \frac{8}{3}\nabla \cdot \boldsymbol{F}_1) \right.\right. \\
&\quad \left.\left. + t^{-2/3}(\frac{3}{2}E_2 - \frac{1}{2}\nabla \cdot \boldsymbol{F}_2) + t^{-5/3}(\frac{3}{2}\nabla \cdot \boldsymbol{F}_3)) + \boldsymbol{F}_2^t t^{-2/3} - 3\boldsymbol{F}_3^t t^{-5/3} \right\} \right] \\
&= tP_0 + P_1 + t^{-1}P_2 + t^{-2}P_3, \qquad (3.44)
\end{aligned}$$

where

$$\begin{aligned}
P_0 &= -\nabla \cdot \frac{1}{7}\left[(5E_1 - 2\nabla \cdot \boldsymbol{F}_1)\nabla\nabla^{-2}(-\frac{2}{3}A) \right. \\
&\quad \left. + A\nabla\nabla^{-2}(-2E_1 + \frac{8}{3}\nabla \cdot \boldsymbol{F}_1) \right], \qquad (3.45) \\
P_1 &= -\nabla \cdot \left[\frac{3}{2}(-E_2 + \nabla \cdot \boldsymbol{F}_2)\nabla\nabla^{-2}(-\frac{2}{3}A) + A\nabla\nabla^{-2}(\frac{3}{2}E_2 - \frac{1}{2}\nabla \cdot \boldsymbol{F}_2) \right. \\
&\quad \left. + \frac{1}{7}(5E_1 - 2\nabla \cdot \boldsymbol{F}_1)\boldsymbol{C} \right], \qquad (3.46) \\
P_2 &= -\nabla \cdot \left[(\frac{9}{4}\nabla \cdot \boldsymbol{F}_3)\nabla\nabla^{-2}(-\frac{2}{3}A) + \frac{3}{2}(-E_2 + \nabla \cdot \boldsymbol{F}_2)\boldsymbol{C} \right. \\
&\quad \left. + A\nabla\nabla^{-2}(\frac{3}{2}\nabla \cdot \boldsymbol{F}_3) - 3A\boldsymbol{F}_3^t \right], \qquad (3.47) \\
P_3 &= -\nabla \cdot \left[(\frac{9}{4}\nabla \cdot \boldsymbol{F}_3)\boldsymbol{C} \right]. \qquad (3.48)
\end{aligned}$$

P_0 contains all pure longitudinal couplings, P_1 and P_2 contain mixed couplings, and P_3 contains the purely rotational coupling.

Similarly, to third order, equation [3.2] becomes

$$\begin{aligned}
\frac{\partial}{\partial t}(\frac{\boldsymbol{v}_3}{a}) + \frac{\boldsymbol{v}_3}{a}\frac{4}{3}t^{-1} + \frac{2}{3}t^{-2}\nabla\nabla^{-2}\delta_3 &= -\frac{\boldsymbol{v}_1}{a} \cdot \nabla\frac{\boldsymbol{v}_2}{a} - \frac{\boldsymbol{v}_2}{a} \cdot \nabla\frac{\boldsymbol{v}_1}{a} \\
&= \boldsymbol{Q}_0 + \boldsymbol{Q}_1 t^{-1} + \boldsymbol{Q}_2 t^{-2} + \boldsymbol{Q}_3 t^{-3}, \qquad (3.49)
\end{aligned}$$

where

$$\begin{aligned}
\boldsymbol{Q}_0 &= -[\nabla\nabla^{-2}(-\frac{2}{3}A)\cdot\nabla][\nabla\nabla^{-2}\frac{1}{7}(-2E_1+\frac{8}{3}\nabla\cdot\boldsymbol{F}_1)] \\
&\quad -[\nabla\nabla^{-2}\frac{1}{7}(-2E_1+\frac{8}{3}\nabla\cdot\boldsymbol{F}_1)\cdot\nabla][\nabla\nabla^{-2}(-\frac{2}{3}A)] \\
\boldsymbol{Q}_1 &= -[\nabla\nabla^{-2}(-\frac{2}{3}A)\cdot\nabla][\nabla\nabla^{-2}(\frac{3}{2}E_2-\frac{1}{2}\nabla\cdot\boldsymbol{F}_2)+\boldsymbol{F}_2^t] \\
&\quad -[(\nabla\nabla^{-2}(\frac{3}{2}E_2-\frac{1}{2}\nabla\cdot\boldsymbol{F}_2)+\boldsymbol{F}_2^t)\cdot\nabla][\nabla\nabla^{-2}(-\frac{2}{3}A)] \\
&\quad -(\boldsymbol{C}\cdot\nabla)[\nabla\nabla^{-2}\frac{1}{7}(-2E_1+\frac{8}{3}\nabla\cdot\boldsymbol{F}_1)] \\
&\quad -[(\nabla\nabla^{-2}\frac{1}{7}[-2E_1+\frac{8}{3}\nabla\cdot\boldsymbol{F}_1])\cdot\nabla]\boldsymbol{C}, \\
\boldsymbol{Q}_2 &= -[\nabla\nabla^{-2}(-\frac{2}{3}A)\cdot\nabla][\nabla\nabla^{-2}(\frac{3}{2}\nabla\cdot\boldsymbol{F}_3)-3\boldsymbol{F}_3^t] \\
&\quad -[(\nabla\nabla^{-2}[\frac{3}{2}\nabla\cdot\boldsymbol{F}_3]-3\boldsymbol{F}_3^t)\cdot\nabla][\nabla\nabla^{-2}(-\frac{2}{3}A)] \\
&\quad -[\boldsymbol{C}\cdot\nabla][\nabla\nabla^{-2}(\frac{3}{2}E_2-\frac{1}{2}\nabla\cdot\boldsymbol{F}_2)+\boldsymbol{F}_2^t] \\
&\quad -[(\nabla\nabla^{-2}[\frac{3}{2}E_2-\frac{1}{2}\nabla\cdot\boldsymbol{F}_2]+\boldsymbol{F}_2^t)\cdot\nabla]\boldsymbol{C}, \\
\boldsymbol{Q}_3 &= -(\boldsymbol{C}\cdot\nabla)(-3\boldsymbol{F}_3^t)-(-3\boldsymbol{F}_3^t\cdot\nabla)\boldsymbol{C}. \qquad (3.50)
\end{aligned}$$

As before, we combine the divergence of equation [3.44] with equation [3.49] to produce one second order differential equation for δ_3. This is

$$\begin{aligned}
\ddot{\delta}_3+\frac{4}{3}t^{-1}\dot{\delta}_3-\frac{2}{3}t^{-2}\delta_3 &= (-\frac{7}{3}P_0+\nabla\cdot\boldsymbol{Q}_0)+(\frac{4}{3}P_1+\nabla\cdot\boldsymbol{Q}_1)t^{-1} \\
&\quad +(-\frac{1}{3}P_2+\nabla\cdot\boldsymbol{Q}_2)t^{-2}+(\frac{2}{3}P_3+\nabla\cdot\boldsymbol{Q}_3)t^{-3}, \qquad (3.51)
\end{aligned}$$

which admits a solution of the form

$$\delta_3 = Rt^2+St+U+Vt^{-1}. \qquad (3.52)$$

Plugging in this solution and matching powers of t gives us the final solution

$$\begin{aligned}
\delta_3 &= \frac{1}{4}(-\frac{7}{3}P_0+\nabla\cdot\boldsymbol{Q}_0)t^2+\frac{3}{2}(\frac{4}{3}P_1+\nabla\cdot\boldsymbol{Q}_1)t \\
&\quad -\frac{3}{2}(-\frac{1}{3}P_2+\nabla\cdot\boldsymbol{Q}_2)-\frac{1}{2}(\frac{2}{3}P_3+\nabla\cdot\boldsymbol{Q}_3)t^{-1}. \qquad (3.53)
\end{aligned}$$

The first term is the purely longitudinal mode, and is again the fastest growing term. The second term, however, is also growing, and contains a mixture of longitudinal and rotational couplings. The third term is a constant in time and is also a mixture of couplings. The fourth, and still decaying, term contains purely rotational couplings.

Putting this solution into equation [3.44], we find

$$\begin{aligned}\frac{\boldsymbol{v}_3}{a} &= \nabla\nabla^{-2}\left[t(\frac{13}{6}P_0+\nabla\cdot\boldsymbol{Q}_0)-(P_1+\nabla\cdot\boldsymbol{Q}_1)+t^{-1}P_2+t^{-2}(\frac{2}{3}P_3+\nabla\cdot\boldsymbol{Q}_3)\right]\\ &+ \text{ divergence-free part.}\end{aligned} \tag{3.54}$$

To find the divergence-free part, we note that $\nabla\times\boldsymbol{Q}_0=0$ and look at the purely rotational part of equation [3.49],

$$\frac{\partial}{\partial t}\left(\frac{\boldsymbol{v}_3^t}{a}\right)+\frac{\boldsymbol{v}_3^t}{a}\frac{4}{3}t^{-1}=\boldsymbol{Q}_1^t t^{-1}+\boldsymbol{Q}_2^t t^{-2}+\boldsymbol{Q}_3^t t^{-3}, \tag{3.55}$$

which admits a solution of the form

$$\frac{\boldsymbol{v}_3^t}{a}=\boldsymbol{W}+\boldsymbol{Y}t^{-1}+\boldsymbol{Z}t^{-2}. \tag{3.56}$$

Matching powers of t, we obtain the final result

$$\begin{aligned}\frac{\boldsymbol{v}_3}{a} &= \nabla\nabla^{-2}\left[t(\frac{13}{6}P_0+\nabla\cdot\boldsymbol{Q}_0)-(P_1+\nabla\cdot\boldsymbol{Q}_1)+t^{-1}P_2+t^{-2}(\frac{2}{3}P_3+\nabla\cdot\boldsymbol{Q}_3)\right]\\ &+\frac{3}{4}\boldsymbol{Q}_1^t+3\boldsymbol{Q}_2^t t^{-1}-\frac{3}{2}\boldsymbol{Q}_3^t t^{-2}.\end{aligned} \tag{3.57}$$

The fastest growing mode of this solution is the purely longitudinal peice, but there are several other growing terms as well (remembering that the a in the denominator of the left side is proportional to $t^{2/3}$.) The second term is a potential flow, growing in time, which derives from a mixture of initially longitudinal and rotational modes. The other growing term, $(3/4)\boldsymbol{Q}_1^t$, is a purely rotational mode deriving from a mixture of initially longitudinal and rotational modes. Thus it is at third order in perturbation theory that we find growing terms in the peculiar velocity associated with the initial rotational flow. This should be somewhat important in quasi-linear

regimes where δ is approaching unity, although perturbation theory at third order and higher has a fairly small window of applicability.

3.5 Evolution of Vorticity

As a corollary to the discussion above, we look at the evolution of vorticity in perturbation theory. We define the vorticity, $\boldsymbol{\zeta}$, to be the curl of the transverse velocity. Remembering the first order solution for the peculiar velocity,

$$\boldsymbol{v} = \frac{Haf}{4\pi}\nabla \int d^3x' \delta(\boldsymbol{x}') \frac{1}{|\boldsymbol{x}' - \boldsymbol{x}|} + \frac{\boldsymbol{F}(\boldsymbol{x})}{a} = a\dot{D}\boldsymbol{\eta}_0 + \frac{\boldsymbol{v}_{0t}}{a}, \tag{3.58}$$

we find that the first oder vorticity is

$$\boldsymbol{\zeta}^{(1)} = \nabla \times \boldsymbol{v}_t^{(1)} = \nabla \times \frac{\boldsymbol{v}_0}{a} \equiv \frac{\boldsymbol{\zeta}_0}{a}. \tag{3.59}$$

Thus to first order, the vorticity decays as the inverse of the scale factor, a. To explore the time dependence of the next order term, we start with equation [2.17] from the last chapter. We then use the vector identity

$$\boldsymbol{v} \times (\nabla \times \boldsymbol{v}) = \nabla(\frac{1}{2}v^2) - (\boldsymbol{v} \cdot \nabla)\boldsymbol{v}, \tag{3.60}$$

which gives us

$$\frac{1}{a}\frac{\partial}{\partial t}(a\boldsymbol{v}) + \frac{1}{a}\nabla\left(\frac{1}{2}v^2\right) - \frac{1}{a}\boldsymbol{v} \times (\nabla \times \boldsymbol{v}) + \frac{1}{a}\nabla\phi = 0. \tag{3.61}$$

Taking the curl of this equation and writing it in terms of $\boldsymbol{\zeta}$, we have

$$\frac{\partial}{\partial t}(a\boldsymbol{\zeta}) = \nabla \times (\boldsymbol{v} \times \boldsymbol{\zeta}). \tag{3.62}$$

Using the first order velocity and vorticity as the source for the second order vorticity, we find

$$\frac{\partial}{\partial t}(a\boldsymbol{\zeta}^{(2)}) = \nabla \times (\boldsymbol{v}^{(1)} \times \boldsymbol{\zeta}^{(1)}) = \dot{D}\nabla \times (\boldsymbol{\eta}_0 \times \boldsymbol{\zeta}_0) + \frac{1}{a^2}\nabla \times (\boldsymbol{v}_{0t} \times \boldsymbol{\zeta}_0). \tag{3.63}$$

The first term dominates for late times and so, disregarding the second term, we see that

$$\zeta^{(2)} = \frac{D}{a}\nabla \times (\boldsymbol{\eta}_0 \times \boldsymbol{\zeta}_0). \tag{3.64}$$

The interesting aspect of this result is that it is the interaction between the first order vorticity and the first order longitudinal mode. This of course just echoes the result of equation [3.14] and the fact that as an object collapses any small rotational velocity is amplified due to angular momentum conservation.

CHAPTER 4
THE CMB AND THE SUNYAEV-ZELDOVICH EFFECT

4.1 Introduction

One possible place in which the effect of rotational velocities may be important is in the scattering of the cosmic microwave background (CMB) by foreground ionized gas. One of the major predictions of the now almost universally accepted hot big bang theory is the existence of background relic radiation. This is the radiation seen from the surface of last scattering. Early in the universe ($z >\sim 1000$) temperatures were high enough that neutral atoms could not form. At this time photons scattered readily off the densely packed charged particles. At about $z = 1000$ the temperature dropped enough to allow the production of neutral hydrogen and photons were "frozen out." It is from this epoch that we receive the background radiation. The existence of this radiation was first predicted by Gamow, Alpher, and Herman in he 1950's, and the search for it began in earnest in the mid 1960's. It was discovered, rather accidentally, by Arno Penzias and Robert Wilson in 1965.[25] Since that time a great many measurements of the temperature and polarization of the CMB have been made. The intensity of the CMB has been measured very accurately over more than three orders of magnitude in frequency and the spectrum is found to be that of a blackbody with a temperature of 2.725 ± 0.002K.[26] Figure [4–1] shows how well the data fit a Planckian spectrum. One very intriguing aspect of the CMB is its near total isotropy. The temperature in every direction is identical to a part in 10^{-3}. This thermal equilibrium over so many causally disconnected regions is now reasonably well explained by theories of inflation. (In fact, it was one of the principle motivations for the development of inflationary theories.)

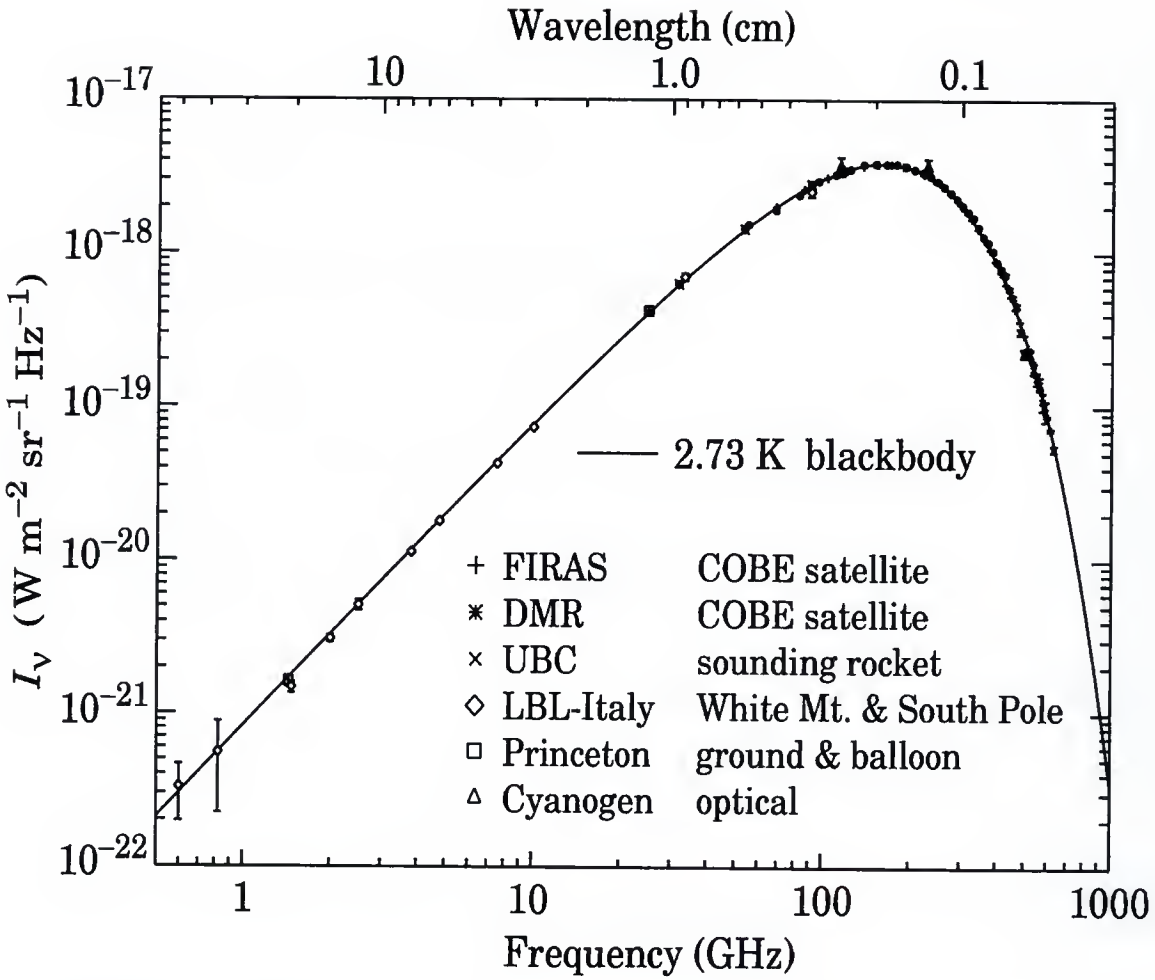

Figure 4–1. Measurements of the intensity of the CMBR as a function of frequency. The solid line represents a perfect blackbody at 2.73 K. The figure is taken from Smoot.[26] (See references therein for sources of data.)

4.2 Anisotropies in the CMB

Perhaps more interesting than the problem of explaining the isotropy of the CMB is explaining its anisotropies. These anisotropies are typically expressed in terms of an expansion in spherical harmonics,

$$\frac{\Delta T}{T}(\theta,\phi) = \sum_{lm} a_{lm} Y_{lm}(\theta,\phi). \tag{4.1}$$

We can then define an angular correlation function by

$$C(\theta) = \langle \frac{\Delta T}{T}(\hat{n_1}) \frac{\Delta T}{T}(\hat{n_2}) \rangle = \sum_{l} \frac{2l+1}{4\pi} C_l P_l(\hat{n_1} \cdot \hat{n_2}), \tag{4.2}$$

where P_l are the Legendre polynomials and $C_l \equiv \langle |a_l^m|^2 \rangle$, is the angular power spectrum. The first, and dominant, anisotropy is the $l = 1$ dipole moment. This is simply interpreted as due to the motion of the earth relative to the "cosmic rest frame" as defined by the CMB. Utilizing a simple special relativistic calculation, Peebles and Wilkinson,[27] first noted that the temperature measured by an observer in a frame moving with respect to the homogeneous background, at an angle θ with respect to the motion is

$$T'(\theta) = \frac{T(1-\frac{v^2}{c^2})^{1/2}}{1-(v/c)\cos\theta}, \tag{4.3}$$

which can be expanded as

$$T'(\theta) = T[1 + \frac{v}{c}\cos\theta + \frac{1}{2}\frac{v^2}{c^2}\cos 2\theta + O(v^3)]. \tag{4.4}$$

The amplitude of the dipole anisotropy, as measured by the Cosmic Background Explorer (COBE) satellite, is $\Delta T/T = 3.372 \pm 0.014$mK.[28] This implies a solar system velocity of 371 ± 1km/s towards galactic coordinates $(\ell, b) = (264°.14 \pm 0.30, 48°.26 \pm 0.30)$.

4.3 Primary Anisotropies

After the dipole anisotropy, which, as we saw, is at the $\Delta T/T \approx 10^{-3}$ level, is accounted for, the next level of anisotropies are found at $\Delta T/T \approx 10^{-5}$. These

anisotropies are believed to be due to inhomogeneities in the surface of last scattering. The effect of density perturbations present at that time can be divided into three categories. The first, known as the Sachs-Wolfe effect, is due to the photons climbing out of the gravitational potentials of the density perturbations. The magnitude of the effect is really the combination of two effects. First, as the photons climb out of the well, they are redshifted, or cooled, which gives

$$\frac{\Delta T}{T} = \frac{\delta\phi}{c^2}. \tag{4.5}$$

The photons are also heated, due to the associated time dilation, and you seem to be looking at a younger, hotter universe. This effect is

$$\frac{\Delta t}{t} = \frac{\delta\phi}{c^2} \Longrightarrow \frac{\Delta T}{T} = -\frac{2\delta\phi}{3c^2}, \tag{4.6}$$

since $T \propto 1/a$ and $a \propto t^{2/3}$. Thus the total Sachs-Wolfe effect is given by

$$\frac{\Delta T}{T} = \frac{\delta\phi}{3c^2} \tag{4.7}$$

The second effect related to density perturbations at the surface of last scattering is called the adiabatic, or intrinsic, perturbation effect. It is simply due to the fact that denser regions would recombine later, thus look hotter. This effect yields a temperature perturbation equal to the density perturbation responsible for the late recombination. The final important source of primary anisotropy is simply the doppler shift of the photons coming off the moving plasma at last scattering. This yields a temperature perturbation of

$$\frac{\delta T}{T} = \frac{\delta \boldsymbol{v} \cdot \hat{r}}{c}, \tag{4.8}$$

where $\hat{r}$ represents the unit vector along the line of sight. The combination of these effects lead to the famous acoustic peaks in the angular power spectrum of the CMB anisotropies. Before recombination, adiabatically overdense regions initially

collapse due to gravity, but are then pushed apart by radiation pressure, setting up acoustic waves. These standing waves are frozen out at decoupling and are seen, via the aforementioned effects, in the angular power spectrum. The first, and largest, peak is associated with a length scale equal to the Hubble radius at the time of recombination. The size, shape, and position of this peak, as well as the subsequent peaks, tell us a great deal about allowed cosmologies and the values of cosmological parameters. For example, as previously mentioned in chapter 1, the location of the first peak at $\ell \approx 200$ strongly indicates that the universe is flat, or very close to it.

As mentioned, the first significant detection of the CMB anisotropies was by the COBE satellite. Since that time, many ground and balloon based measurements have been attempted. In 2003 the most significant of these missions, the Wilkinson Microwave Anisotropy Probe (WMAP) completed its first year of data acquisition. Figure [4–2] shows the angular power spectrum measured by WMAP. The first acoustic peak is very clearly seen. The second peak is also clear and the beginnings of a third are hinted at. Figure [4–3] shows the results of a number of other experiments and how they relate to the WMAP data. The agreement among the variety of different measurements shows the robustness of the results. WMAP provides a very accurate picture of the anisotropy spectrum from about $\ell = 10$ to about $\ell = 800$. The large error bars at very low ℓ are due to the fact that we have only one universe to observe, and at large angular scales one cannot average over significantly many independent pieces of sky. (This is equivalent to saying that there are only $2\ell+1$ m's to average over.) The limits at high ℓ's are due to resolution limits for the WMAP satellite. The European Space Agency plans launch of the PLANCK satellite in or around 2007, which hopes to extend measurements to perhaps $\ell \sim 1200$.

4.4 Secondary Anisotropies

The primary temperature anisotropies, due to the nature of the surface of last scattering, dominate the angular power spectrum at small and medium ℓ's, but

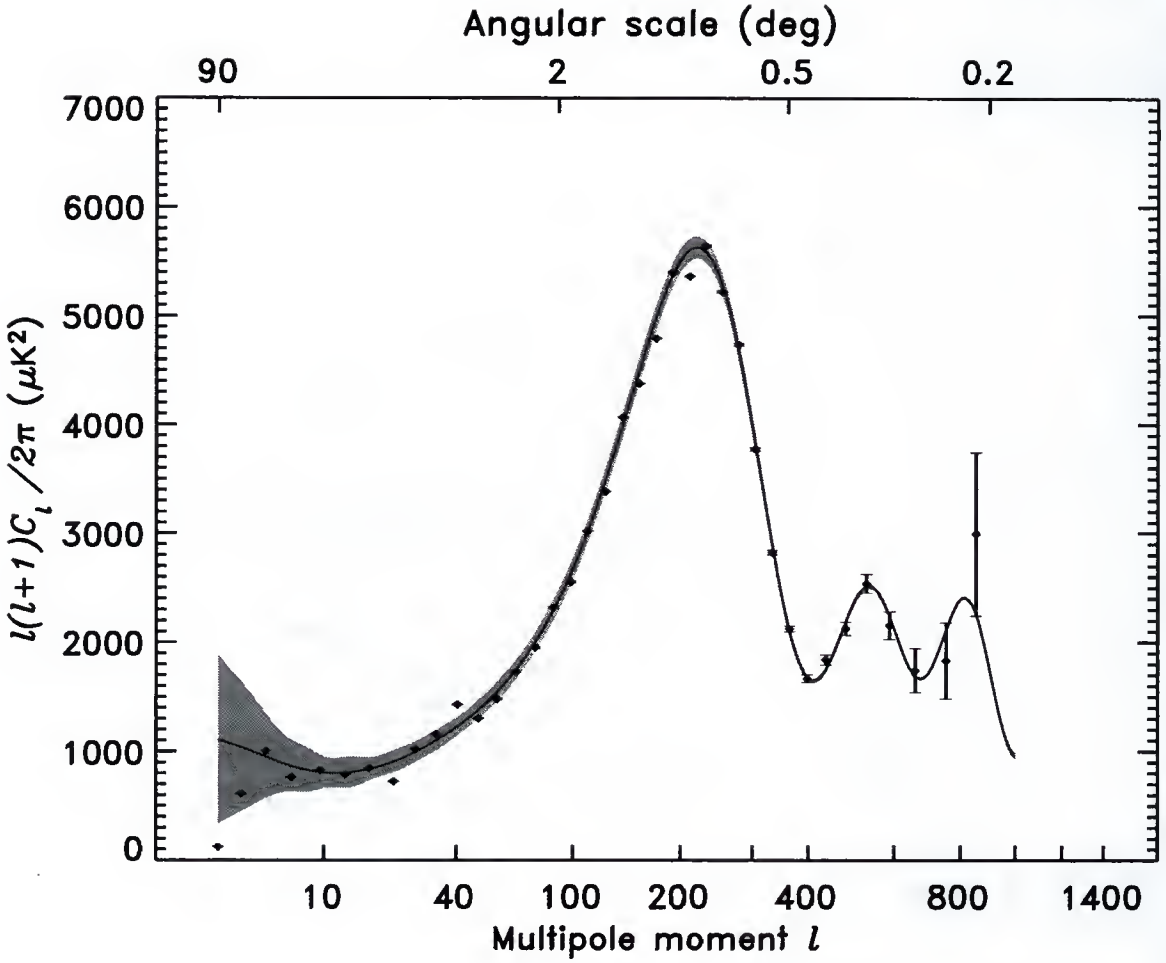

Figure 4–2. The points represent the data obtained from the first year run of the WMAP satellite, along with 1σ error bars. The line represents a best fit ΛCDM model, and the gray shading represents the 1σ error due to cosmic variance. Taken from Hinshaw et al.[29]

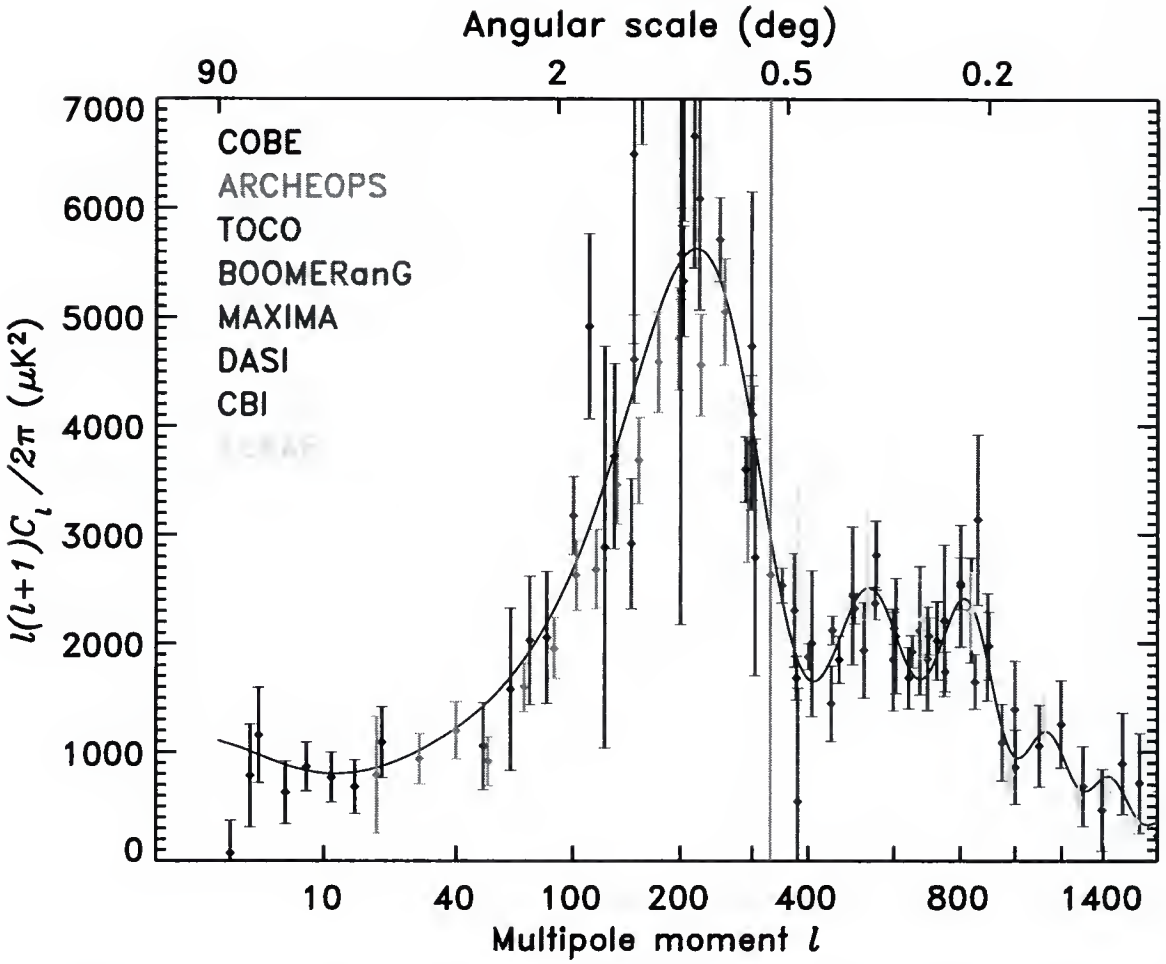

Figure 4–3. A collection of recent data from various CMB anisotropy measurement experiments. The line is again the best fit ΛCDM model based on the first year WMAP results. Taken from Hinshaw et. al.[29]

they are by no means the only contributors to the spectrum. At smaller scales, or larger ℓ's, secondary anisotropies are expected to dominate the angular power spectrum. These effects include the Integrated Sachs-Wolfe (ISW) effect, which, although it is a secondary effect, is expected to only be seen at large angular scales, and the thermal and kinetic Sunyaev-Zeldovich (SZ) effects,[30,31] which should be the major contributions to the spectrum at ℓ's greater than about 1200. The ISW effect is the secondary analog to the primary Sachs-Wolfe effect. When a CMB photon falls into a potential well on its journey to us it is heated, or blueshifted, then cooled, or redshifted, as it climbs back out. If the depth of the well remains constant while the photon traverses it, then the redshift exactly cancels the blueshift and no trace is seen in the CMB. However, if the depth of the well changes over the time that the photon takes to traverse the well, then there is a net change in the photon temperature. The photon may traverse many such regions on its path to us, thus the word "integrated" in its name. The ISW can further be split into two contributions, an "early" effect, due the changeover from a radiation dominated universe to a matter dominated universe, and a "late" effect, due to the changeover from a matter dominated universe to a Λ dominated one. (Thought to happening around now.) The origin of the early ISW lies in the fact that when radiation is controlling the expansion of the universe, potentials on the scale of the sound horizon are damped, giving photons crossing them an overall boost in energy. The early effect provides a contribution to the angular power spectrum in the region of the first acoustic peak, at low ℓ's. This effect has been seen by comparing data from WMAP to data from the Sloan Digital Sky Survey (SDSS).[32] The late effect is expected to be strongly damped at medium and higher ℓ's as well, as the photons pass through a great many regions of overdensities and underdensities. It is hoped that detections of the late ISW effect at low ℓ's will provide more information about

the dark energy content of the universe, as it is sensitive to the time of switch-over from matter domination to Λ domination.

4.5 Thermal and Non-Thermal Sunyaev-Zeldovich Effects

At small angular scales, corresponding to ℓ's over about 1200, the thermal and kinetic SZ effects should be dominant. The SZ effect is the result of the interaction of the CMB photons with regions of charged particles between the observer and the surface of last scattering. The thermal SZ effect is an inverse Compton scattering of the CMB off thermal electron populations. The result is a temperature fluctuation, which, at low frequencies, like those of most of the CMB photons, is

$$\frac{\Delta T}{T} = -2 \int \frac{k_B T_e}{m_e c^2} n_e \sigma_T dl. \tag{4.9}$$

Recent analysis of the data obtained by the WMAP satellite confirms that the SZ effect is swamped by the primary anisotropies for all angular scales available to it, corresponding to ℓ's up to roughly 900.[33] Though there is not yet a large amount of angular power spectrum data taken at high ℓ's (see figure [4–3]), at least one mission, the Cosmic Background Imager, has measured power up to $\ell \approx 3500$ which seems to be consistent with the power expected from the thermal SZ effect.[34,35] More accurate measures of this power may be useful in constraining the values of some cosmological parameters.[36]

There is an additional effect due to scattering off non-thermal electron populations, such as would be found in cluster radio halo sources. Computation of this effect is made difficult by the highly relativistic nature of the electrons, but the low density of such electrons, and the relative rarity of such populations, lead to insignificant contributions to the angular power spectrum. (Though the search for the non-thermal SZ effect in specific clusters can prove useful.)

4.6 Kinetic Sunyaev-Zeldovich Effect

There is an additional temperature fluctuation induced in the CMB if the foreground material is in bulk motion. This effect, called the kinetic SZ effect, is simply due to the doppler shift induced by the motion. The temperature fluctuation along a line-of-sight direction, $\hat{\gamma}$, is given by

$$\frac{\Delta T}{T} = \int dl e^{-\tau} \sigma_T n_e \hat{\gamma} \cdot \frac{\boldsymbol{v}}{c}, \tag{4.10}$$

where τ is the optical depth to scattering through the electron cloud, n_e is the number density of electrons in the cloud, and $\boldsymbol{v}$ is the peculiar velocity of the cloud.

Measurement of this effect for particular clusters can be used to calculate the radial component of its peculiar velocity, which is of significant interest, as the method does not require an independent distance measurement.[37] (It does, however, require an accurate estimation of optical depth and electron density.) In addition, one must disentangle it from the thermal effect, as well as other small-scale anisotropies. This is typically done by making use of the fact that the kinetic SZ effect has a different frequency dependence than the thermal effect.[38]

CHAPTER 5
KINETIC SZ ANGULAR POWER SPECTRUM INGREDIENTS

5.1 Introduction

In this chapter we lay out the ingredients for calculating the angular power spectrum of CMB anisotropies due to the kinetic Sunyaev-Zeldovich effect. The angular power spectrum can be written in terms of a projection of the actual three-dimensional power spectrum, which we will explore in the first few sections of the chapter. We will compare several of the popular models used to build these power spectra. The final sections will include calculations of the angular spectrum in both the perturbative regime and the nonlinear regime, without inclusion of the rotational modes. This gives us the necessary background for the calculation including rotational modes in the next chapter.

5.2 Linear Power Spectrum

One of the main ingredients in all the calculations to follow is a linear order density-density power spectrum. The most commonly used model is one originated by Bardeen et al.[39] The authors matched a fitting function to results from numerical simulation to produce an analytic form for the spectrum. A slightly improved version, used by Ma,[40] and to be used as the input linear power spectrum in all that follows is given by

$$P(k,a) = \frac{Ak^n[D(a)/D_0]^2[\ln(1+\alpha_1 q)/\alpha_1 q]^2}{[1+\alpha_2 q+(\alpha_3 q)^2+(\alpha_4 q)^3+(\alpha_5 q)^4]^{1/2}}, \tag{5.1}$$

where

$$q = \frac{k}{\Gamma h} \tag{5.2}$$

$$\Gamma = \frac{\Omega_m h}{e^{\Omega_b(1+1.3/\Omega_m)}} \tag{5.3}$$

$$D(a) = ag(a) \tag{5.4}$$

$$D_o = D(a=0) \tag{5.5}$$

$$g(a) = \frac{2.5\Omega_m(a)}{\Omega_m(a)^{4/7} - \Omega_\Lambda(a) + [1+\Omega_m(a)/2][1+\Omega_\Lambda(a)/70]} \tag{5.6}$$

$$A = \frac{\delta_H^2 (c/H_0)^{n+3}}{4\pi} \tag{5.7}$$

$$\delta_H = (1.94\times10^{-5})\Omega_m^{-\beta_1-\beta_2\ln(\Omega_m)} e^{-\beta_3(n-1)-\beta_4(n-1)^2} \tag{5.8}$$

$$\Omega_m(a) = \frac{\Omega_m}{\Omega_m + a^3\Omega_\Lambda} \tag{5.9}$$

$$\Omega_\Lambda(a) = 1 - \Omega_m(a). \tag{5.10}$$

When the cosmological parameters $\Omega_m, \Omega_\Lambda, \Omega_b$ appear without functional dependence on a, they refer to the values today. Which values to use are determined by the cosmology one wants to explore. The values used in the calculations that follow are based on a ΛCDM cosmological model and values found by recent observations,[4] and they can be found in Appendix C. The values of the numerical constants are given in table [5–1].

Table 5–1. Linear Power Spectrum Parameters

Parameter	Value
α_1	2.34
α_2	3.89
α_3	16.1
α_4	5.46
α_5	6.71
β_1	0.785
β_2	0.05
β_3	0.95
β_4	0.169

The factor of k^n reflects the assumption that the initial power spectrum, (at decoupling) was a scale-free Guassian process and thus the initial spectrum was a simple power law. We typically define a dimensionless version of the power spectrum, given by, $\Delta = k^3 P(k)/2\pi^2$. Figure [5–1] shows a plot of the dimensionless linear power spectrum given above.

5.3 Nonlinear Power Spectrum

Here we present a model for the nonlinear power spectrum first constructed by Ma and Fry.[41] Before moving on, we note that there are other persciptions for describing the nonlinear power spectrum, the most notable due to Zhang et al.,[42] but we follow the Ma and Fry description.

As we noted in chapter 2, the two main ingredients in this construction are the halo mass function and the halo density profile. We use three different models for the halo density profile. The first two are the NFW and Moore profiles mentioned in chapter 2. Following the convention of Ma and Fry we write the profiles, given by equations [2.38] and [2.39], as

$$\frac{\rho(r)}{\rho_0} = \delta_a u(r/r_s), \tag{5.11}$$

where

$$\begin{aligned} u_{NFW}(x) &= \frac{1}{x(1+x)^2}, \\ u_M(x) &= \frac{1}{x^{1.5}(1+x^{1.5})}. \end{aligned} \tag{5.12}$$

A commonly introduced parameter, which we can use to write δ_a and r_s in terms of contained mass, is the concentration parameter, $c \equiv r_{200}/r_s$, where r_{200} is the radius within which the density is 200 times the mean. This radius can be written in terms of mass by, $M = 800\pi\rho_0 r_{200}^3/3$. Thus we can write the scale radius as

$$r_s = \frac{1}{c}\left(\frac{3M}{800\pi\rho_0}\right)^{1/3}. \tag{5.13}$$

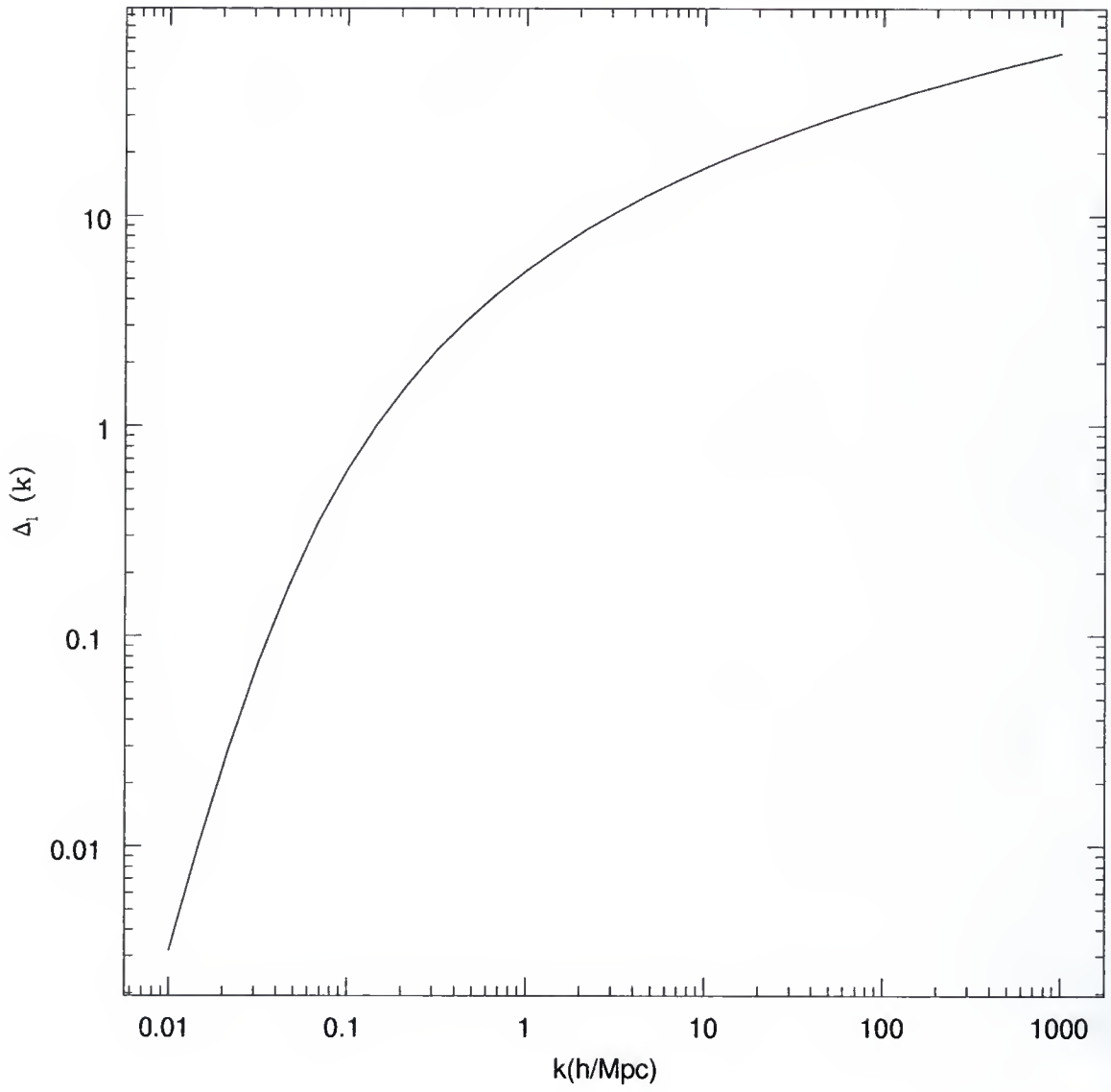

Figure 5–1. A plot of the dimensionless linear power spectrum, $\Delta_l = k^3 P(k)/2\pi^2$, for use in upcoming calculations. This represents the linear power spectrum today, $a = 1$.

The characteristic density, δ_a can also be written in terms of the concentration parameter, and is given by

$$\delta_{a,NFW} = \frac{200c^3}{3[\ln(1+c) - c/(1+c)]} \tag{5.14}$$

$$\delta_{a,M} = \frac{100c^3}{\ln(1+c^{3/2})}. \tag{5.15}$$

For the plots in this section we use a model for the concentration parameter based on N-body simulation data of Jing and Suto[43] given by

$$c = \begin{cases} 5\sigma(M) & : \quad (M/M_\odot) < 10^{14} \\ 9\sigma(M) & : \quad (M/M_\odot) > 10^{14} \end{cases} \tag{5.16}$$

$M_\odot = 1.989 \times 10^{30}$ kg is one solar mass. The third halo profile we will use is simply a combination of the previous two, as suggested by Jing and Suto.[43] Their simluations imply that the NFW profile is appropriate for cluster halos and the Moore profile is appropriate for galactic halos and the halos of small groups of galaxies. The cutoff between the mass of a cluster and that of a small group of galaxies is about $M/M_\odot = 10^{14}$, so the halo profile we refer to as "mixed" is Moore's for $(M/M_\odot) < 10^{14}$ and NFW's for $(M/M_\odot) > 10^{14}$.

The other important ingredient is the halo mass function. In this section, we will look at both the Press-Schechter mass function, given in equation [2.36] and the Sheth-Tormen mass function, given in equation [2.37]. The principle ingredient in each of the mass functions, as we saw in chapter 2, is σ, the standard deviation of the density contrast, which is a function of the radius of the sphere within which we are interested. Written in terms of the power spectrum, we have

$$\sigma^2(R) = \int_0^\infty \frac{4\pi k^2 dk}{(2\pi)^3} P(k)\tilde{W}^2(kR), \tag{5.17}$$

where $\tilde{W}$ is the Fourier transform of the top-hat window function,

$$\tilde{W}(x) = \frac{3(\sin x - x\cos x)}{x^3}. \tag{5.18}$$

The top hat window function has the value one within the radius R and zero everywhere else and is used to remove the need to worry about tiny fluctuations outside the region of interest. This can also be expressed as a function of enclosed mass using the relation, $M = 4\pi\rho_0 R^3/3$. Figure [5–2] shows a plot of σ vs. M for the input linear power spectrum given in equation [5.1].

Finally, we must put this together to make a power spectrum. We first note that we can write the spectrum as a sum of two distinct contributions, a one-halo term, from particles within the same halo, and a halo-halo term, from particles in two separate halos. From Fry and Ma,[41] we can write these terms as

$$P_{1h}(k) = \int dM \frac{dn}{dM}[r_s^3 \delta_a \tilde{u}(kr_s)]^2, \tag{5.19}$$

$$P_{2h}(k) = \left[\int dM \frac{dn}{dM} r_s^3 \delta_a \tilde{u}(kr_s) b(M)\right]^2 P_{lin}(k), \tag{5.20}$$

where $b(M)$ is a bias factor given by Jing (1998),[44] as

$$b(M) = \left(1 + \frac{\nu^2 - 1}{\delta_c}\right)\left(\frac{1}{2\nu^4} + 1\right)^{0.06-0.02n}, \tag{5.21}$$

where, as before, $\nu \equiv \delta_c/\sigma(M)$. This bias factor is introduced to account for the fact that dark matter halos cluster differently than the general mass density field. Clusters form at the peaks of the density fields, thus the bias accounts for the difference between the statistics of the the peaks and those of the general field. Figure [5–3] shows the behavior of $b(M)$. Its value is near unity for masses of the most common clusters. It becomes very large for very large mass clusters, but these are exceedingly rare occurances. (Which is, of course, the very reason the bias is so high.) The second factor in the bias parameter is a phenomenological addition to the original formula based on N-body results and the Sheth-Tormen perscription, and

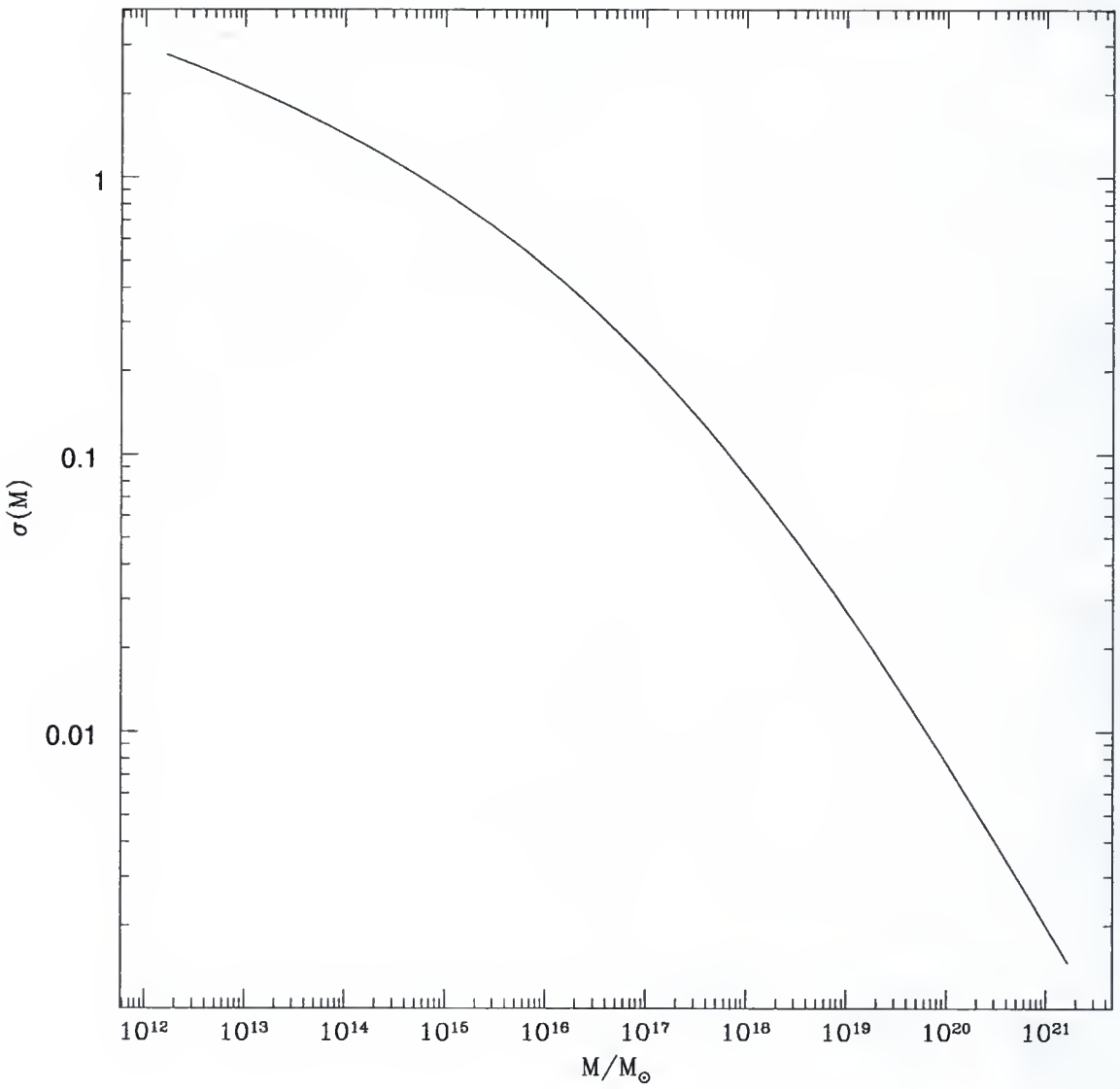

Figure 5–2. The linear rms fluctuation of the density contrast as a function of the mass within a top hat window. The mass is expressed in multiples of one solar mass ($1M_\odot = 1.989 \times 10^{30} kg$).

it is therefore neglected when the Press-Schechter formalism is used in the figures below.

Figures [5–4], [5–5], and [5–6] show the nonlinear power spectra for the NFW, Moore, and mixed halo profiles, respectively. In each plot the spectrum is plotted twice, once for the Press-Schechter mass function and once for the Sheth-Tormen mass function. Also, the linear power spectrum of figure [5–1] is included for comparison.

Figure [5–7] shows the nonlinear power spectrum, using the mixed halo profile and ST mass function, as we will henceforth, broken down into its one-halo and halo-halo contributions. Of course the halo-halo term dominates at small k, corresponding to large distances, or large masses, and the one-halo term dominates at large k, corresponding to small scales.

5.4 Angular Power Spectrum Machinery

Now that we have three dimensional power spectra for both linear and nonlinear regimes, we need to know how to use these to calculate the angular spectrum of CMB temperature fluctuations due to the kinetic SZ effect. This machinery is due to Ma and Fry.[45] First we remember from chapter 4 that the fractional temperature anisotropy due to the kSZ effect is

$$\frac{\Delta T}{T}(\hat{\boldsymbol{\gamma}}) = \int dl e^{-\tau} n_e \sigma_T \hat{\boldsymbol{\gamma}} \cdot (\boldsymbol{v}/c). \tag{5.22}$$

We write the electron density as $n_e = \bar{n}_e(1+\delta)$ where the mean electron density can be written, $\bar{n}_e = X_e \Omega_b \rho_c (1+z)^3/m_p$. Here X_e is the ionization fraction, m_p is the mass of the proton, and $\rho_c = 3H^2/8\pi G$ is the critical density for closure of the universe. We can then write the temperature fluctuation as

$$\frac{\Delta T}{T}(\hat{\boldsymbol{\gamma}}) = \int dl e^{-\tau} \bar{n}_e \sigma_T \hat{\boldsymbol{\gamma}} \cdot (\boldsymbol{q}/c), \tag{5.23}$$

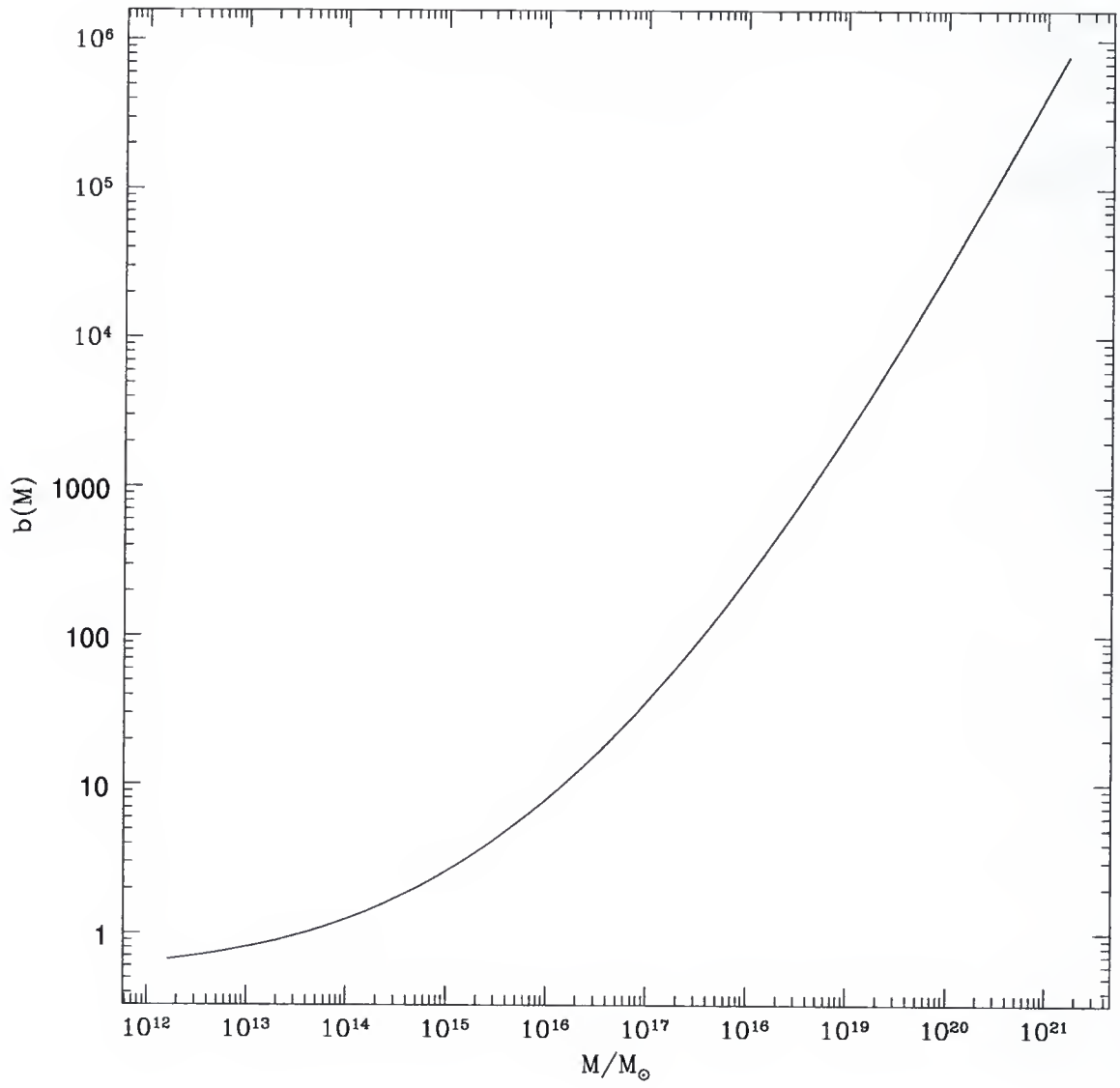

Figure 5–3. The bias parameter plotted as a function of halo mass. Most halos fall into the mass range $M/M_\odot = 10^{12} - 10^{15}$, where the bias is near unity.

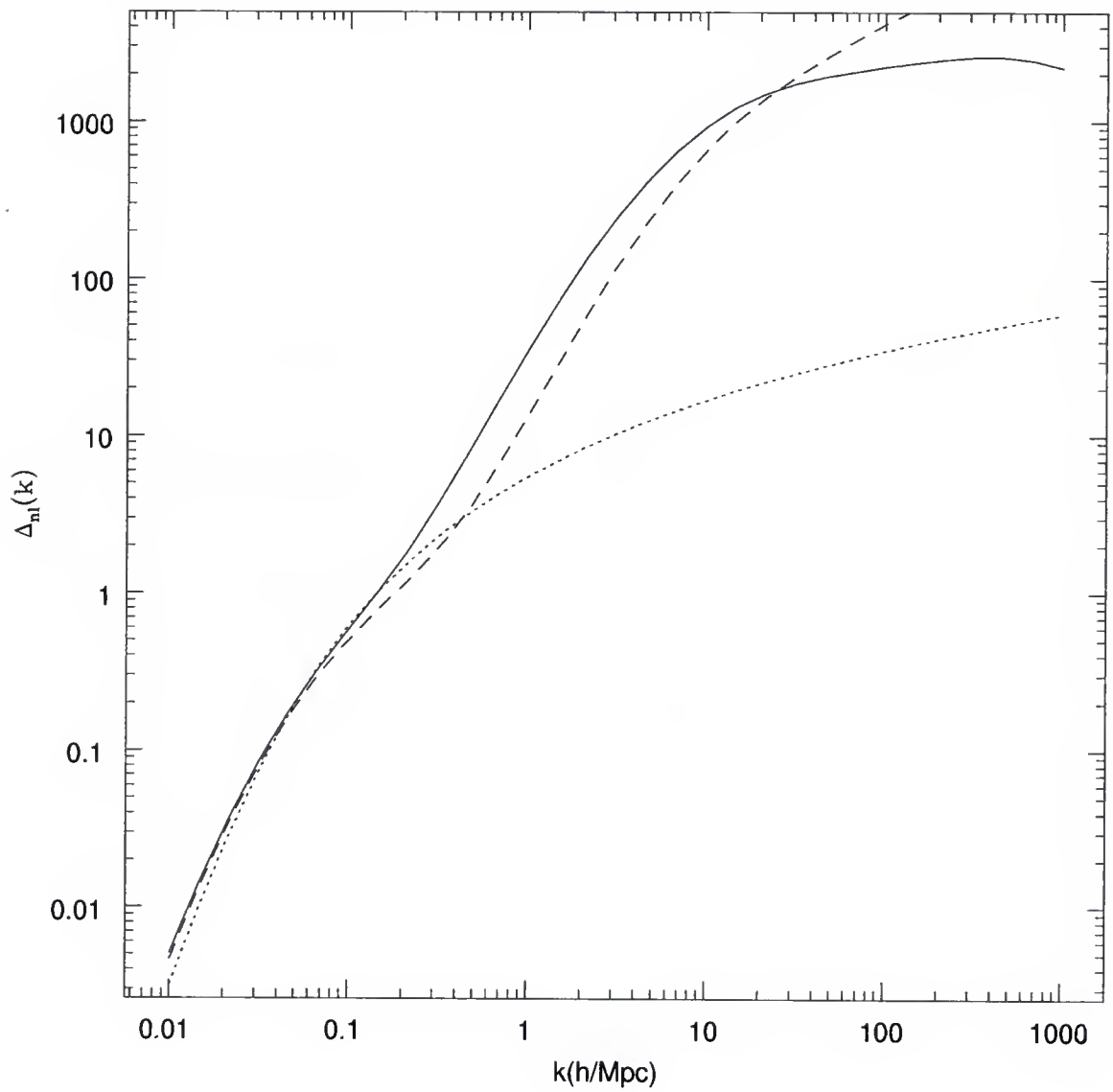

Figure 5–4. Dimensionless nonlinear power spectra using the NFW halo profile. The solid line uses the Press-Schechter mass function, the dashed line the Sheth-Tormen mass function. The dotted line shows the linear power spectrum for comparison.

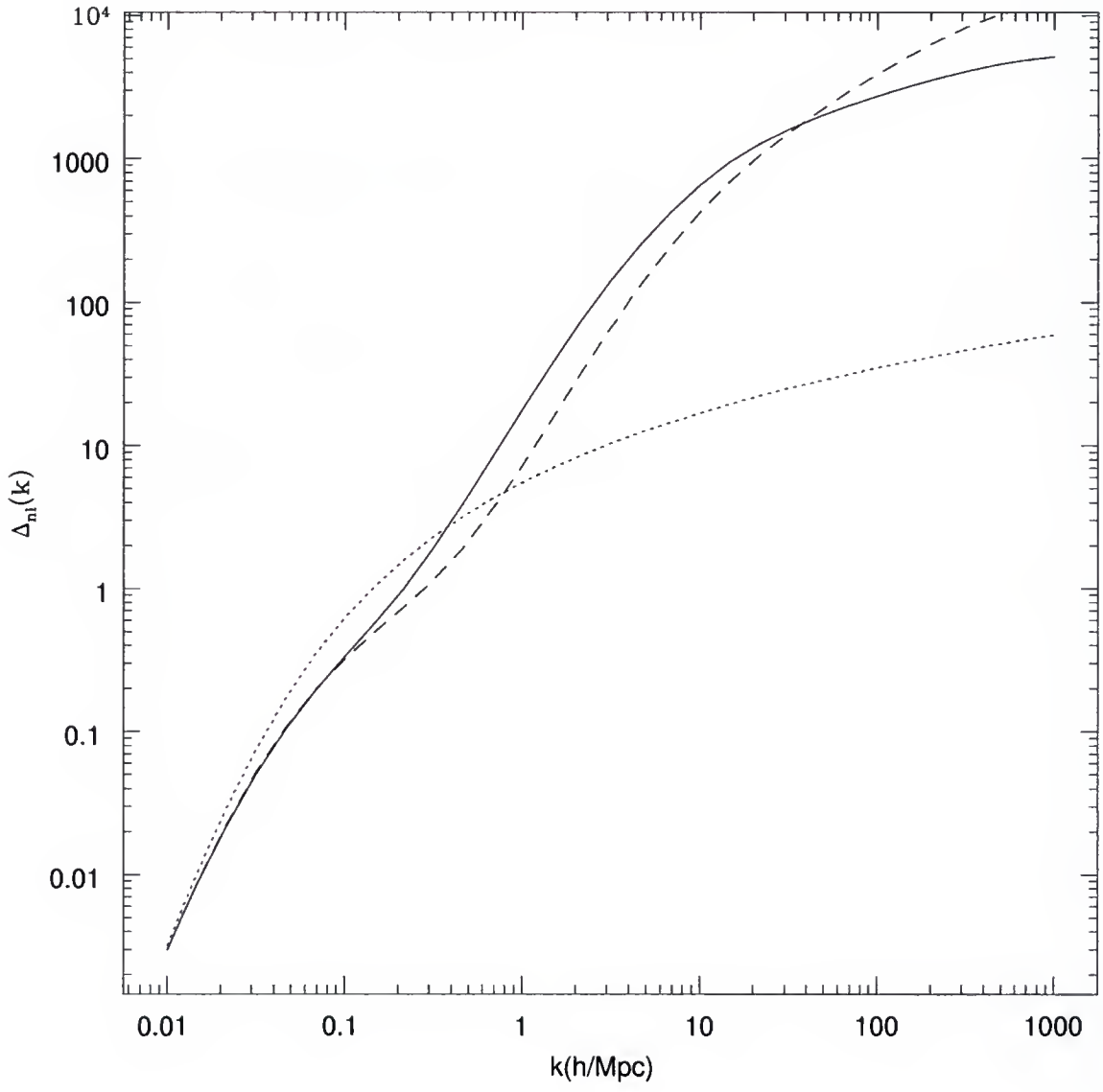

Figure 5–5. Dimensionless nonlinear power spectra using the Moore halo profile. The solid line uses the Press-Schechter mass function, the dashed line the Sheth-Tormen mass function. The dotted line shows the linear power spectrum for comparison.

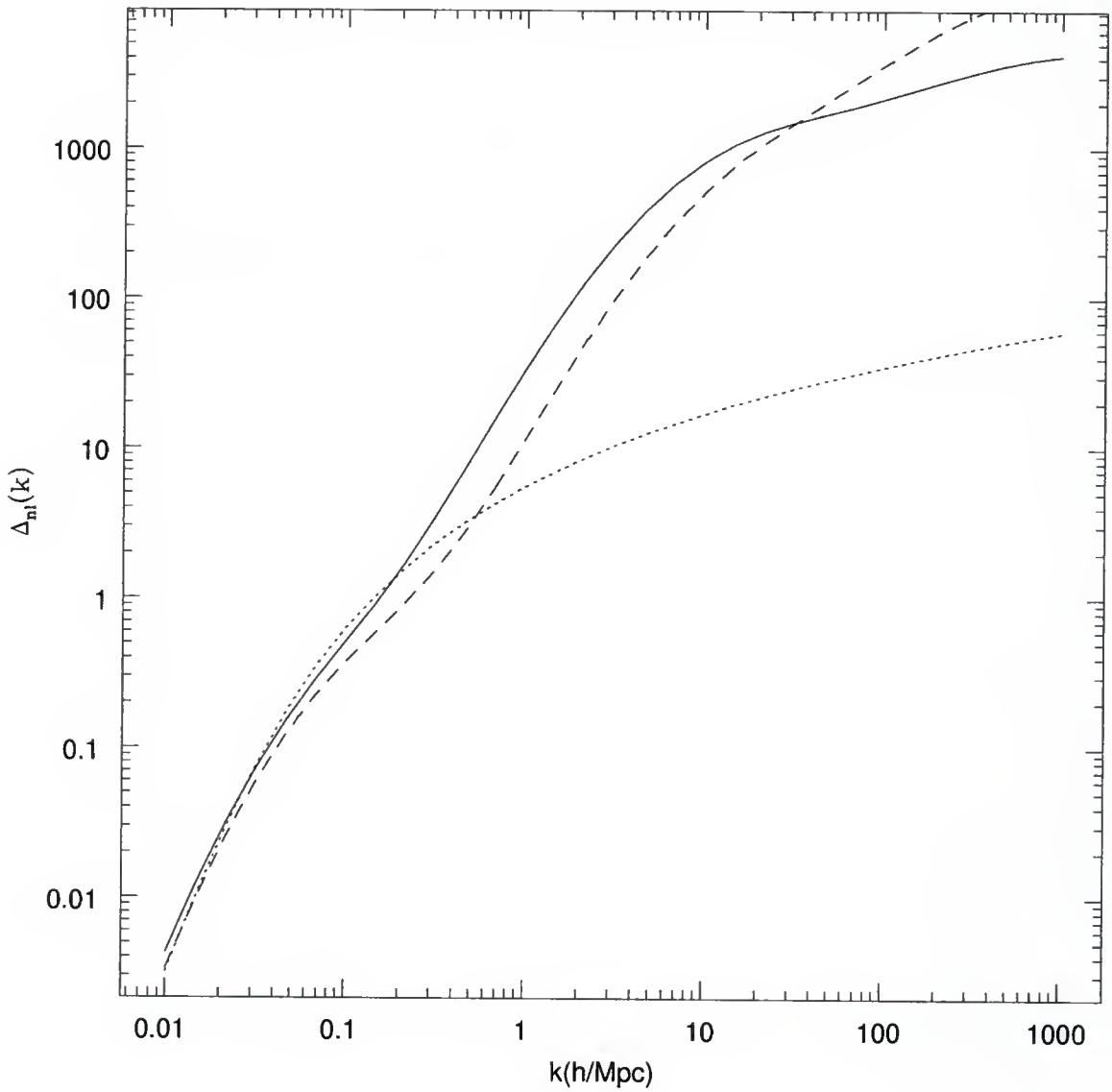

Figure 5–6. Dimensionless nonlinear power spectra using the NFW profile for large mass halos and the Moore profile for smaller mass halos. The solid line uses the Press-Schechter mass function, the dashed line uses the Sheth-Tormen function. The dotted line shows the linear power spectrum for comparison.

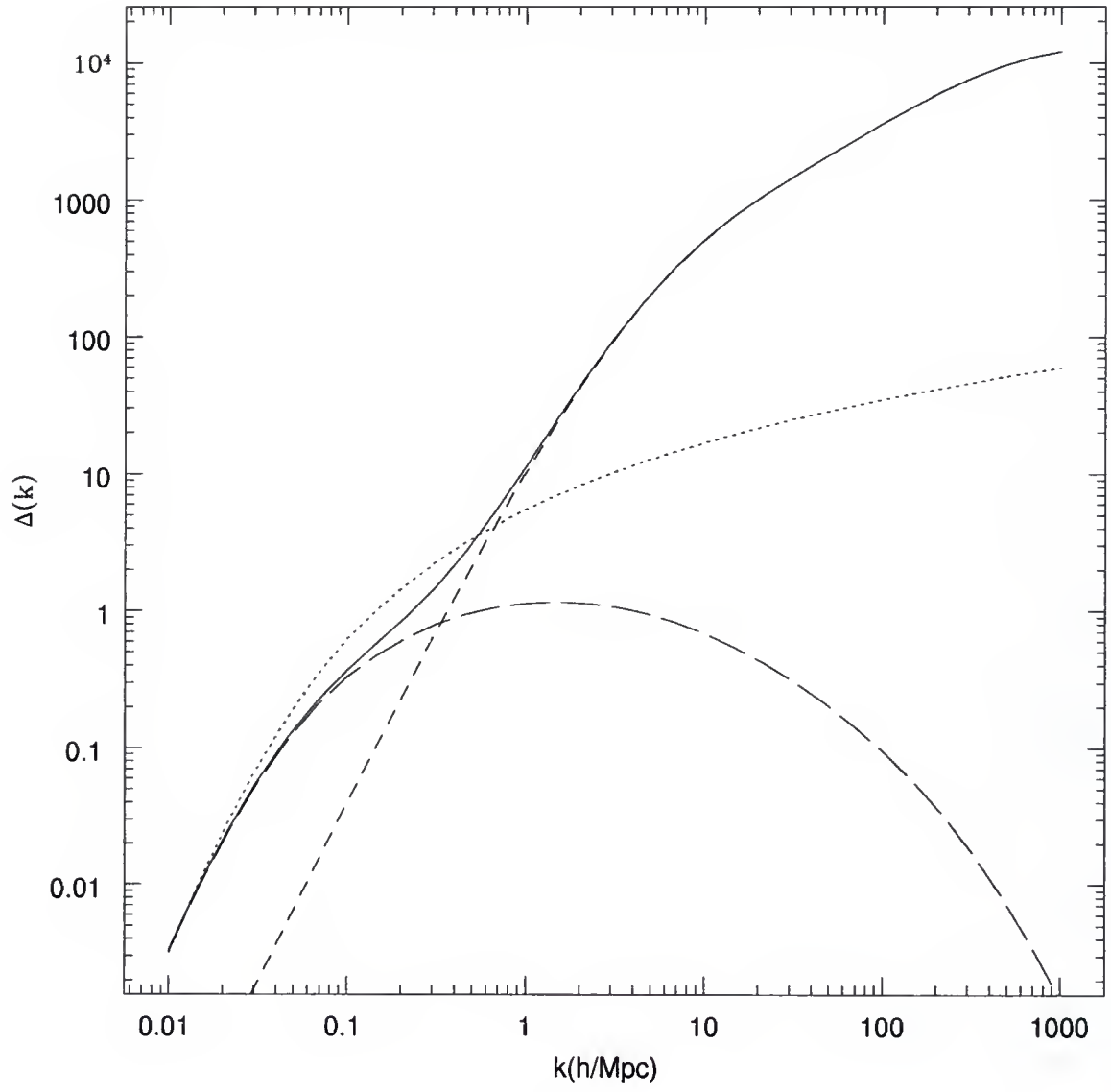

Figure 5–7. Dimensionless nonlinear power spectrum compared to linear version. The solid line is the nonlinear spectrum, using the mixed halo profile and the ST mass function. The dotted line represents the linear power spectrum. The short dashed line is the one-halo contribution to the nonlinear spectrum and the long dashed line is the contribution from the halo-halo term.

where $\boldsymbol{q} = \boldsymbol{v}(1+\delta)$ is the density weighted peculiar velocity, which has the Fourier transform

$$\tilde{\boldsymbol{q}} = \tilde{\boldsymbol{v}} + \int \frac{d^3k'}{(2\pi)^3}\tilde{\boldsymbol{v}}(\boldsymbol{k}')\tilde{\delta}(\boldsymbol{k}-\boldsymbol{k}'). \tag{5.24}$$

The angular two-point correlation function of the CMB temperature fluctuations is defined by equation [4.2]. The power spectrum, C_ℓ can be calculated as a projection of the three-dimensional power spectrum. This result is due to Kaiser,[46] and is simply the Fourier version of a projection originally due to Limber.[47]

For the density weighted velocity, Ma and Fry arrive at an expression for the angular power spectrum for the kSZ effect,

$$C_\ell = \frac{\bar{n}_{e,0}^2\sigma_T^2}{H_0^2}\int \frac{dx}{x^2}(1+z)^4 e^{-2\tau} P_{q\gamma}\left(\frac{\ell}{x}, z\right), \tag{5.25}$$

where $P_{q\gamma}$ is the power spectrum of $\boldsymbol{q}$ along the line of sight vector. The integration variable, x, is simply the co-moving distance to an object of redshift z. In a model with matter and cosmological constant, but no curvature, the relationship between x and z is given by

$$dx = \frac{dz}{H_0\sqrt{\Omega_m(1+z)^3+\Omega_\Lambda}}. \tag{5.26}$$

Figure [5–8] shows this distance plotted against $(1+z)$.

One very interesting aspect of a projection such as this is that modes parallel to the wave-vector $\boldsymbol{k}$ do not contribute, as the crests and troughs cancel each other when collapsed on top of one other.[48] (In actuality this cancellation is only approximate for long wavelengths, or large angular scales, but is very near total at the small angular scales we are interested in.) This implies that what we really need to find is $P_{q\perp} \approx 2P_{q\gamma}$. The factor of two comes from the fact that there are two independent directions perpendicular to $\boldsymbol{k}$. It also implies that there is no linear perturbative contribution to this effect, as in linear theory (without the rotational mode) $\tilde{\boldsymbol{q}} = \tilde{\boldsymbol{v}}(\boldsymbol{k}) \propto \hat{\boldsymbol{k}}$. It is the second order contribution, called the Ostiker-Vishniac (OV) effect, that we will look at in the next section.

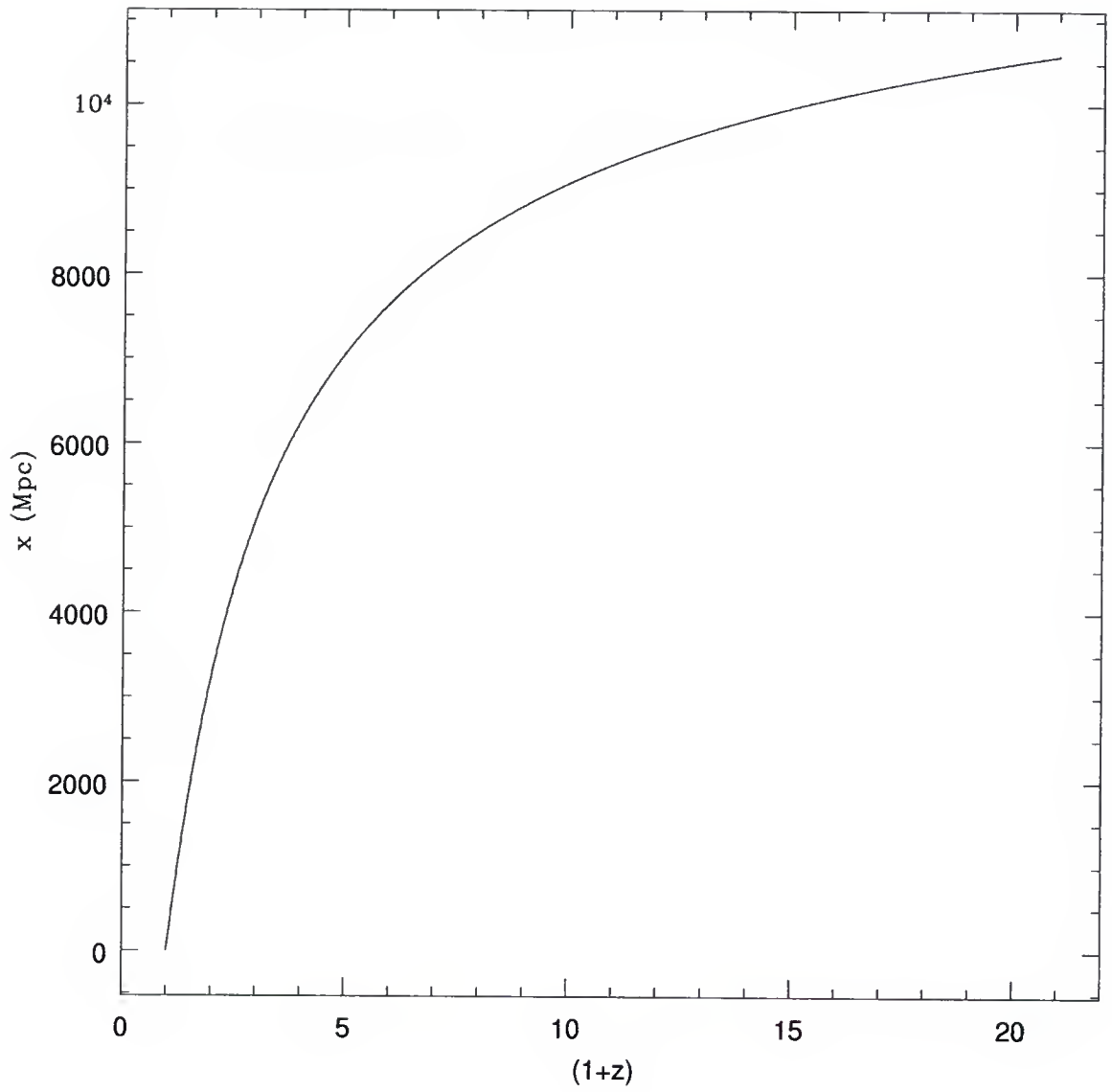

Figure 5–8. The relationship between redshift and distance to an object in a zero-curvature universe.

The result obtained by Ma and Fry for $P_{q\perp}$ is

$$\begin{aligned} P_{q\perp}(k) &= \int \frac{d^3k'}{(2\pi)^3}\Bigg[(1-\mu'^2)P_{\delta\delta}(|\boldsymbol{k}-\boldsymbol{k}'|)P_{vv}(k') \\ &\quad -\frac{(1-\mu'^2)k'}{|\boldsymbol{k}-\boldsymbol{k}'|}P_{\delta v}(|\boldsymbol{k}-\boldsymbol{k}'|)P_{\delta v}(k')\Bigg] \\ &\quad +\int \frac{d^3k'}{(2\pi)^3}\frac{d^3k''}{(2\pi)^3}\sqrt{1-\mu'^2}\sqrt{1-\mu''^2}\cos(\phi'-\phi'') \\ &\quad \times P_{\delta\delta vv}(\boldsymbol{k}-\boldsymbol{k}',-\boldsymbol{k}-\boldsymbol{k}'',\boldsymbol{k}',\boldsymbol{k}"), \end{aligned} \tag{5.27}$$

where $\mu' \equiv \hat{\boldsymbol{k}}\cdot\hat{\boldsymbol{k}}'$, $\mu'' \equiv \hat{\boldsymbol{k}}\cdot\hat{\boldsymbol{k}}"$, and the power spectra are defined by

$$\langle\tilde{\delta}(\boldsymbol{k}_a)\tilde{\delta}(\boldsymbol{k}_b)\rangle = (2\pi)^3\delta_D(\boldsymbol{k}_a+\boldsymbol{k}_b)P_{\delta\delta}(k_a) \tag{5.28}$$

$$\langle\tilde{\boldsymbol{v}}^i(\boldsymbol{k}_a)\tilde{\boldsymbol{v}}^j(\boldsymbol{k}_b)\rangle = (2\pi)^3\delta_D(\boldsymbol{k}_a+\boldsymbol{k}_b)\hat{\boldsymbol{k}}_a^i\hat{\boldsymbol{k}}_b^j P_{vv}(k_a) \tag{5.29}$$

$$\langle\tilde{\delta}(\boldsymbol{k}_a)\tilde{\boldsymbol{v}}^i(\boldsymbol{k}_b)\rangle = (2\pi)^3\delta_D(\boldsymbol{k}_a+\boldsymbol{k}_b)\hat{\boldsymbol{k}}_b^i P_{\delta v}(k_a) \tag{5.30}$$

$$\langle\tilde{\delta}(\boldsymbol{k}_a)\tilde{\delta}(\boldsymbol{k}_b)\tilde{\boldsymbol{v}}^i(\boldsymbol{k}_c)\tilde{\boldsymbol{v}}^j(\boldsymbol{k}_d)\rangle_c = (2\pi)^3\delta_D(\Sigma\boldsymbol{k}_\alpha)\hat{\boldsymbol{k}}_c^i\hat{\boldsymbol{k}}_d^j P_{\delta\delta vv}(\boldsymbol{k}_a,\boldsymbol{k}_b,\boldsymbol{k}_c,\boldsymbol{k}_d). \tag{5.31}$$

The subscript c in the last equation refers to the connected, or irreducible, moment. It is important to note that equations [5.29], [5.30], and [5.31] all depend on the assumption of $\boldsymbol{v} \propto \hat{\boldsymbol{k}}$, a condition we will later modify.

5.5 Ostriker-Vishniac Angular Power Spectrum

Calucluation of the angular power of CMB fluctuations in the quasi-linear regime, using second-order perturbation theory, produces the Ostiker-Vishniac spectrum.

In this regime, we use first order peculiar velocities and density perturbations to get the second order power spectra. Taking the Fourier transform of equation [2.22], we have

$$\tilde{\boldsymbol{v}}(\boldsymbol{k}) = \frac{\dot{a}f}{k}\tilde{\delta}\hat{k}, \tag{5.32}$$

so that

$$P_{vv}^{(1)} = \left(\frac{\dot{a}f}{k}\right)^2 P_{\delta\delta}^{(1)} \tag{5.33}$$

$$P_{\delta v}^{(1)} = \left(\frac{\dot{a}f}{k}\right) P_{\delta\delta}^{(1)}. \tag{5.34}$$

Here the superscripts refer to the linear order power spectra. Putting these in equation [5.27] we have

$$P_{q\perp}^{(2)}(k) = \dot{a}^2 f^2 \int \frac{d^3k'}{(2\pi)^3} P_{\delta\delta}^{(1)}(k') \frac{k(k - 2k'\mu')(1 - \mu'^2)}{k'^2(k^2 + k'^2 - 2kk'\mu')}. \tag{5.35}$$

Using the linear power spectrum given in section [5.2] and inserting this in equation [5.25] produces the spectrum plotted in figure [5–9]. In that figure we have integrated equation [5.25] from the present, $z = 0$, to several different possible redshifts of reionization, z_r. The OV spectrum, and the more refined nonlinear spectrum of the next section, are sensitive to z_r and thus observations of this effect will put good constraints on the ionization history of the universe.[42]

5.6 Nonlinear Angular Power Spectrum

In the nonlinear regime Ma and Fry suggest an approximate form for $P_{q\perp}$ which is valid for high k, the region of interest in a nonlinear analysis. They use

$$P_{q\perp}(k) = \frac{2}{3} \int \frac{d^3k'}{(2\pi)^3} P_{\delta\delta}(k) P_{vv}(k') = \frac{2}{3} \langle v^2 \rangle P_{\delta\delta}(k). \tag{5.36}$$

In figure [5–10] we plot the angular spectrum obtained from this form, using the one-halo power spectrum given in section [5.3]. We use a value of $\langle v^2 \rangle^{1/2} = 200\text{km/s}$ for the velocity dispersion. The key feature is that the OV spectrum underestimates the power at high ℓ's. In figure [5–11] we show the nonlinear kSZ spectrum as it compares to the expected spectrum from the thermal SZ effect. Note that for very high ℓ the kSZ effect is dominant.

One factor that is not taken into account in this model is the bias on small scales between baryonic matter and dark matter. The SZ effect is due to scattering

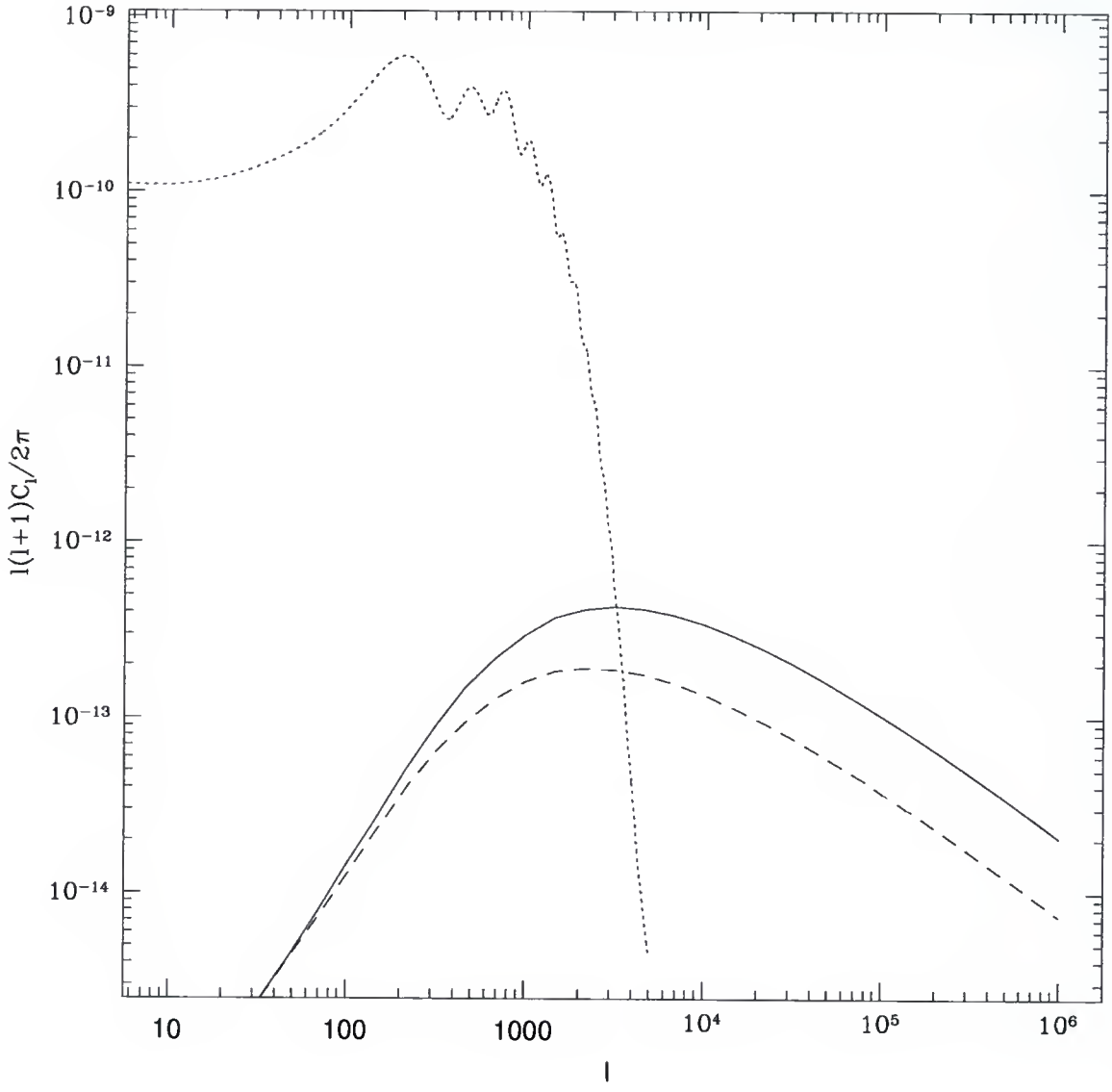

Figure 5–9. The second-order, perturbative Ostriker-Vishniac angular power spectrum. The solid line is the OV spectrum, calculated using a redshift of reionization of 20, the dashed line is the same with reionization redshift of 6, and, for reference, the dotted line is the primary anisotropy spectrum.

off free electrons which may (in fact, most certainly do) cluster differently than the surrounding dark matter halo. Ma and Fry do address this by also plotting the spectrum using a somewhat different profile function based on the modeling of hot gas in galaxies and clusters. This generally causes the power to be lower, but still greater than in the linear model.

Before moving on to the next chapter and the effect of rotational velocities on these power spectra, we note that we have not considered the possibility of non-uniform reionization in these calculations.[49,50] Santos et al. calculate that such "patchy" reionization would lead to significantly higher values for the temperature power spectrum, and in fact would likely swamp the effect of density perturbations. Since little is known about the actual inhomogeneity of reionization, we have chosen to assume it uniform for all that follows.

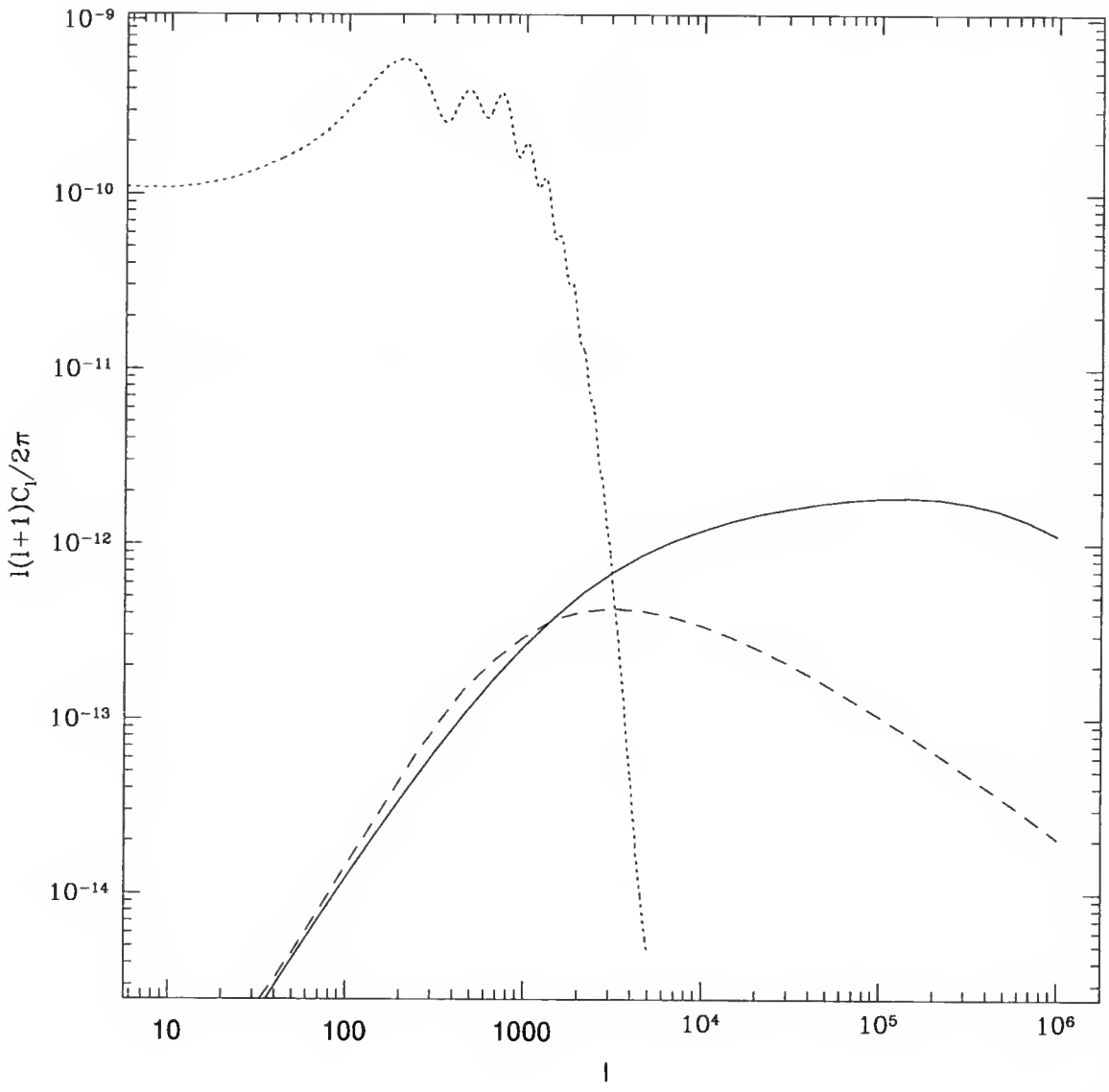

Figure 5–10. The nonlinear angular power spectrum, based on the model of Ma and Fry. (solid line) The dashed line is the OV spectrum and the dotted line is the primary anisotropy spectrum. Both the nonlinear and OV spectra are evaluated to $z_r = 20$.

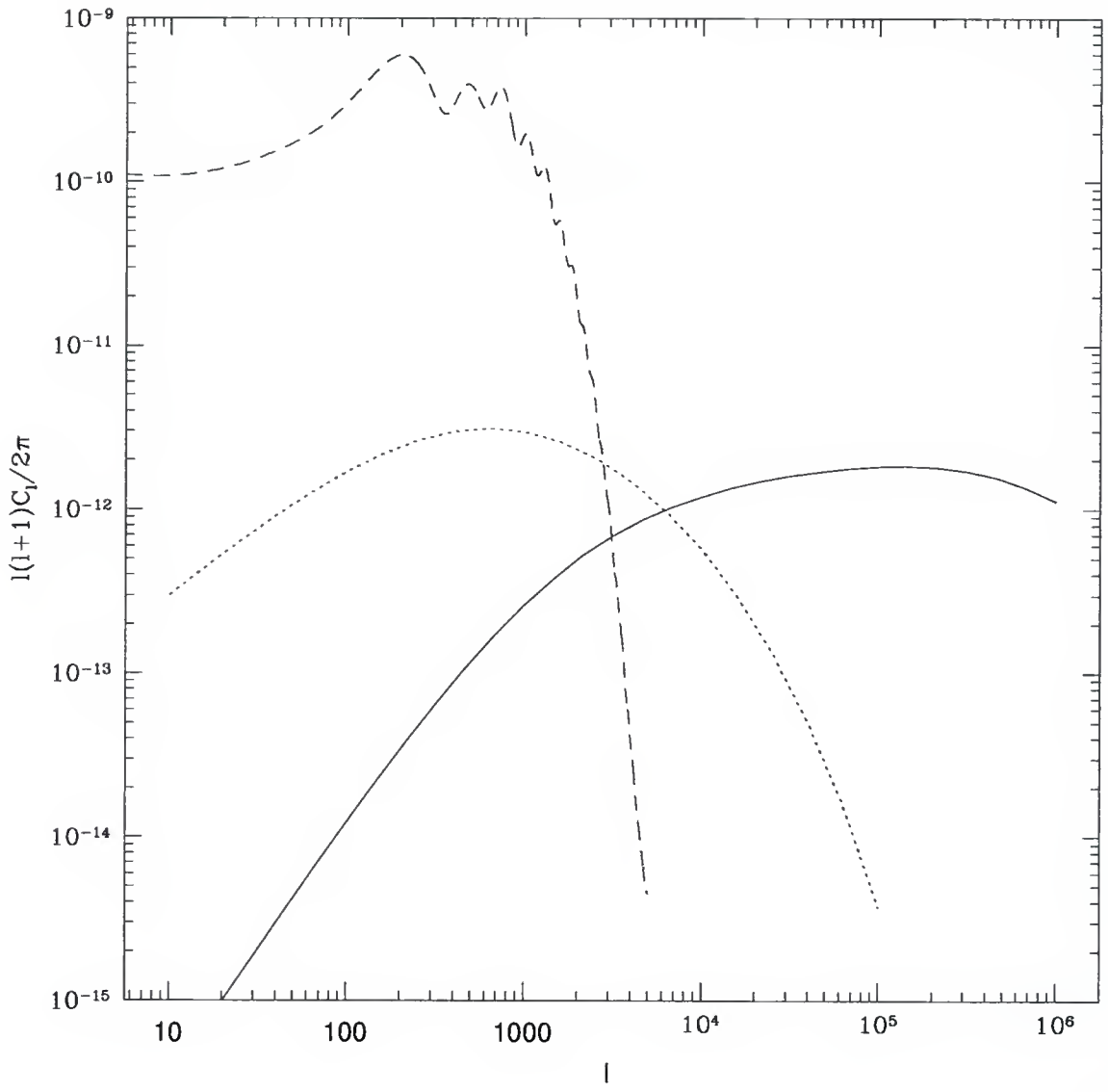

Figure 5–11. The solid line represents the nonlinear kSZ effect spectrum, while the dotted line represents the thermal SZ spectrum. (Plot for this spectrum was obtained from C.-P. Ma.) The dashed line is the primary spectrum.

CHAPTER 6
SZ POWER SPECTRUM INCLUDING ROTATIONAL MODES

6.1 Introduction

In this chapter we calculate the angular power spectrum of temperature anisotropies in the CMB due to the kinetic SZ effect with the inclusion of rotational velocity modes. Before beginning our discussion, we note that attempts have been made to include rotation in a calculation of the kinetic SZ effect. Cooray and Chen (2002)[51] calculate the angular power spectrum of the rotational kSZ effect using a perscription for the halo rotations based on work by Bullock and collaborators.[52] Importantly, however, this is angular momentum gained through events such as halo interactions and is different from the rotational modes that would be present due to conservation of initial angular momentum. Cooray and Chen find a power spectrum contribution several orders of magnitude smaller than the contributions seen in the previous chapter, and in fact they anticipate this result given the accuracy with which Ma and Fry's spectrum matches the N-body data. Of course these N-body simulations do not include the initial rotational modes, so they would not be expected to include the contribution we calculate here.

6.2 First-Order Results

We now include the effect of rotational velocities in the SZ angular spectrum by following the procedure, due to Ma and Fry, laid out in the last chapter. Remembering that we are looking for the power spectrum of the density weighted peculiar velocity, we had written the Fourier transform of this quantity as

$$\tilde{\boldsymbol{q}}(\boldsymbol{k}) = \tilde{\boldsymbol{v}}(\boldsymbol{k}) + \int \frac{d^3k'}{(2\pi)^3} \tilde{\boldsymbol{v}}(\boldsymbol{k}')\tilde{\delta}(\boldsymbol{k}-\boldsymbol{k}'). \tag{6.1}$$

We have previously ignored the contribution from the first term above, because for the growing mode $\boldsymbol{v} \propto \hat{\boldsymbol{k}}$. The first order rotational mode, however, is perpendicular to $\boldsymbol{k}$ so we have the simple relationship, $P_{q\perp} = (a_i/a)P^0_{v_\perp v_\perp}$, where $P^0_{v_\perp v_\perp}$ is the power spectrum of the rotational velocity at decoupling and a_i is the scale factor at decoupling.

We expect the rotational velocity dispersion at decoupling to be approximately equal to the longitudinal dispersion, which is approximately 20 km/s. This means

$$\int \frac{d^3k'}{(2\pi)^3} P^0_{v_\perp v_\perp}(k') = \langle (v_t^0)^2 \rangle \approx 400(\mathrm{km/s})^2. \tag{6.2}$$

We can determine the functional dependence of the initial spectrum on the wavenumber by considering the mass contained within the horizon at a time t.

$$M_H = \rho_0 r_H^3 = \rho_0 (ct_H)^3 = (6\pi G \rho_0 t_H^2)(\frac{c^3 t_H}{6\pi G}). \tag{6.3}$$

We write it in this manner because the solution to equation [2.9], for zero curvature, is $6\pi G\rho_0 t^2 = 1$. This means that $t_H \propto M_H \propto k^{-3}$. Finally, we note that

$$\Delta(k) = k^3 P(k) \propto \left(\frac{a_H}{a}\right)^2 \propto \left(\frac{t_H}{t}\right)^{4/3} \propto (k^{-3})^{4/3} = k^{-4}, \tag{6.4}$$

which means that $P^0_{v_\perp v_\perp}(k) = Ak^{-7}$. We see that we need a low k cutoff for the integral above to converge. We choose a cutoff of $k = 10^{-5}(h/\mathrm{Mpc})$. This gives us the value $A = 3 \times 10^{-16} h(\mathrm{Mpc})^{-4}(\mathrm{km/s})^2$. Inserting this spectrum into equation [5.25] gives us the angular spectrum of CMB temperature fluctuations. The result is given in figure [6–1]. As expected, the contribution is many orders of magnitude below other contributions because, to linear order, the rotational mode decays with the expansion of the universe.

6.3 Non-Linear Results

Seeing that the first order rotational contribution is negligible, we look to the second term in equation [6.1].

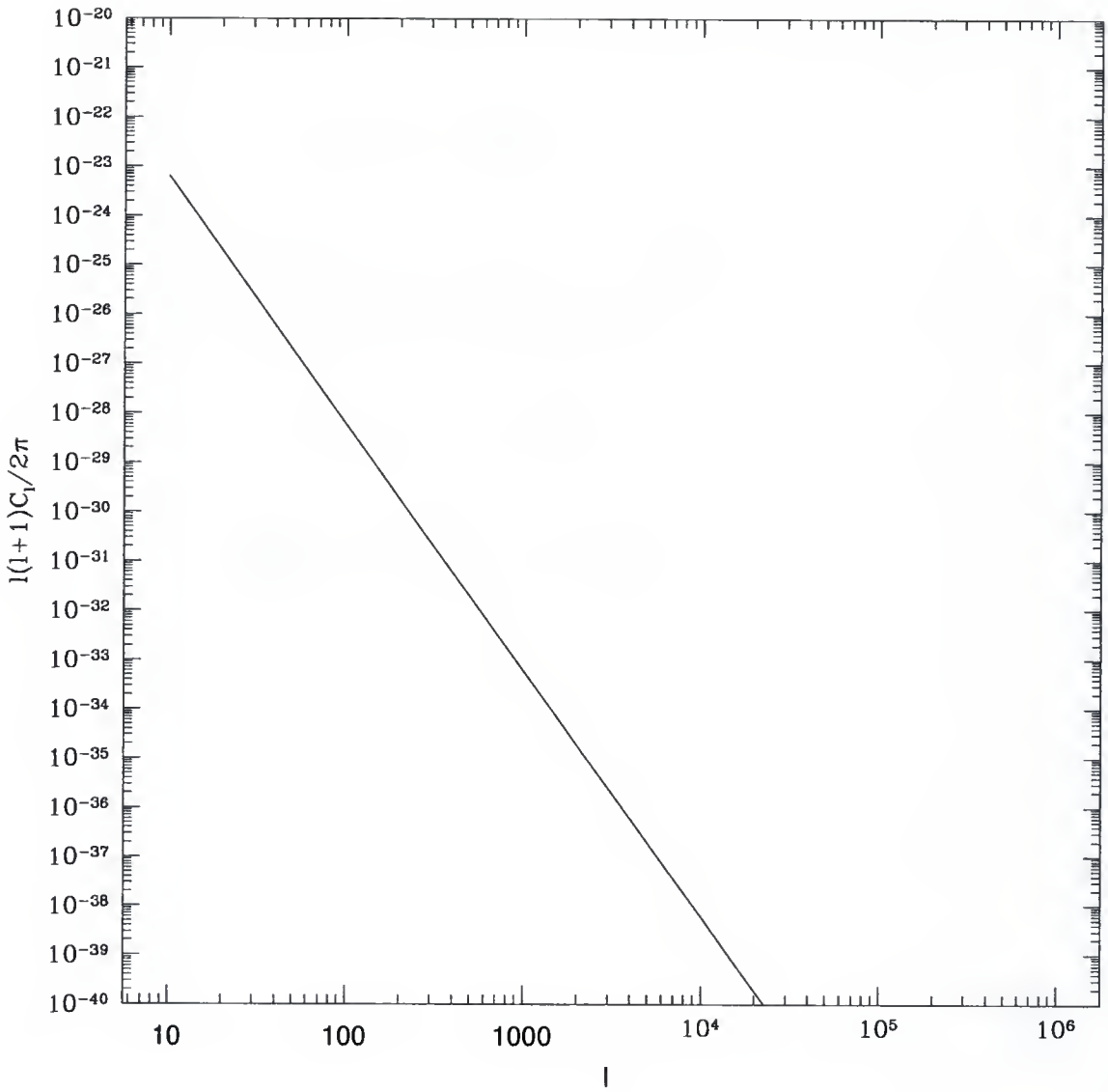

Figure 6–1. Angular power spectrum of temperature variation on the CMB due to the first order rotational velocities.

Before we do so we need a way to describe the rotational velocity field. We find this by imposing angular momentum conservation on a collapsing object. As we saw previously, collapsed objects have density profiles as given in equations [5.11] and [5.12]. We consider the mass contained within an initial co-moving radius x, in a region with a nearly homogeneous density. (The "nearly" indicating the slight overdensity which will lead the region to collapse.) We denote the final co-moving radial coordinate y and write the mass as

$$M = \frac{4\pi}{3}\rho_{0,i}a_i^3x^3 = \rho_0 a^3\left[\frac{4\pi}{3}y^3 + \int_0^y dy' 4\pi y'^2 \delta_a u(y/y_s)\right], \tag{6.5}$$

which is just expressing the fact that we are superimposing the halos onto a uniform background. This will allow us to define the mapping from x to y for a given $u(y/y_s)$. For the Moore profile ($u(x) = 1/[x^{1.5}(1+x^{1.5})]$) we find

$$\frac{4\pi}{3}\rho_{0,i}a_i^3x^3 = \rho_0 a^3\left[\frac{4\pi}{3}y^3 + y_s^3\frac{8\pi}{3}\delta_a \ln\left[1+(y/y_s)^{3/2}\right]\right], \tag{6.6}$$

but since $\rho_0 \propto a^{-3}$, $\rho_{0,i}a_i^3 = \rho_0 a^3$ and we have

$$x^3 = y^3 + 2\delta_a y_s^3 \ln\left[1+(y/y_s)^{3/2}\right] \tag{6.7}$$

As our interest is in the small y regime, we find the asymptotic behavior at low y to be

$$x^3 = 2\delta_a(yy_s)^{3/2}. \tag{6.8}$$

Figure [6–2] shows this behavior.

For the NFW profile ($u(x) = 1/[x(1+x)^2]$) we find

$$x^3 = y^3 + 3\delta_a y_s^3\left[\frac{1-(y/y_s)}{1+(y/y_s)} + \ln[1+(y/y_s)]\right], \tag{6.9}$$

which asymptotes to

$$x^3 = 3\delta_a y_s^3 \tag{6.10}$$

for low y. (See figure [6–3].)

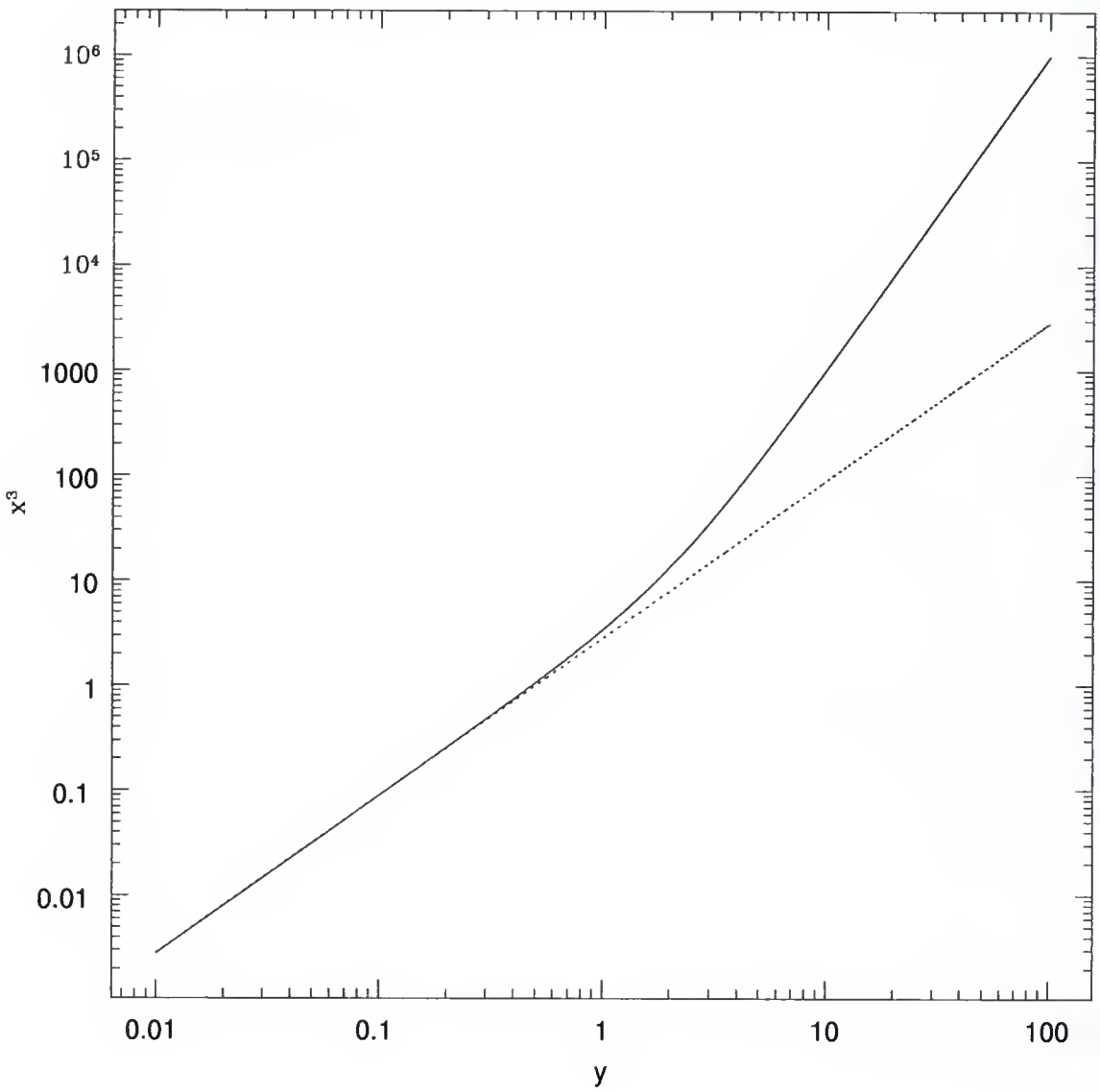

Figure 6–2. Mapping of the initial co-moving radius, x, to final co-moving radius, y for a Moore profile cluster. The values $\delta_a = 1/2$ and $y_s = 2$ have been used. The dotted line represents the limiting behavior at low y.

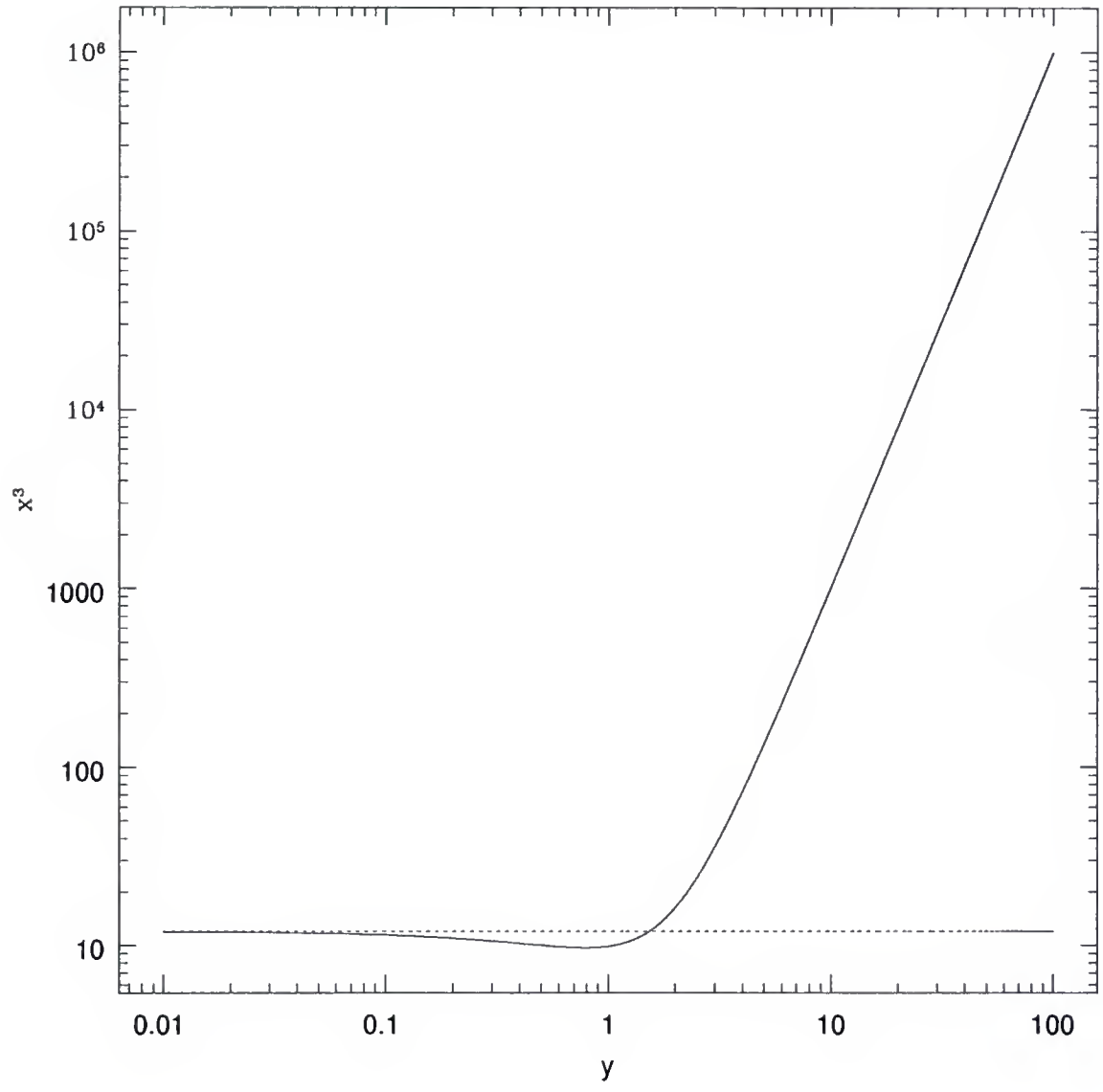

Figure 6–3. Mapping of the initial co-moving radius, x, to final co-moving radius, y for a NFW profile cluster. The values $\delta_a = 1/2$ and $y_s = 2$ have been used. The dotted line represents the limiting behavior at low y.

We can express conservation of angular momentum as

$$\boldsymbol{v}_t(y) = \boldsymbol{v}_{0,t}\frac{a_i x}{a y} \equiv \frac{a_i}{a}\boldsymbol{v}_{0,t}\lambda(y), \tag{6.11}$$

where

$$\lambda_M(y) = \left(1 + 2\delta_a (y_s/y)^3 \ln\left[1 + (y/y_s)^{3/2}\right]\right)^{1/3}, \tag{6.12}$$

$$\lambda_{NFW}(y) = \left(1 + 3\delta_a (y_s/y)^3 \left[\frac{1-(y/y_s)}{1+(y/y_s)} + \ln[1+(y/y_s)]\right]\right)^{1/3}. \tag{6.13}$$

Now, returning to the definition, $\boldsymbol{q} = (1+\delta)\boldsymbol{v}$, we see that in the nonlinear regime, where the second term above will be dominant, we have, for the rotational velocity mode, $\boldsymbol{q} = \delta\boldsymbol{v}_t = (a_i/a)\delta\lambda\boldsymbol{v}_{0,t}$. We then make the definition $\delta' = (a_i/a)\delta\lambda$ and write $\boldsymbol{q} = \delta'\boldsymbol{v}_{0,t}$. This may, at first, seem like an odd thing to do, but we will find that we just absorb the collapse factor into the halo density profile to produce a new profile, making the calculation very similar to that in the last chapter.

The second moment of the components of $\tilde{\boldsymbol{q}}$ obey

$$\begin{aligned}
\langle \tilde{\boldsymbol{q}}^i(\boldsymbol{k}_1)\tilde{\boldsymbol{q}}^j(\boldsymbol{k}_2)\rangle &= (2\pi)^3\delta_D(\boldsymbol{k}_1+\boldsymbol{k}_2)\Big[\langle \tilde{\boldsymbol{v}}_1^i\tilde{\boldsymbol{v}}_2^j\rangle \\
&\quad + \int \frac{d^3k'}{(2\pi)^3}\frac{d^3k''}{(2\pi)^3}\langle \tilde{\boldsymbol{v}}^i(\boldsymbol{k}')\tilde{\delta}(\boldsymbol{k}_1-\boldsymbol{k}')\tilde{\boldsymbol{v}}^j(\boldsymbol{k}'')\tilde{\delta}(\boldsymbol{k}_2-\boldsymbol{k}'')\rangle\Big] \\
&= (2\pi)^3\delta_D(\boldsymbol{k}_1+\boldsymbol{k}_2)\Big[\langle \tilde{\boldsymbol{v}}_1^i\tilde{\boldsymbol{v}}_2^j\rangle \\
&\quad + \int \frac{d^3k'}{(2\pi)^3}\frac{d^3k''}{(2\pi)^3}\Big[\langle \tilde{\boldsymbol{v}}^i(\boldsymbol{k}')\tilde{\delta}(\boldsymbol{k}_1-\boldsymbol{k}')\rangle\langle \tilde{\boldsymbol{v}}^j(\boldsymbol{k}'')\tilde{\delta}(\boldsymbol{k}_2-\boldsymbol{k}'')\rangle \\
&\quad + \langle \tilde{\boldsymbol{v}}^i(\boldsymbol{k}')\tilde{\delta}(\boldsymbol{k}_1-\boldsymbol{k}'')\rangle\langle \tilde{\boldsymbol{v}}^j(\boldsymbol{k}'')\tilde{\delta}(\boldsymbol{k}_2-\boldsymbol{k}')\rangle \\
&\quad + \langle \tilde{\boldsymbol{v}}^i(\boldsymbol{k}')\tilde{\boldsymbol{v}}^j(\boldsymbol{k}'')\rangle\langle \tilde{\delta}(\boldsymbol{k}_1-\boldsymbol{k}')\tilde{\delta}(\boldsymbol{k}_2-\boldsymbol{k}'')\rangle + \langle\rangle_c\Big]\Big].
\end{aligned} \tag{6.14}$$

In the nonlinear regime behavior is dominated by the terms of higher order, so we will neglect the first term above, which is the lowest order term. The second term above is zero by our assumption of isotropy. The last term is the irreducible fourth order term. If we had kept the collapse factor with the rotational velocity, we would expect this irreducible term to be the term of interest, as then the velocity would

couple strongly to the density. However, as we have associated the collapse with the density, we now expect the important term to be similar to the important term for the longitudinal mode. Thus the irreducible fouth moment will vanish, just as in Ma and Fry, and we drop it.

We now write the transformed velocity as

$$\tilde{\boldsymbol{v}}(\boldsymbol{k}) = \tilde{\boldsymbol{v}}_{\parallel}(\boldsymbol{k}) + \tilde{\boldsymbol{v}}_{\perp}(\boldsymbol{k}) = \hat{\boldsymbol{k}} v_{\parallel}(k) + \hat{\boldsymbol{\varepsilon}} v_{\perp}(k), \tag{6.15}$$

where $\hat{\boldsymbol{\varepsilon}}$ represents a unit vector perpendicular to $\boldsymbol{k}$. This term could be written,

$$\hat{\boldsymbol{\varepsilon}}^i = \frac{(\delta_{ij} - \hat{\boldsymbol{k}}^i \hat{\boldsymbol{k}}^j)\tilde{\boldsymbol{v}}^j}{v_{\perp}} \tag{6.16}$$

Using this velocity we have the general definitions,

$$\begin{aligned}
\langle \tilde{\delta}(\boldsymbol{k}_1)\tilde{\delta}(\boldsymbol{k}_2)\rangle &= (2\pi)^3 \delta_D(\boldsymbol{k}_1 + \boldsymbol{k}_2) P_{\delta\delta}(k_1) && (6.17)\\
\langle \tilde{\boldsymbol{v}}^i(\boldsymbol{k}_1)\tilde{\boldsymbol{v}}^j(\boldsymbol{k}_2)\rangle &= \langle [\tilde{\boldsymbol{v}}^i_{\parallel}(\boldsymbol{k}_1) + \tilde{\boldsymbol{v}}^i_{\perp}(\boldsymbol{k}_1)][\tilde{\boldsymbol{v}}^j_{\parallel}(\boldsymbol{k}_2) + \tilde{\boldsymbol{v}}^j_{\perp}(\boldsymbol{k}_2)]\rangle \\
&= \langle \tilde{\boldsymbol{v}}^i_{\parallel}(\boldsymbol{k}_1)\tilde{\boldsymbol{v}}^j_{\parallel}(\boldsymbol{k}_2)\rangle + \langle \tilde{\boldsymbol{v}}^i_{\perp}(\boldsymbol{k}_1)\tilde{\boldsymbol{v}}^j_{\perp}(\boldsymbol{k}_2)\rangle \\
&= (2\pi)^3 \delta_D(\boldsymbol{k}_1 + \boldsymbol{k}_2)[\hat{\boldsymbol{k}}^i_1 \hat{\boldsymbol{k}}^j_2 P_{v_{\parallel} v_{\parallel}}(k_1) + \hat{\boldsymbol{\varepsilon}}^i_1 \hat{\boldsymbol{\varepsilon}}^j_2 P_{v_{\perp} v_{\perp}}(k_1)] && (6.18)\\
\langle \tilde{\delta}(\boldsymbol{k}_1)\tilde{\boldsymbol{v}}^i(\boldsymbol{k}_2)\rangle &= \langle \tilde{\delta}(\boldsymbol{k}_1)\tilde{\boldsymbol{v}}^i_{\parallel}(\boldsymbol{k}_2)\rangle + \langle \tilde{\delta}(\boldsymbol{k}_1)\tilde{\boldsymbol{v}}^i_{\perp}(\boldsymbol{k}_2)\rangle \\
&= (2\pi)^3 \delta_d(\boldsymbol{k}_1 + \boldsymbol{k}_2)[\hat{\boldsymbol{k}}^i_2 P_{\delta v_{\parallel}}(k_1) + \hat{\boldsymbol{\varepsilon}}^i_2 P_{\delta v_{\perp}}(k_1)], && (6.19)
\end{aligned}$$

The cross terms in the second expression vanish because the components are independent. The last term in equation [6.19] is zero by isotropy.

Now, remembering that wherever we have a δ associated with a rotational velocity, we will replace it with a δ', and we will replace the velocity with $\boldsymbol{v}_{0,t}$, we

have

$$
\begin{aligned}
P^{ij}_{qq}(k) &= \int \frac{d^3k'}{(2\pi)^3}\frac{d^3k''}{(2\pi)^3} \\
&\times\big[(2\pi)^3\delta_D(\boldsymbol{k}-\boldsymbol{k}'-\boldsymbol{k}'')[\hat{\boldsymbol{k}}'^i\hat{\boldsymbol{k}}'^j P_{v_\parallel v_\parallel}(k')P_{\delta\delta}(k'') + \hat{\boldsymbol{\varepsilon}}'^i\hat{\boldsymbol{\varepsilon}}''^j P^0_{v_\perp v_\perp}(k')P_{\delta'\delta'}(k'') \\
&+\hat{\boldsymbol{k}}'^i\hat{\boldsymbol{k}}''^j P_{\delta v_\parallel}(k')P_{\delta v_\parallel}(k'') + \hat{\boldsymbol{k}}'^i\hat{\boldsymbol{\varepsilon}}''^j P_{\delta v_\parallel}(k')P_{\delta' v_\perp}(k'') \\
&+\hat{\boldsymbol{\varepsilon}}'^i\hat{\boldsymbol{k}}''^j P_{\delta' v_{\perp,0}}(k')P_{\delta v_\parallel}(k'') + \hat{\boldsymbol{\varepsilon}}'^i\hat{\boldsymbol{\varepsilon}}''^j P_{\delta' v_{\perp,0}}(k')P_{\delta' v_{\perp,0}}(k'')]\big]. \qquad (6.20)
\end{aligned}
$$

Note that $\hat{\boldsymbol{\varepsilon}}', \hat{\boldsymbol{\varepsilon}}''$ refer to unit vectors perpendicular to $\hat{\boldsymbol{k}}'$ and $\hat{\boldsymbol{k}}''$, respectively. We now calculate the quantity of interest using

$$P_{q\perp}(k) = 2\hat{\boldsymbol{\gamma}}^i\hat{\boldsymbol{\gamma}}^j P^{ij}_{qq}(k). \qquad (6.21)$$

The inner products of interest are

$$
\begin{aligned}
\hat{\boldsymbol{\gamma}}^i\hat{\boldsymbol{\gamma}}^j\hat{\boldsymbol{k}}'^i\hat{\boldsymbol{k}}'^j &= (1-\mu'^2)\nu'^2 && (6.22)\\
\hat{\boldsymbol{\gamma}}^i\hat{\boldsymbol{\gamma}}^j\hat{\boldsymbol{k}}'^i\hat{\boldsymbol{\varepsilon}}'^j &= (\mu'(1-\mu'^2)^{1/2})\nu'^2 && (6.23)\\
\hat{\boldsymbol{\gamma}}^i\hat{\boldsymbol{\gamma}}^j\hat{\boldsymbol{\varepsilon}}'^i\hat{\boldsymbol{\varepsilon}}'^j &= \mu'^2\nu'^2 && (6.24)\\
\hat{\boldsymbol{\gamma}}^i\hat{\boldsymbol{\gamma}}^j\hat{\boldsymbol{k}}'^i\hat{\boldsymbol{k}}''^j &= (1-\mu'^2)^{1/2}\nu'\hat{\boldsymbol{\gamma}}\cdot\hat{\boldsymbol{k}}'' && (6.25)\\
\hat{\boldsymbol{\gamma}}^i\hat{\boldsymbol{\gamma}}^j\hat{\boldsymbol{k}}'^i\hat{\boldsymbol{\varepsilon}}''^j &= (1-\mu'^2)^{1/2}\hat{\boldsymbol{\gamma}}\cdot\hat{\boldsymbol{\varepsilon}}'' && (6.26)\\
\hat{\boldsymbol{\gamma}}^i\hat{\boldsymbol{\gamma}}^j\hat{\boldsymbol{\varepsilon}}'^i\hat{\boldsymbol{k}}''^j &= \mu'\nu'\hat{\boldsymbol{\gamma}}\cdot\hat{\boldsymbol{k}}'' && (6.27)\\
\hat{\boldsymbol{\gamma}}^i\hat{\boldsymbol{\gamma}}^j\hat{\boldsymbol{\varepsilon}}'^i\hat{\boldsymbol{\varepsilon}}''^j &= \mu'\nu'\hat{\boldsymbol{\gamma}}\cdot\hat{\boldsymbol{\varepsilon}}'', && (6.28)
\end{aligned}
$$

where μ' is defined as before and $\nu' \equiv \cos(\phi')$. In equations [6.25] and [6.27] we have the expression, $\hat{\boldsymbol{\gamma}}\cdot\hat{\boldsymbol{k}}''$, which we evaluate by noting that in the next step we will integrate over the delta function in equation [6.20], and thus replace $\hat{\boldsymbol{k}}''$ with $\hat{\boldsymbol{k}}-\hat{\boldsymbol{k}}'$. Since $\hat{\boldsymbol{k}}'' \to (\boldsymbol{k}-\boldsymbol{k}')/|\boldsymbol{k}-\boldsymbol{k}'|$ and $\hat{\boldsymbol{\gamma}}\cdot\hat{\boldsymbol{k}} = 0$, we end up with

$$
\begin{aligned}
\hat{\boldsymbol{\gamma}}^i\hat{\boldsymbol{\gamma}}^j\hat{\boldsymbol{k}}'^i\hat{\boldsymbol{k}}''^j &= \frac{(1-\mu'^2)k'\nu'}{|\boldsymbol{k}-\boldsymbol{k}'|} && (6.29)\\
\hat{\boldsymbol{\gamma}}^i\hat{\boldsymbol{\gamma}}^j\hat{\boldsymbol{\varepsilon}}'^i\hat{\boldsymbol{k}}''^j &= \frac{\mu'(1-\mu'^2)^{1/2}\nu'k'}{|\boldsymbol{k}-\boldsymbol{k}'|}. && (6.30)
\end{aligned}
$$

Additionally, in equations [6.26] and [6.28], $\hat{\boldsymbol{\gamma}}\cdot\hat{\boldsymbol{\varepsilon}}''$ becomes $\hat{\boldsymbol{\gamma}}\cdot\hat{\boldsymbol{\varepsilon}}'''$ where $\hat{\boldsymbol{\varepsilon}}'''$ is a unit vector perpendicular to $\boldsymbol{k}-\boldsymbol{k}'$.

Putting these in, we have

$$\begin{aligned}
P_{q\perp}(k) &= \int \frac{d^3k'}{(2\pi)^3}\big[(1-\mu'^2)\nu'^2 P_{v_\parallel v_\parallel}(k')P_{\delta\delta}(|\boldsymbol{k}-\boldsymbol{k}'|) \\
&\quad +\mu'^2\nu'^2 P^0_{v_\perp v_\perp}(k')P_{\delta'\delta'}(|\boldsymbol{k}-\boldsymbol{k}'|) \\
&\quad +\frac{(1-\mu^2)\nu'^2 k'}{|\boldsymbol{k}-\boldsymbol{k}'|}P_{\delta v_\parallel}(k')P_{\delta v_\parallel}(|\boldsymbol{k}-\boldsymbol{k}'|) \\
&\quad +(1-\mu'^2)^{1/2}\nu'\hat{\boldsymbol{\gamma}}\cdot\hat{\boldsymbol{\varepsilon}}''' P_{\delta v_\parallel}(k')P_{\delta' v_{\perp,0}}(|\boldsymbol{k}-\boldsymbol{k}'|) \\
&\quad +\frac{\mu'(1-\mu'^2)^{1/2}\nu'^2 k'}{|\boldsymbol{k}-\boldsymbol{k}'|}P_{\delta' v_{\perp,0}}(k')P_{\delta v_\parallel}(|\boldsymbol{k}-\boldsymbol{k}'|) \\
&\quad +\mu'\nu'\hat{\boldsymbol{\gamma}}\cdot\hat{\boldsymbol{\varepsilon}}''' P_{\delta' v_{\perp,0}}(k')P_{\delta' v_{\perp,0}}(|\boldsymbol{k}-\boldsymbol{k}'|)\big]. \qquad (6.31)
\end{aligned}$$

Now, noting, as per Ma and Fry, that we are interested in high k, beyond the k' peak of the above integrals, we drop terms of order k'/k and perform the integrations over μ' and ν'. First, we notice that

$$\hat{\boldsymbol{\gamma}}\cdot\hat{\boldsymbol{\varepsilon}}''' \to \hat{\boldsymbol{\gamma}}\cdot\hat{\boldsymbol{\varepsilon}} = 1, \qquad (6.32)$$

in this limit. To perform the angular integrations, we note that

$$\begin{aligned}
\int d^3k' \cos^2(\phi')f(\mu',k,) &= \pi\int_{-1}^{1}d\mu'\int_0^\infty dk'k'^2 f(\theta',k') \\
&= \frac{1}{2}\int d^3k' f(\theta',k'), \qquad (6.33) \\
\int d^3k' \cos(\phi')f(\mu',k') &= 0, \qquad (6.34) \\
\int d^3k'(1-\mu'^2)f(k') &= 2\pi\frac{4}{3}\int dk'k'^2 f(k') \\
&= \frac{2}{3}\int d^3k' f(k'), \qquad (6.35) \\
\int d^3k'\mu'^2 f(k') &= 2\pi\frac{2}{3}\int dk'k'^2 f(k') \\
&= \frac{1}{3}\int d^3k' f(k'), \qquad (6.36) \\
\int d^3k'\mu'(1-\mu'^2)^{1/2}f(k') &= 0. \qquad (6.37)
\end{aligned}$$

Putting this together gives us our result,

$$P_{q\perp}(k) = \int \frac{d^3k'}{(2\pi)^3} \left[\frac{2}{3} P_{v_\parallel v_\parallel}(k') P_{\delta\delta}(k) + \frac{1}{3} P^0_{v_\perp v_\perp}(k') P_{\delta'\delta'}(k) \right]. \tag{6.38}$$

The first term is, of course, the term introduced last chapter, due to Ma and Fry. It is the second term we calculate here.

First, we must calculate $P_{\delta'\delta'}(k)$. As we hinted at earlier, the collapse factor, λ, simply multiplies the halo density profile, giving us a new profile, $w(y/y_s) = \lambda u(y/y_s)$. Since we are ultimately interested in behaviors at low y, or equivalently, high k, we will use the low y asymptotic form of λ. For the Moore profile,

$$w(y/y_s) = (2\delta_a)^{1/3} \frac{1}{(y/y_s)^2(1 + (y/y_s)^{3/2})}. \tag{6.39}$$

It is the Fourier transform of this function that we will need. Figure [6–4] shows this transform as compared to the transform of the full w. The discrepancy is is the relatively unimportant small k region.

Figure [6–5] shows the transform of w and an analytical fit, which we will use to increase computational efficiency. This fit is given by

$$\tilde{w}(q) = (2\delta_a)^{1/3} \frac{4\pi \left[\ln(e + \frac{1}{k^{1/3}}) + 0.25 \ln(\ln(e + \frac{1}{k^{1/3}})) \right]}{(1 + 0.6k^{1.3})^{0.77}}. \tag{6.40}$$

For the NFW profile, we have

$$w(y/y_s) = (3\delta_a)^{1/3} \frac{1}{(y/y_s)^2(1 + (y/y_s))^2}. \tag{6.41}$$

This transform and the transform of using the full version of λ are shown in figure [6–6].

The analytical fit of the transform of this profile is

$$\tilde{w}(q) = (3\delta_a)^{1/3} \frac{4\pi}{1 + 0.6q}. \tag{6.42}$$

Figure [6–7] shows this fit compared to the transform.

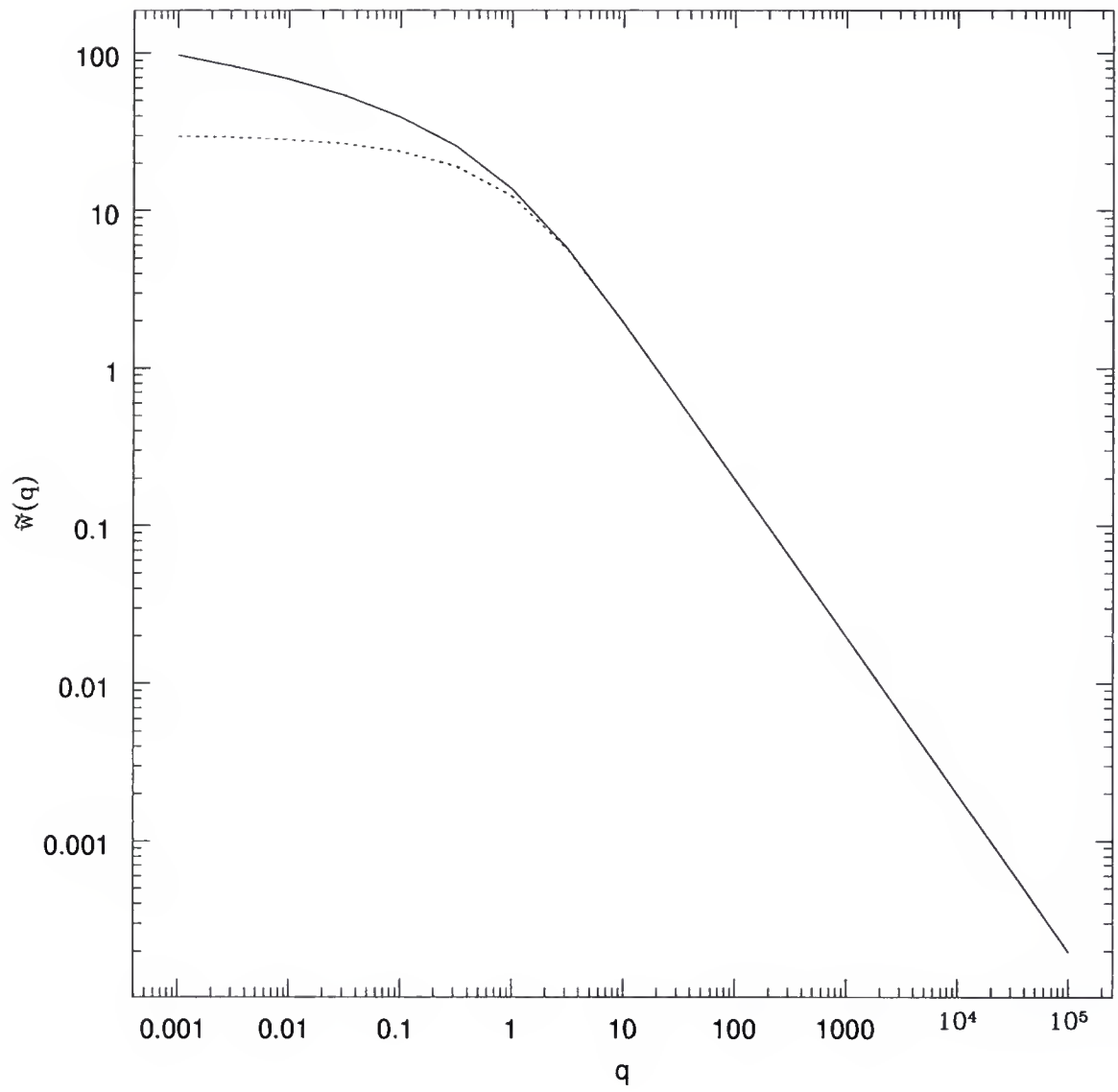

Figure 6–4. The Fourier transform of the Moore $w(y)$. The solid line represents the use of the full version of λ, while the dotted line represents the use of the high k asymptotic form of λ. In both versions we set $\delta_a = 1/2$.

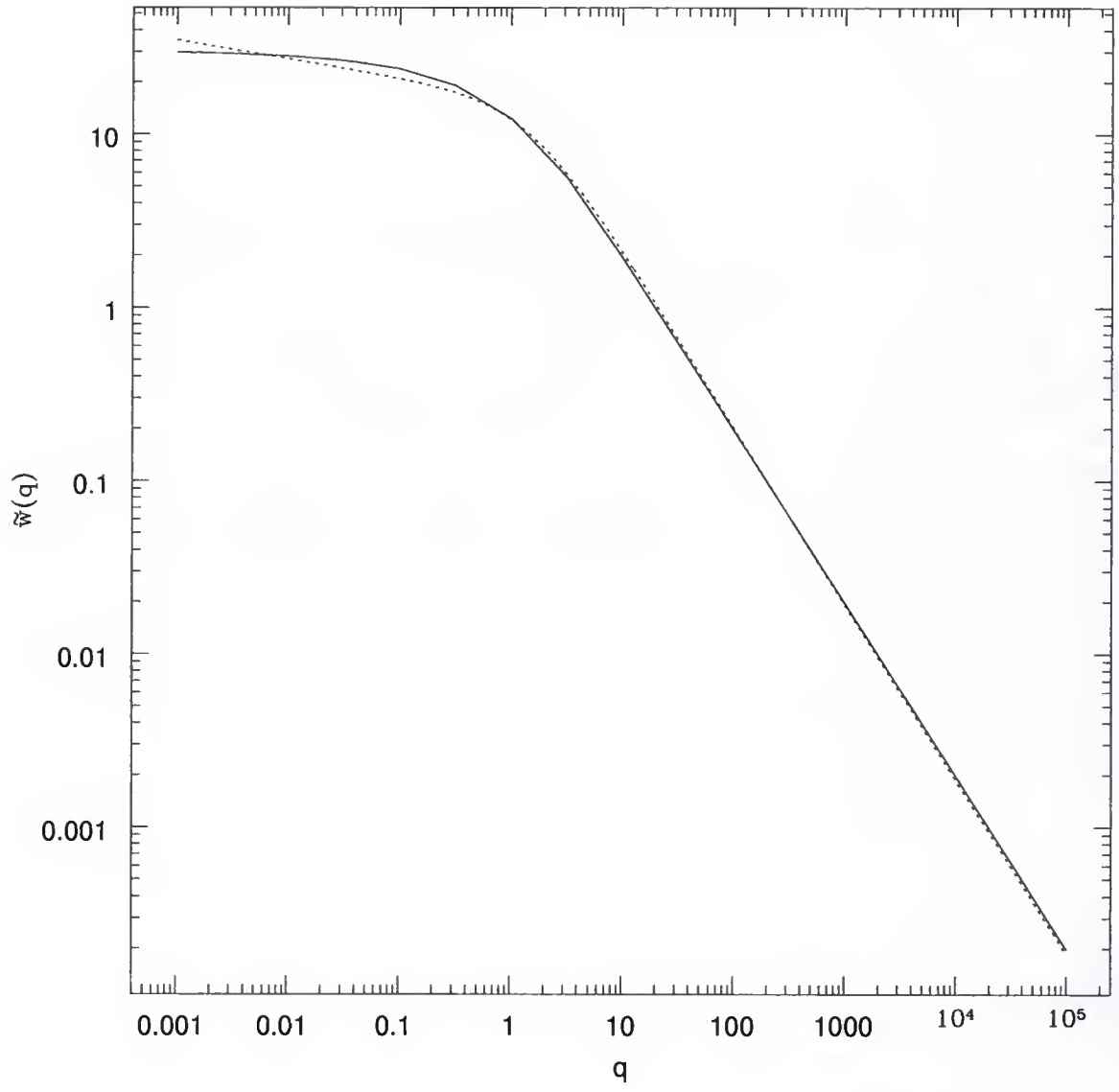

Figure 6–5. The Fourier transform of $w(y)$ for the Moore profile using the asymptotic form of λ. The solid line represents the actual transform and the dotted line represents the fit given in equation [6.40]

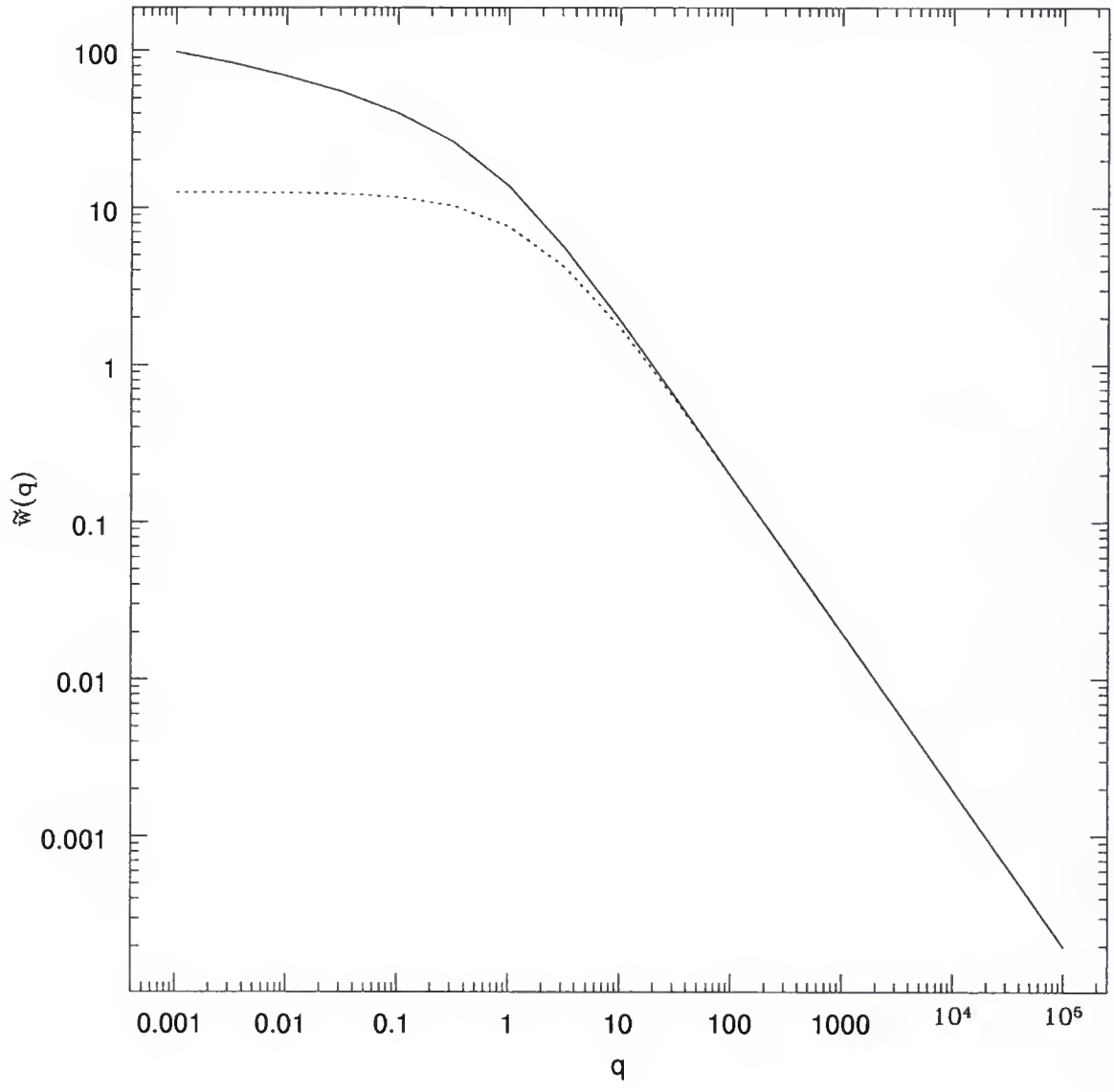

Figure 6–6. The Fourier transform of the NFW $w(y)$. The solid line represents the use of the full version of λ, while the dotted line represents the use of the high k asymptotic form of λ. In both versions we set $\delta_a = 1/3$.

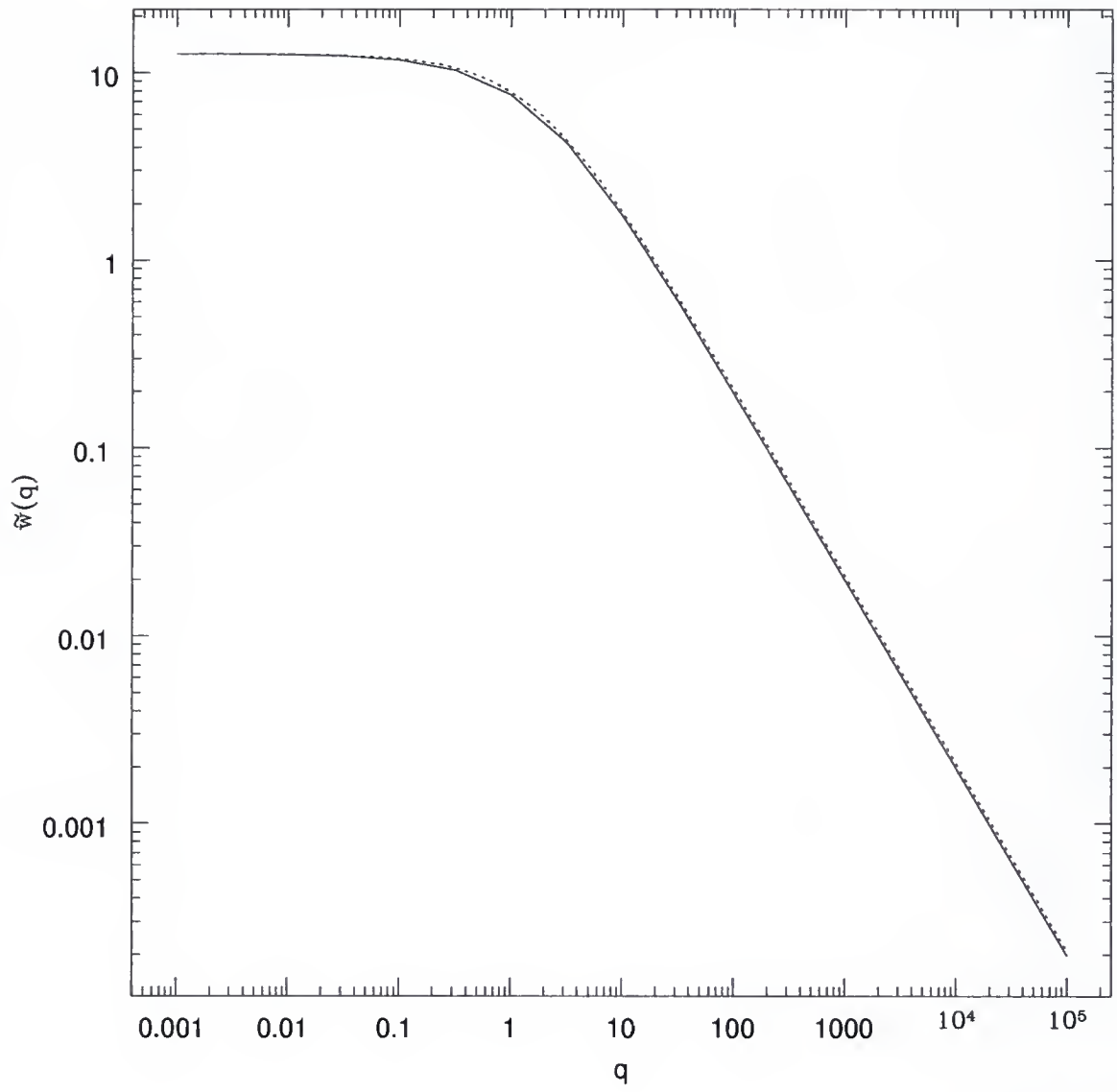

Figure 6–7. The Fourier transform of $w(y)$ for the NFW profile using the asymptotic form of λ. The solid line represents the actual transform and the dotted line represents the fit given in equation [6.42]

We now simply calculate $P_{\delta'\delta'}(k)$ just as we did before, in equation [5.19], with the substitution of w for u. Figure [6–8] shows $P_{\delta'\delta'}(k)$, with the factor of $(a_i/a)^2$ left out, as compared to $P_{\delta\delta}(k)$. Both the overall magnitude and the shape are, of course, markedly different.

Figure [6–9] shows the difference in $P_{\delta'\delta'}(k)$ when the different halo profiles are used. Notice that use of the NFW profile, rather than the Moore profile, leads to a difference of about a factor of ten in the spectrum for high k.

We now have

$$P_{q\perp} = \frac{1}{3}\langle v_{0,t}^2\rangle P_{\delta'\delta'}(k). \tag{6.43}$$

We will use a value of $\langle v_{0,t}^2\rangle^{1/2} = 20\text{km/s}$, as we did in the first section of this chapter.

Putting this into equation [5.25], we find the result given in figures [6–10] and [6–11].

Figure [6–12] shows how the nonlinear rotational velocity contribution compares to the linear contibution. This shows, in stark fashion, that this study was well motivated.

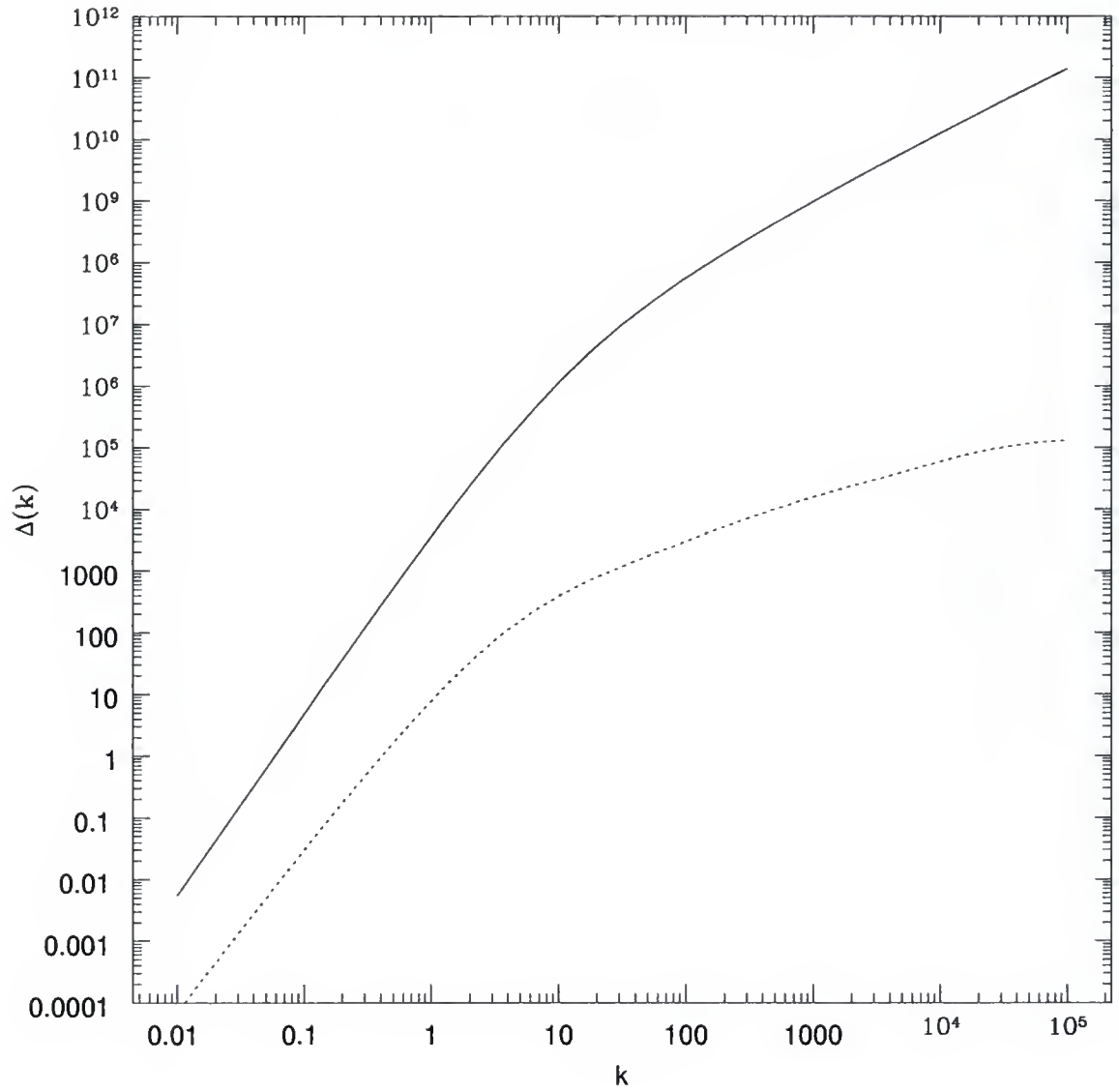

Figure 6–8. Plots of $P_{\delta'\delta'}(k)$, the solid line, and $P_{\delta\delta}(k)$, the dashed line.

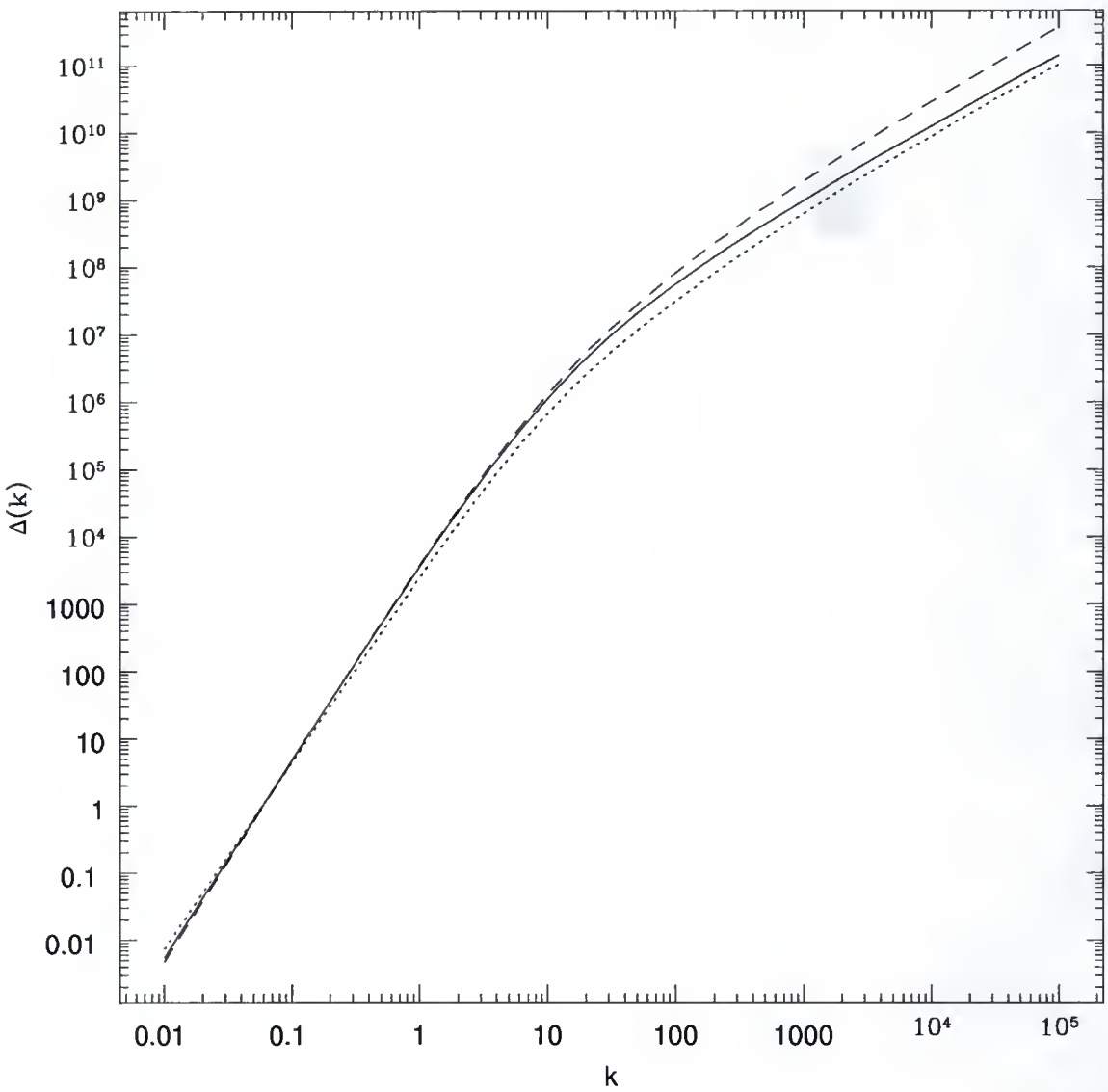

Figure 6–9. $P_{\delta'\delta'}(k)$ plotted using the NFW, dashed line, Moore, dotted line, and mixed, solid line, halo profiles.

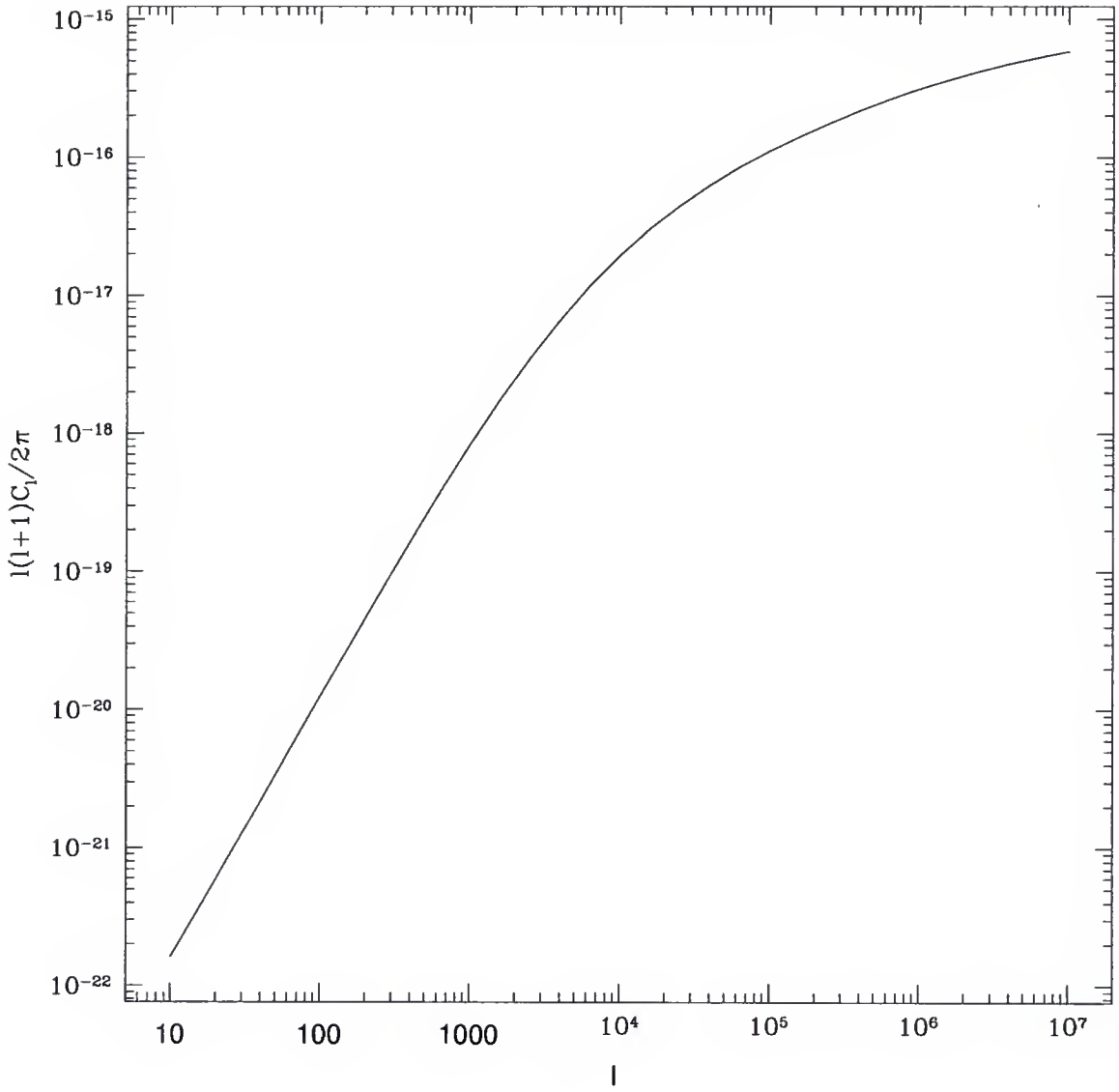

Figure 6–10. Angular power spectrum of temperature fluctuations in the CMB due to nonlinear rotational velocity contribution.

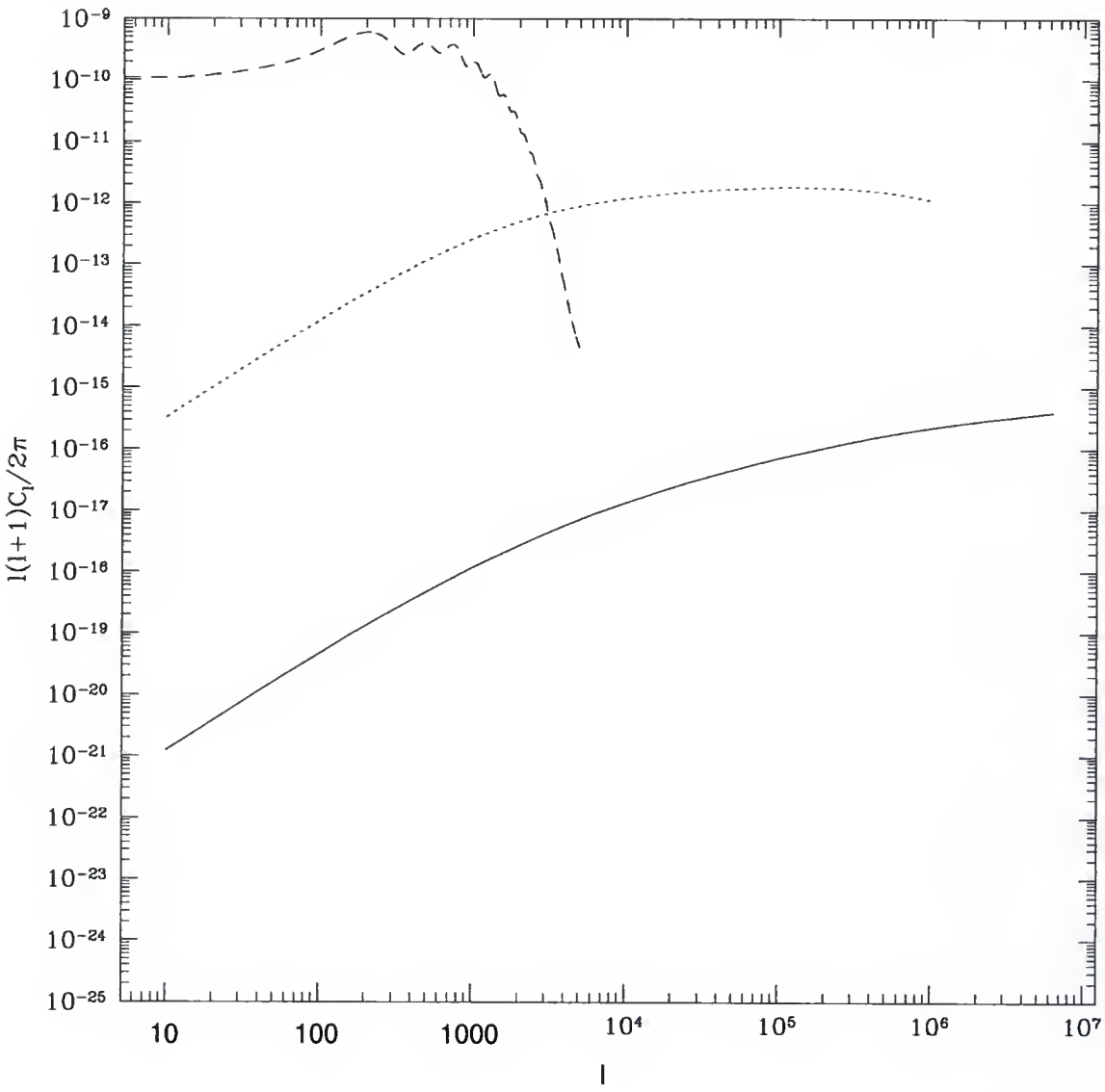

Figure 6–11. The solid line shows the angular spectrum due to the rotational velocity mode. The nonlinear spectrum due to the longitudinal mode, dotted line, and the primary anisotropy spectrum, dashed line, are shown for comparison.

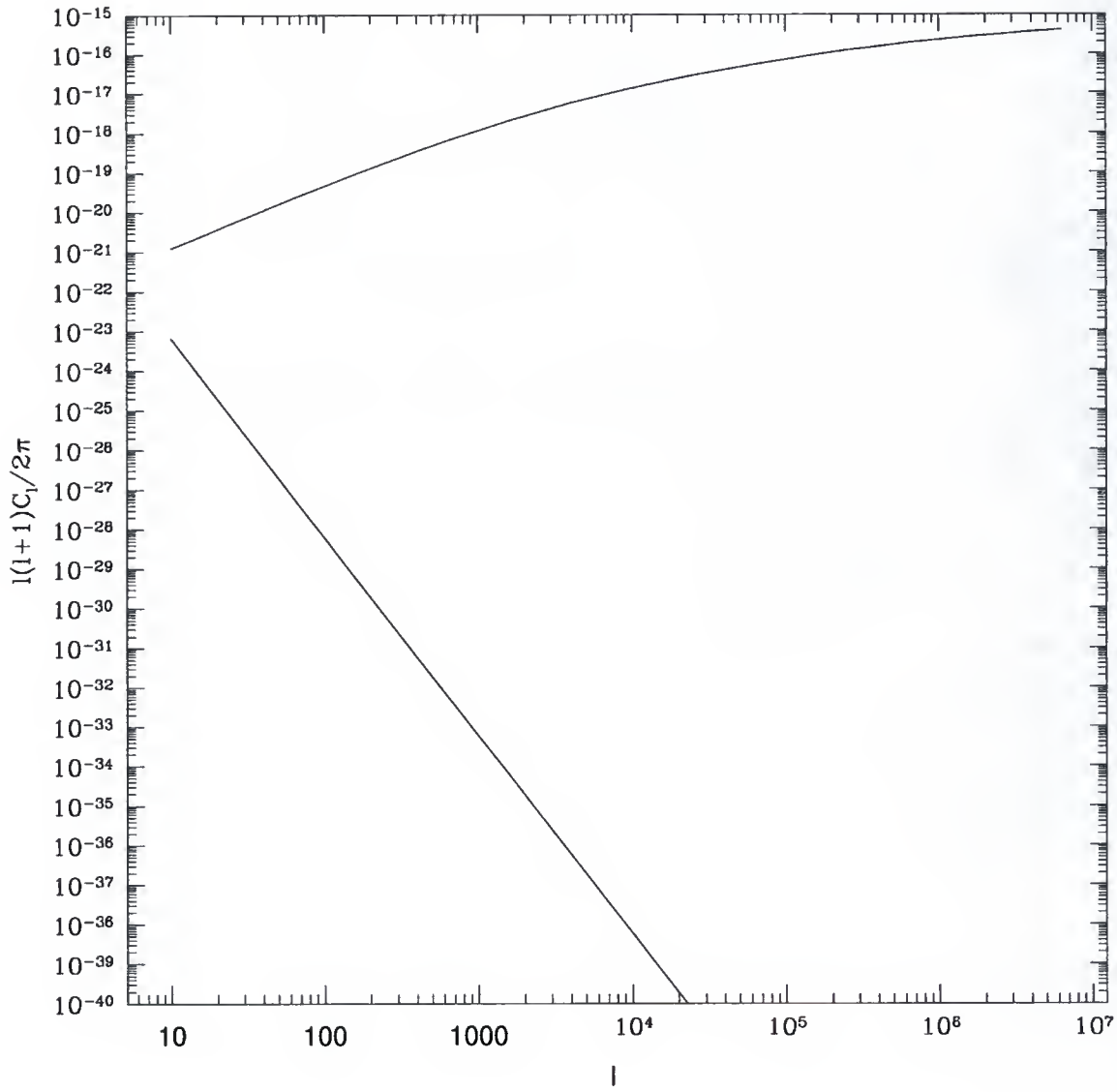

Figure 6–12. The angular power spectrum of CMB temperature fluctuations due rotational velocity modes. The top line is the nonlinear contribution, the bottom line the linear contribution.

CHAPTER 7
CONCLUSION

Our goal in this dissertation has been to include the effects of an initial rotational velocity mode in large-scale structure calculations. We have retained this mode in perturbation theory and we found that, although it decays with time in linear theory, at higher orders it couples to the longitudinal mode and plays a nontrivial role in quasi-linear theory.

We expected that the rotational velocity mode might play an even more significant role in the nonlinear regime. Specifically, we believed that the inclusion of this mode in a calculation of the kinetic Sunyaev-Zeldovich effect might prove significant. The results of last chapter indicate, however, that the inclusion of such modes is not significant on any angular scales available to observation now or in the near future.

This fact provides evidence for the validity of the assumption typically made in previous calculations that the rotational mode is largely unimportant in most cosmological situations. It is important, however, to note that the inclusion of rotational modes in the nonlinear calculation leads to temperature fluctuations many orders of magnitude higher than those in the linear regime. It seems that the success of the a priori exclusion of initial rotational modes was fortuitous.

It is important to note that there are many possible ways to improve upon our results. One important factor is that the halo profiles used to build the halo model are the result of N-body simulations which do not include the initial rotational mode. It is certainly conceivable that the profile in the central regions of halos would be considerably different if this mode were included in the simulations. Analytical calculations which allow for the inclusion of angular momentum do indicate that a shallower inner profile is likely.[53] One would expect that if a numerical simulation

were performed where the initial rotational velocities were retained, such a profile would be seen. Having said this, we note that, as suggested by the fairly small profile differences seen in figure [6–9] even a somewhat different inner profile would not be likely to produce an observable effect on the angular power spectrum of temperature fluctuations.

Besides the aforementioned inclusion of rotational modes in N-body simulations, there are many ways in which the work begun in this dissertation could continue. First, the role of the rotational modes in quasi-linear theory should be further explored. We have shown here that it plays potentially important roles, but not fully explored what those roles might be. Additionally, the inclusion of rotational velocities will also have an impact on the thermal Sunyaev-Zeldovich effect. An initial rotational velocity dispersion should contribute to the overall velocity dispersion, and thus effective temperature, of collapsed objects.

APPENDIX A
CONSERVATION OF ANGULAR MOMENTUM IN AN EXPANDING UNIVERSE

We begin by defining the angular momentum about an arbitrary origin as

$$\boldsymbol{L} = \int d^3r \rho \boldsymbol{r} \times \boldsymbol{v}, \tag{A.1}$$

which we can express in comoving coordinates as

$$\boldsymbol{L} = \int d^3x \rho_0 a^3 (1+\delta) a\boldsymbol{x} \times \boldsymbol{v}. \tag{A.2}$$

We want to look at the time derivative of the angular momentum. Noting that the quantity $\rho_0 a^3$ is constant in time (remembering that $\rho_0 \propto a^{-3}$) we have

$$\frac{d\boldsymbol{L}}{dt} = \rho_0 a^3 \int d^3x \boldsymbol{x} \times \frac{\partial}{\partial t}[(1+\delta)a\boldsymbol{v}]. \tag{A.3}$$

Using the fluid flow equations from chapter 2, equations [2.12] and [2.15], this becomes

$$\begin{aligned} \frac{d\boldsymbol{L}}{dt} &= -\rho_0 a^3 \int d^3x \Big[\boldsymbol{x} \times \{(1+\delta)[(\boldsymbol{v}\cdot\nabla)\boldsymbol{v} + \nabla\phi] + \boldsymbol{v}(\nabla\cdot[(1+\delta)\boldsymbol{v}])\}\Big] && \text{(A.4)} \\ &= -\rho_0 a^3 \int d^3x \Big[\boldsymbol{x} \times \{([\nabla\cdot(1+\delta)\boldsymbol{v}]\boldsymbol{v}) + (1+\delta)\nabla\phi\}\Big]. && \text{(A.5)} \end{aligned}$$

The cross product of $\boldsymbol{x}$ with the second term vanishes because ϕ leads to a central force. Writing the remainder in component notation, we have

$$\frac{dL_i}{dt} = \int d^3x \varepsilon_{ijk} x_j \nabla_l [(1-\delta) v_k v_l], \tag{A.6}$$

which we can write as

$$\frac{dL_i}{dt} = \int d^3x \varepsilon_{ijk} [\nabla_l x_j (1+\delta) v_k v_l + (1+\delta) v_k v_l \nabla_l x_j]. \tag{A.7}$$

The first term is a surface term and is thus zero, and the second term is just

$$\frac{dL_i}{dt} = \int d^3x \varepsilon_{ijk} \delta_{lj} v_k v_l (1 + \delta) = 0, \tag{A.8}$$

as it is just proportional to the cross product of $\boldsymbol{v}$ with itself. Thus $d\boldsymbol{L}/dt = 0$, and, as we would suspect, the total angular momentum in an expanding universe is conserved.

APPENDIX B
SPHERICAL COLLAPSE AND THE DERIVATION OF δ_C

A reasonable value for the critical density contrast required for collapse of a halo can be obtained through a simple analysis of spherical collapse model. We begin by writing the Newtonian equation of motion for a mass shell surrounding a mass, M.

$$\frac{d^2r}{dt^2} = -\frac{GM}{r^2}. \tag{B.1}$$

This can be solved using the parametric approach,

$$r = A(1 - \cos\theta) \tag{B.2}$$

$$t = B(\theta - \sin\theta). \tag{B.3}$$

Simple substitution will verify this solution and provide the relation

$$A^3 = GMB^2. \tag{B.4}$$

Figure [B–1] shows the radius and time plotted as functions of the parameter θ.

Now, expanding these solutions for small θ, corresponding to small initial over-densities, we have

$$r(\theta) \approx A\left(\frac{\theta^2}{2} - \frac{\theta^4}{24}\right), \tag{B.5}$$

$$t(\theta) \approx B\left(\frac{\theta^3}{6} - \frac{\theta^5}{120}\right). \tag{B.6}$$

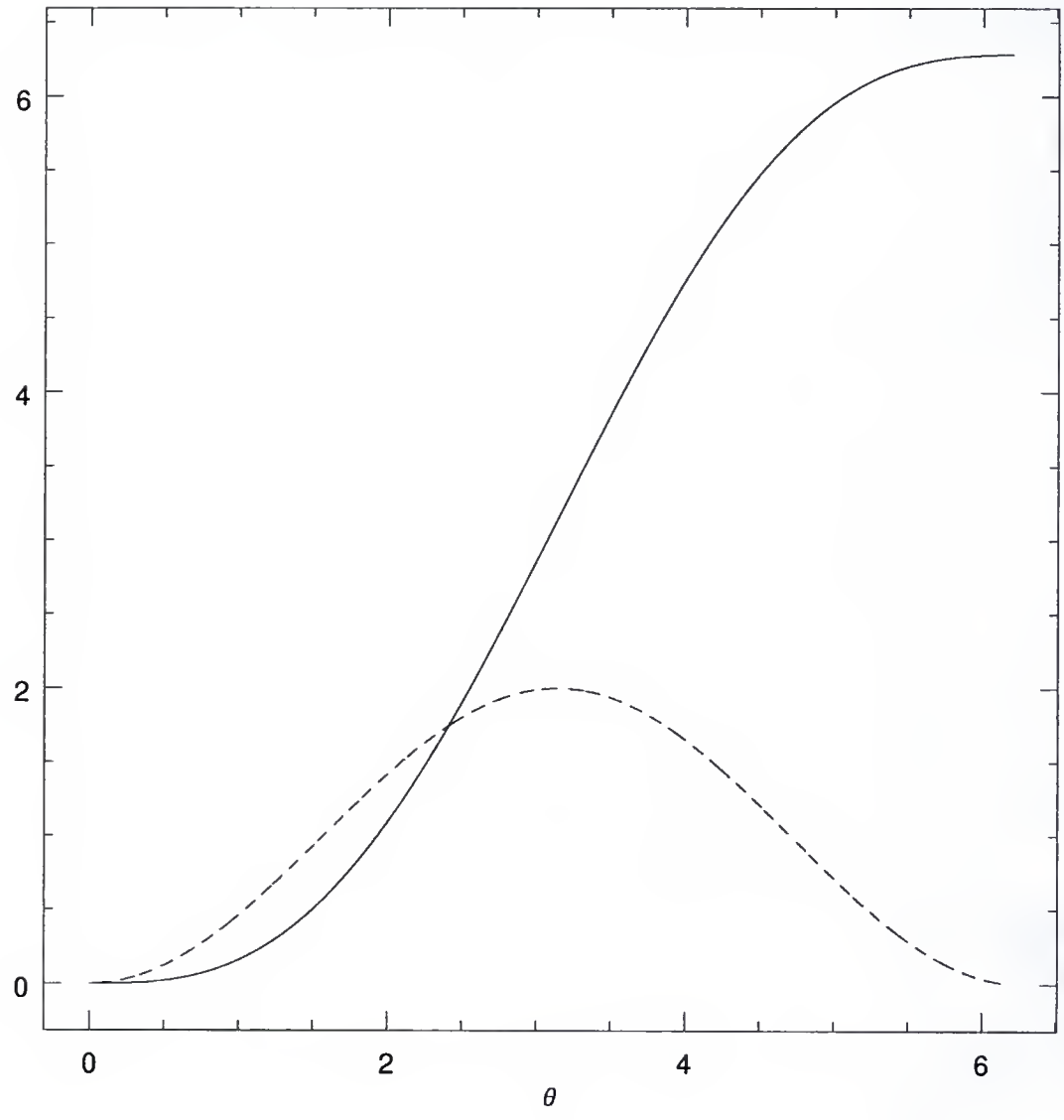

Figure B–1. Plots of radius and time as functions of the parameter θ. t/A is the solid line, r/B is dashed.

Feeding the leading order solution for t into the expression for r we find

$$r(\theta) \approx \frac{A}{2}\left(\frac{6t}{B}\right)^{2/3}\left[1-\frac{1}{20}\left(\frac{6t}{B}\right)^{2/3}\right] \tag{B.7}$$

$$\approx \frac{1}{2}(6t)^{2/3}(GM)^{1/3}\left[1-\frac{1}{20}\left(\frac{6t}{B}\right)^{2/3}\right]. \tag{B.8}$$

Remembering that $\bar{\rho} = M/(4\pi r^3/3)$ (this is actually the mean density within a sphere of radius r) and $\rho_0 = 1/6\pi t^2 G$, we find

$$\delta = \frac{\rho-\rho_0}{\rho_0} \approx \frac{3}{20}\left(\frac{6t}{B}\right)^{2/3}. \tag{B.9}$$

Equation [B.2] tells us that total collapse occurs at $\theta = 2\pi$, where $t = 2\pi B$. Putting this in we get the result, $\delta_c \approx 1.686$. The reader may object, as $\theta = 2\pi$ is clearly not $\ll 1$, however, all this is saying is that collapse takes place when linear theory predicts an overdensity of 1.686.

As a point of further interest, we can calculate the exact density run for this spherical collapse. To start we consider the energy of a spherical shell at its turnaround,

$$E = -\frac{GM(x)}{2A}, \tag{B.10}$$

as, at turnaround, all energy is potential and $r = 2A$. Here x refers to the co-moving radius. We also note that $E \propto 1/x$ because we are perturbing an Einstein-De Sitter universe, where $E = 0$, by an initial overdensity a co-moving distance x from the shell. When combined with the fact that $M(x) \propto x^3$ we see that $A \propto x^4$ and $B \propto x^{9/2}$. Using these scale relations we can write

$$\frac{r}{r_{ta}} = \frac{A(1-\cos\theta)}{2A_{ta}} = \left(\frac{x^4}{x_{ta}^4}\right)\frac{1-\cos\theta}{2}, \tag{B.11}$$

and

$$\left(\frac{x}{x_{ta}}\right)^{9/2} = \frac{B}{B_{ta}} = \frac{\pi}{\theta-\sin\theta}, \tag{B.12}$$

so that

$$\frac{r}{r_{ta}} = \left(\frac{\pi}{\theta - \sin\theta}\right)^{8/9} \frac{1-\cos\theta}{2}. \tag{B.13}$$

In each of the previous equations the subscript "ta" indicates a quantity for the shell at turnaround at the chosen time t. We compute the mass density run using

$$\rho(r) = \frac{dM}{dr}\frac{1}{4\pi r^2}, \tag{B.14}$$

and using the chain rule,

$$\frac{dM}{dr} = \frac{dM}{dx}\frac{dx}{d\theta}\left(\frac{dr}{d\theta}\right)^{-1}, \tag{B.15}$$

and the dependences we found above. The result, when divided by the mean density, becomes

$$\frac{\rho(r)}{\rho_0} = \frac{9}{2}\frac{(\theta-\sin\theta)^2}{(1-\cos\theta)^3}\left[4 - \frac{9}{2}\frac{\sin\theta(\theta-\sin\theta)}{(1-\cos\theta)^2}\right]^{-1}. \tag{B.16}$$

We can also write down the mean density within the sphere, to compare with the linear prediction,

$$\frac{\bar{\rho}}{\rho_0} = \frac{M}{\frac{4}{3}\pi r^3} 6\pi G t^2 = \frac{9}{2}\frac{MGt^2}{r^3} = \frac{9}{2}\frac{(\theta-\sin\theta)^2}{(1-\cos\theta)^3}. \tag{B.17}$$

Figure [B–2] shows the density contrast as a function of the scaled radius, for the mean density, as above, and for the linear prediction of equation [B.9]. Also shown the the density run. None of these are expected to be accurate at small r, where shell crossing causes virialization.

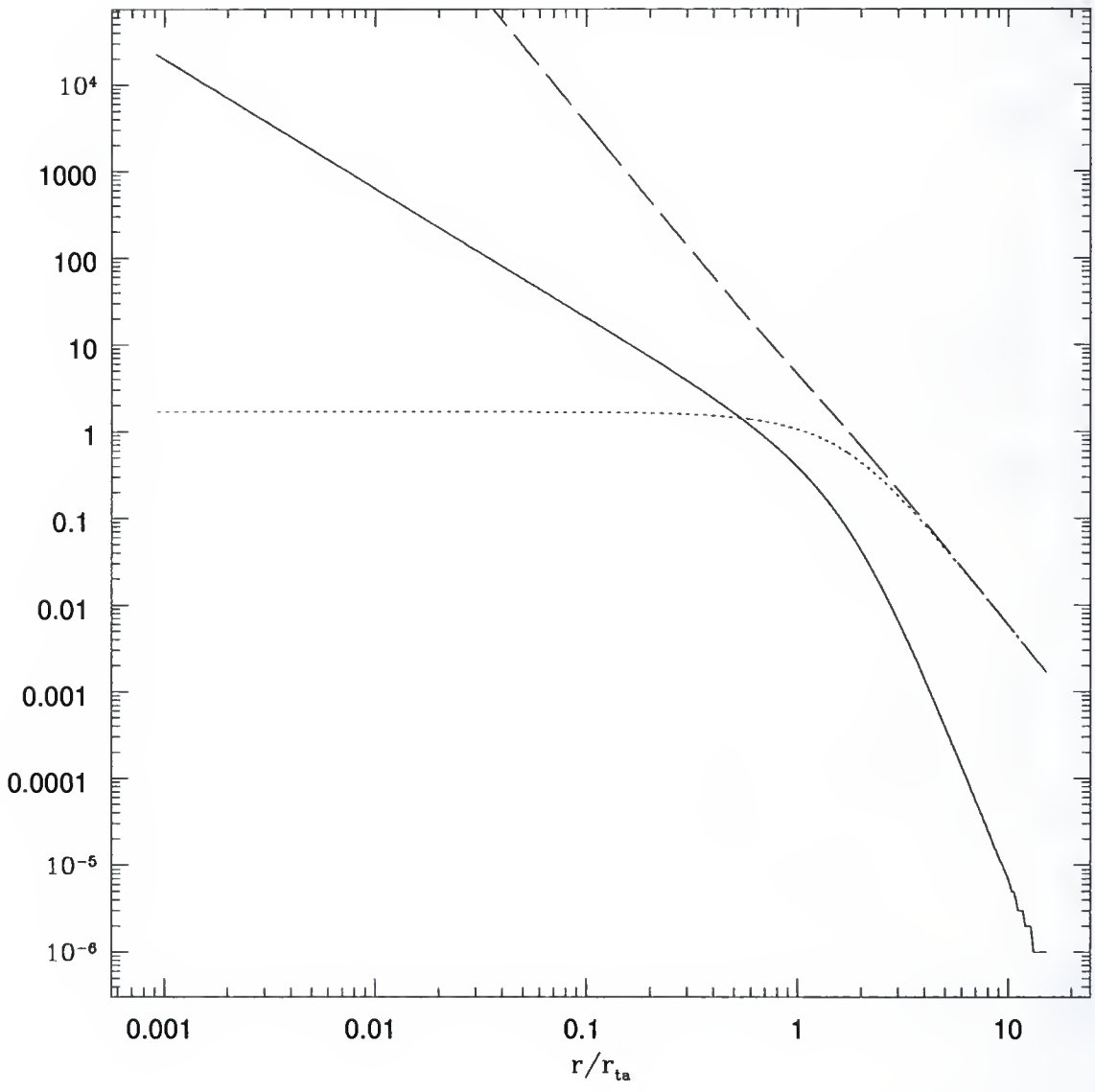

Figure B–2. Density contrasts plotted as a function of the scaled radius. The dashed line is the exact solution for the mean density contrast within the radius. The dotted line is the linear model prediction. The solid line is the actual density run.

APPENDIX C
PHYSICAL CONSTANTS AND COSMOLOGICAL PARAMETERS

Table C–1. A list of constants and parameters used in calculations.

Parameter	Symbol	Value	Units
Speed of Light	c	299792.458	km/s
Mass of Proton	m_p	1.672621×10^{-27}	kg
Gravitational Constant	G	6.673×10^{-20}	$km^3kg^{-1}s^{-2}$
Thompson Cross-Section	σ_T	6.65245×10^{-35}	km^2
Fractional Matter Density	Ω_m	0.3	-
Fractional Λ Density	Ω_Λ	0.7	-
Fractional Baryon Density	Ω_b	0.05	-
Primordial Helium Fraction	Y	0.74	-
Ionization Fraction	X_e	1.0	-
Initial Power Index	n	1.0	-
Dimensionless Hubble Constant	h	0.71	-

APPENDIX D
CODE FOR CALCULATING ANGULAR SZ SPECTRUM

The integration elements of this code were adapted from routines given in Press et al.[54]

```
/* rvcl.c
-----------------------------------------------
Calculates the rotational contribution to Cl's
-----------------------------------------------*/

#include <math.h>
#include <stdio.h>
#include "./cosmodefs.h"
#define FUNC(x) ((*funk)(1.0/(x))/((x)*(x)))
#define FUNCY(x) ((*funk)(x))
#define FUNT(x) ((*funk) (tan(x))*(1.0+(tan(x))*(tan(x))))
#define EPS 1.0e-3
#define JMAX 14
#define JMAXP 15
#define K 5
#define NR_END 1
#define FREE_ARG char*
#define ZMAX 20.0
#define MMAX 0
#define TMAX 30.0
#define LLMAX 6.0
#define ZZMAX 6.0
#define Do 0.31124
#define V2 400.0

double kay, z1temp, rad, rsptemp, kprimetemp;
int l;

double qromo(double (*func)(double), double a, double b,
    double (*choose)(double(*)(double), double, double, int))
     /*Romberg Integration on an open interval*/
{
  void polint(double xa[], double ya[], int n, double x, double *y
  , double *dy);
  int j;
  double ss, dss, h[JMAXP+1], s[JMAXP];

  h[1]=1.0;
  for (j=1;j<=JMAX;j++) {
    s[j]=(*choose)(func,a,b,j);
    if (j >= K) {
      polint(&h[j-K],&s[j-K],K,0.0,&ss,&dss);
      if (fabs(dss) <= EPS*fabs(ss)) return ss;
    }
    h[j+1]=h[j]/9.0;
  }
  printf("Too many steps in routine qromo\n");
```

```
  exit(1);
  return 0.0;
}

double midtan(double (*funk)(double), double aaa, double bbb, int n)
{
  double x,tnm,sum,del,ddel,b,a;
  static double s;
  int it,j;

  b=atan(bbb);
  a=atan(aaa);
  if (n==1) {
    return (s=(b-a)*FUNT(0.5*(a+b)));
  } else {
    for (it=1,j=1;j<n-1;j++) it *= 3;
    tnm=it;
    del=(b-a)/(3.0*tnm);
    ddel=del+del;
    x=a+0.5*del;
    sum=0.0;
    for (j=1;j<=it;j++) {
      sum += FUNT(x);
      x += ddel;
      sum += FUNT(x);
      x += del;
    }
    return (s=(s+(b-a)*sum/tnm)/3.0);
  }
}

double midtan1(double (*funk)(double), double aaa, double bbb, int n)
{
  double x,tnm,sum,del,ddel,b,a;
  static double s;
  int it,j;

  b=atan(bbb);
  a=atan(aaa);
  if (n==1) {
    return (s=(b-a)*FUNT(0.5*(a+b)));
  } else {
    for (it=1,j=1;j<n-1;j++) it *= 3;
    tnm=it;
    del=(b-a)/(3.0*tnm);
    ddel=del+del;
    x=a+0.5*del;
    sum=0.0;
    for (j=1;j<=it;j++) {
      sum += FUNT(x);
      x += ddel;
      sum += FUNT(x);
      x += del;
    }
    return (s=(s+(b-a)*sum/tnm)/3.0);
  }
}


double midtan4(double (*funk)(double), double aaa, double bbb, int n)
{
  double x,tnm,sum,del,ddel,b,a;
  static double s;
```

```
  int it,j;

  b=atan(bbb);
  a=atan(aaa);
  if (n==1) {
    return (s=(b-a)*FUNT(0.5*(a+b)));
  } else {
    for (it=1,j=1;j<n-1;j++) it *= 3;
    tnm=it;
    del=(b-a)/(3.0*tnm);
    ddel=del+del;
    x=a+0.5*del;
    sum=0.0;
    for (j=1;j<=it;j++) {
      sum += FUNT(x);
      x += ddel;
      sum += FUNT(x);
      x += del;
    }
    return (s=(s+(b-a)*sum/tnm)/3.0);
  }
}

double midtan5(double (*funk)(double), double aaa, double bbb, int n)
{
  double x,tnm,sum,del,ddel,b,a;
  static double s;
  int it,j;

  b=atan(bbb);
  a=atan(aaa);
  if (n==1) {
    return (s=(b-a)*FUNT(0.5*(a+b)));
  } else {
    for (it=1,j=1;j<n-1;j++) it *= 3;
    tnm=it;
    del=(b-a)/(3.0*tnm);
    ddel=del+del;
    x=a+0.5*del;
    sum=0.0;
    for (j=1;j<=it;j++) {
      sum += FUNT(x);
      x += ddel;
      sum += FUNT(x);
      x += del;
    }
    return (s=(s+(b-a)*sum/tnm)/3.0);
  }
}

double midtan6(double (*funk)(double), double aaa, double bbb, int n)
{
  double x,tnm,sum,del,ddel,b,a;
  static double s;
  int it,j;

  b=atan(bbb);
  a=atan(aaa);
  if (n==1) {
    return (s=(b-a)*FUNT(0.5*(a+b)));
  } else {
    for (it=1,j=1;j<n-1;j++) it *= 3;
    tnm=it;
```

```
    del=(b-a)/(3.0*tnm);
    ddel=del+del;
    x=a+0.5*del;
    sum=0.0;
    for (j=1;j<=it;j++) {
      sum += FUNT(x);
      x += ddel;
      sum += FUNT(x);
      x += del;
    }
    return (s=(s+(b-a)*sum/tnm)/3.0);
  }
}

double midpnt(double (*funk)(double), double a, double b, int n)
     /*Integration workhorse*/
{
  double x,tnm,sum,del,ddel;
  static double s;
  int it,j;

  if (n==1) {
    return (s=(b-a)*FUNCY(0.5*(a+b)));
  } else {
    for (it=1,j=1;j<n-1;j++) it *= 3;
    tnm=it;
    del=(b-a)/(3.0*tnm);
    ddel=del+del;
    x=a+0.5*del;
    sum=0.0;
    for (j=1;j<=it;j++) {
      sum += FUNCY(x);
      x += ddel;
      sum += FUNCY(x);
      x += del;
    }
    return (s=(s+(b-a)*sum/tnm)/3.0);
  }
}

double midpnt1(double (*funk)(double), double a, double b, int n)
     /*Integration workhorse*/
{
  double x,tnm,sum,del,ddel;
  static double s;
  int it,j;

  if (n==1) {
    return (s=(b-a)*FUNCY(0.5*(a+b)));
  } else {
    for (it=1,j=1;j<n-1;j++) it *= 3;
    tnm=it;
    del=(b-a)/(3.0*tnm);
    ddel=del+del;
    x=a+0.5*del;
    sum=0.0;
    for (j=1;j<=it;j++) {
      sum += FUNCY(x);
      x += ddel;
      sum += FUNCY(x);
      x += del;
    }
```

```
    return (s=(s+(b-a)*sum/tnm)/3.0);
  }
}


double midpnt2(double (*funk)(double), double a, double b, int n)
     /*Integration workhorse*/
{
  double x,tnm,sum,del,ddel;
  static double s;
  int it,j;

  if (n==1) {
    return (s=(b-a)*FUNCY(0.5*(a+b)));
  } else {
    for (it=1,j=1;j<n-1;j++) it *= 3;
    tnm=it;
    del=(b-a)/(3.0*tnm);
    ddel=del+del;
    x=a+0.5*del;
    sum=0.0;
    for (j=1;j<=it;j++) {
      sum += FUNCY(x);
      x += ddel;
      sum += FUNCY(x);
      x += del;
    }
    return (s=(s+(b-a)*sum/tnm)/3.0);
  }
}


double midpnt4(double (*funk)(double), double a, double b, int n)
     /*Integration workhorse*/
{
  double x,tnm,sum,del,ddel;
  static double s;
  int it,j;

  if (n==1) {
    return (s=(b-a)*FUNCY(0.5*(a+b)));
  } else {
    for (it=1,j=1;j<n-1;j++) it *= 3;
    tnm=it;
    del=(b-a)/(3.0*tnm);
    ddel=del+del;
    x=a+0.5*del;
    sum=0.0;
    for (j=1;j<=it;j++) {
      sum += FUNCY(x);
      x += ddel;
      sum += FUNCY(x);
      x += del;
    }
    return (s=(s+(b-a)*sum/tnm)/3.0);
  }
}
double *vector(long nl, long nh)
{
  double *v;

  v=(double *)malloc((size_t) ((nh-nl+1+NR_END)*sizeof(double)));
```

```
  if (!v) {
    printf("allocation failure in vector\n");
      exit(1);}
  return v-nl+NR_END;
}

void free_vector(double *v, long nl, long nh)
{
  free((FREE_ARG) (v+nl-NR_END));
}

void polint(double xa[], double ya[], int n, double x,
 double *y, double *dy)
     /*Polynomial Extrapolation*/
{
  double *vector(long nl, long nh);
  void free_vector(double *v, long nl, long nh);
  int i,m,ns=1;
  double den,dif,dift,ho,hp,w;
  double *c,*d;

  dif=fabs(x-xa[1]);
  c=vector(1,n);
  d=vector(1,n);
  for (i=1;i<=n;i++) {
    if ( (dift=fabs(x-xa[i])) < dif) {
      ns=i;
      dif=dift;
    }
    c[i]=ya[i];
    d[i]=ya[i];
  }
  *y=ya[ns--];
  for (m=1;m<n;m++) {
    for (i=1;i<=n-m;i++) {
      ho=xa[i]-x;
      hp=xa[i+m]-x;
      w=c[i+1]-d[i];
      if ( (den=ho-hp) == 0.0) {
printf("Error in routine polint\n");
exit(1);}
      den=w/den;
      d[i]=hp*den;
      c[i]=ho*den;
    }
    *y += (*dy=(2*ns < (n-m) ? c[ns+1] : d[ns--]));
  }
  free_vector(d,1,n);
  free_vector(c,1,n);
}

double ps(double x) /* This is the k dependent part of the linear
                       power spectrum */
{
  double ans, fac, q, p, shape, A, delh, omegamz, omegalz, f, g, D;

  delh=1.94e-5*(pow(OMEGAM, (-0.785-0.05*(log(OMEGAM)))))*
  (exp(-0.95*(INDEXN-1)-0.169*(INDEXN-1)*(INDEXN-1)));
  A=delh*delh*pow(SOL/(H*100.0), INDEXN+3)/(4.0*PI);
  shape=OMEGAM*H/(exp(OMEGAB*(1.0+(1.3/OMEGAM))));
```

```
  q=x/(shape*H);
  p=log(1.0+2.34*q)/(2.34*q);
  fac=1.0*(2.0*PI)*(2.0*PI)*(2.0*PI);  /* To account for difference
  between Ma and Fry */
  omegamz=OMEGAM/(OMEGAM + OMEGAL/(z1temp*z1temp*z1temp));
  omegalz=1.0-omegamz;
  f=pow(omegamz, 0.5714);
  g=omegamz/(f - omegalz + (1.0+0.5*omegamz)*(1.0+0.014*omegalz));
  /* a factor of 2.5 left out of g and of Do*/
  D=g/z1temp;
  ans=(D/Do)*(D/Do)*A*fac*pow(x, INDEXN)*p*p/(sqrt(1.0+3.89*q+16.1*
  16.1*q*q+5.46*5.46*5.46*q*q*q+pow(6.71*q, 4)));
  return ans;
}


double window(double x)

 /*Fourier transform of the top-hat window function */
{
  double win;

  win=3.0*((sin(x*rad))/(x*x*x*rad*rad*rad)-(cos(x*rad))
  /(x*x*rad*rad));
  return win;
}


double grand(double x)
{
  return (x*x*ps(x)*window(x)*window(x)/(2.0*PI*PI));
}



double cee(double lnm)
{
/* concentration factor */
  double result;

  rad=pow((3.0*pow(10.0, lnm)/(4.0*PI*AVDEN))
  , (0.33333333333333));
  result=qromo(grand, 0.0, 1.0e30, midtan6);
  if (lnm < 14.0) {
    return 5.0*sqrt(result);
  }  else {
    return 9.0*sqrt(result);
    }
}


double rs(double lnm)
{

  return ((1.0/cee(lnm))*pow(3.0*pow(10.0, lnm)
  /(800.0*PI*AVDEN),  0.333333333333));
  }

double stmf(double lnm)
```

```
{

/* Sheth-Tormen mass function */

  double dsidm, deltaexp;
  double result, radtemp;
  double invsigmaplus, invsigmaminus;
  double resultplus, resultminus, massfunc, ma;

  ma=pow(10.0, lnm);
  rad=pow((3.0*ma/(4.0*PI*AVDEN)), (0.33333333333333));
  result=qromo(grand, 0.0, 1.0e30, midtan4);
  deltaexp=ma*(1.0e-4);
  radtemp=rad;
  rad=pow((3.0*(ma+deltaexp)/(4.0*PI*AVDEN)),
   (0.33333333333333));
  resultplus=qromo(grand, 0.0, 1.0e30, midtan4);
  invsigmaplus = 1.0/(sqrt(resultplus));
  rad=pow((3.0*(ma-deltaexp)/(4.0*PI*AVDEN)),
   (0.33333333333333));
  resultminus=qromo(grand, 0.0, 1.0e30, midtan4);
  invsigmaminus = 1.0/sqrt(resultminus);
  dsidm=(invsigmaplus-invsigmaminus)/(2.0*deltaexp);
  rad=radtemp;
  massfunc=result*2.0*0.322*dsidm*AVDEN*(1.0+
  1.0/(pow((1.189*DC/sqrt(result)),
  0.6)))*sqrt(1.189*1.189*DC*DC/(result*2.0*PI))
  *exp(-DC*DC/(0.707*2.0*result))/(ma);
  return 0.75*massfunc;
  }

double ftnfw(double lnm)
{

/* Algebraic approximation to Fourier transform
of NFW halo profile */

  double q;

  q=kay*rs(lnm);
  return (4.0*PI*(log(E+1.0/q)-log(log(E+1.0/q)/3.0))
  /pow((1.0+pow(q, 1.1)),
  (2.0/1.1)));
  }

double ftm(double lnm)
{

/* Algebraic approximation to Fourier transform
 of Moore halo profile */

  double q;

  q=kay*rs(lnm);
  return (4.0*PI*(log(E+1.0/q)+0.25*log(log(E+1.0/q)))
  /(1.0+0.8*pow(q, 1.5)));
  }

double ftmp(double lnm)
```

```
{

/* Algebraic approximation to ft of Moore profile times
 collapse factor (high k) */

  double q;

  q=kay*rs(lnm);
  return 12.566*(log(E+1.0/pow(q, 0.3333))+0.25*log
  (log(E+1.0/pow(q, 0.33333))))/pow(1.0+0.6*pow(q, 1.3), 0.77);
 }

double ftnfwp(double lnm)
{

/* algebraic approximation to ft of NFW profile
times collapse factor (high k) */

  double q;

  q=kay*rs(lnm);
  return 12.566/(1.0+0.6*q);
  }

double nfwd(double lnm)
{

/* density amplitude for NFW profile */

  return (200.0*cee(lnm)*cee(lnm)*cee(lnm)
  /(3.0*(log(1.0+cee(lnm))-cee(lnm)/(1.0+cee(lnm)))));
}

double md(double lnm)
{

/* density amplitude for Moore profile */

  return (100.0*cee(lnm)*cee(lnm)*cee(lnm)
  /log(1.0+pow(cee(lnm), 1.5)));
  }

double integrand(double zz1)
{
    double hofz;

    hofz=1.0/sqrt(OMEGAM*zz1*zz1*zz1 + OMEGAL);
    return hofz;
}

double ex(double z1)  /* Calculating comoving
                         postion as a function of z */
{
    double ans2;

    if (z1<1.00001)
     ans2=z1-1.0-3.0*OMEGAM*(z1-1.0)*(z1-1.0)/4.0;
    else
     ans2=(SOL/(H*100.0))
*qromo(integrand, 1.0, z1, midpnt4);
    return ans2;
```

```
}


double onehmintegrand(double lnm)
{

/* Integrand for single halo power.
 Factor of mass from changing to dlnM*/

  double que, rstemp1, mdtemp, nfwdtemp, ftmptemp,
  ftnfwptemp, prefacm, prefacnfw;

  rstemp1=rs(lnm);
  que=kay*rstemp1;
  mdtemp=md(lnm);
  nfwdtemp=nfwd(lnm);
  ftmptemp=ftmp(lnm);
  ftnfwptemp=ftnfwp(lnm);
  prefacm=pow(2.0*mdtemp, 0.66666666);
  prefacnfw=pow(3.0*nfwdtemp, 0.66666666);
  if (lnm > 14.0) {
     return prefacnfw*pow(10.0, lnm)*stmf(lnm)*pow(rstemp1,
     6.0)*nfwdtemp*nfwdtemp*ftnfwptemp*ftnfwptemp;
  } else {
     return prefacm*pow(10.0, lnm)*stmf(lnm)*
     pow(rstemp1, 6.0)*mdtemp*mdtemp*ftmptemp*ftmptemp;
  }
  }

double zintegrand(double z1)  /* Everything to be
                                 integrated from z=0 to zr */
{
  double answer, hover, omegamz, omegalz, dxtodz;
  double g, D, f, pref, extemp, tauh, tau, expt, lamafac;
  int m, t;

  extemp=ex(z1);
  kay=1/extemp;
  z1temp=z1;
  answer=(1.0/3.0)*V2*
  qromo(onehmintegrand, 5.0, 18.0, midpnt1);
  dxtodz=SOL/(H*100.0*sqrt(OMEGAM*z1*z1*z1 + OMEGAL));
  tauh=0.0691*(1.0-Y)*OMEGAB*H;
  tau=(2.0/3.0)*(tauh/OMEGAM)*
  (sqrt(1.0-OMEGAM+OMEGAM*z1*z1*z1)-1.0);
  expt=exp(-2.0*tau);
  lamafac=(8.25e-7)*z1*z1;
  return answer*dxtodz*expt*z1*z1*lamafac/(extemp*extemp);

}

main ()
{
int t;
double ce, ceec, cee2, cu, ccl, cn, ccon,
 constants, ll, z1, zz1, z;
double qromo(double (*func)(double), double a, double b,
 double (*choose)(double(*)(double), double, double, int));
```

```
cu=H*100.0/(3.0856e19*3.0856e19);
 /* dimensional and unit conversion constants */
ccl=XE*XE*OMEGAB*OMEGAB *9.0*H*H*10000.0*ST*ST
/(64.0*PI*PI*G*G*MP*MP);  /* electron
density squared times cross section squared
/Hnaught squared. */
cn=4.0*PI*PI; /* correction for difference in
normalization between Fry and me */
ccon=H*H*10000.0/(8.0*PI*PI);
constants=cu*ccl*cn*ccon/(SOL*SOL);

for (t=0;t<=TMAX;t++) {
ll=1.0+(t*LLMAX/TMAX);
l=pow(10.0, ll);
ce=qromo(zintegrand, 1.0, 21.0, midpnt);
ceec=constants*ce;
cee2=ceec*l*(l+1.0)/(2.0*PI);
printf("%d %e\n", l, cee2);
}

}
```

REFERENCE LIST

[1] P.J.E. Peebles. *The Large-Scale Structure of the Universe.* Princeton University Press, Princeton, NJ, 1980.

[2] A. Guth. Inflation and cosmological perturbations. astro-ph/0306275, 2003.

[3] C.W. Misner, K. Thorne, and J. Wheeler. *Gravitation.* W.H. Freeman, 1973.

[4] D.N. Spergel, L. Verde, H.V. Peiris, E. Komatsu, M.R. Nolta, C.L. Bennett, M. Halpern, G. Hinshaw, N. Jarosik, A. Kogut, M. Limon, S.S. Meyer, L. Page, G.S. Tucker, J.L. Weiland, E. Wollack, and E.L. Wright. First year Wilkinson microwave anisotropy probe (WMAP) observations : determination of comological parameters. *Supplement to the Astrophysical Journal*, 148:175, 2003.

[5] J.N. Fry. The galaxy correlation hierarchy in perturbaton theory. *The Astrophysical Journal*, 279:499, 1984.

[6] M. Goroff, B. Grinstein, S.-J. Rey, and M. Wise. Coupling of modes of cosmological mass density fluctuations. *The Astrophysical Journal*, 311:6, 1986.

[7] N. Makino, M. Sasaki, and Y. Suto. Analytic approach to the perturbative expansion of nonlinear gravitational fluctuations in cosmological density and velocity fields. *Physical Review D*, 46:585, 1992.

[8] M. Chodorowski and E. Łokas. The weakly non-linear density-velocity relation. *Monthly Notices of the Royal Astronomical Society*, 287:591, 1997.

[9] E. Bertschinger and A. Dekel. Recovering the full velocity and density fields from large-scale redshift-distance samples. *The Astrophysical Journal*, 336:L5, 1989.

[10] A. Dekel, E. Bertschinger, and S.M. Faber. Potential, velocity, and density fields from sparse and noisy redshift-distance samples: method. *The Astrophysical Journal*, 364:349, 1990.

[11] A. Hamilton and M. Tegmark. The real space power spectrum of the PSCz survey from 0.01 to 300 h Mpc -1. *Monthly Notices of the Royal Astronomical Society*, 330:506, 2002.

[12] F. Bernardeau. Skewness and kurtosis in large-scale cosmic fields. *The Astrophysical Journal*, 433:1, 1994.

[13] J.N. Fry. The galaxy correlation hierarchy in perturbation theory. Unpublished review, 2000.

[14] W.H. Press and P. Schechter. Formation of galaxies and clusters of galaxies by self-similar gravitational condensation. *The Astrophysical Journal*, 187:425, 1974.

[15] J. Lee and S.F. Shandarin. The cosmological mass distribution function in the Zel'Dovich approximation. *The Astrophysical Journal*, 500:14, 1998.

[16] R.K. Sheth and G. Tormen. Large-scale bias and the peak background split. *Monthly Notices of the Royal Astronomical Society*, 308:119, 1999.

[17] J.F. Navarro, C.S. Frenk, and S.D. White. A universal density profile from hierarchical clustering. *The Astrophysical Journal*, 490:493, 1997.

[18] B. Moore, F. Governato, T. Quinn, J. Stadel, and G. Lake. Resolving the structure of cold dark matter haloes. *The Astrophysical Journal*, 499:L5, 1998.

[19] J.A. Peacock. *Cosmological Physics.* Cambridge University Press, Camgridge, MA, 1999.

[20] J.-C. Hwang. Newtonian cosmological perturbations. *Publications of the Korean Astronomical Society*, 7:148, 1992.

[21] J.-C. Hwang. Cosmological quasilinear analysis including the rotation mode. *Physical Review D*, 48:3557, 1993.

[22] B. Jain and E. Bertschinger. Second-order power spectrum and nonlinear evolution at high redshift. *The Astrophysical Journal*, 431:495, 1994.

[23] F. Bernardeau. The gravity-induced quasi-gaussian correlation hierarchy. *The Astrophysical Journal*, 392:1, 1992.

[24] M. Takada and B. Jain. The kurtosis of the cosmic shear field. *Monthly Notices of the Royal Astronomical Society*, 337:875, 2002.

[25] A.A. Penzias and R. Wilson. A measurement of excess antenna temperature at 4080 Mc/s. *The Astrophysical Journal*, 142:419, 1965.

[26] G.F. Smoot and D. Scott. Cosmic background radiation. Unpublished review, 2000.

[27] P.J.E. Peebles and D.T. Wilkinson. Comment on the anisotropy of the primeval fireball. *Physical Review*, 174:2168, 1968.

[28] D.J. Fixsen, E.S. Cheng, D.A. Cottingham, R.E. Eplee Jr., R.B. Isaacman, J.C. Mather, S.S. Meyer, P.D. Noerdlinger, R.A. Shafer, R. Weiss, E.L. Wright, C.L. Bennett, N.W. Boggess, T. Kelsall, S.H. Moseley, R.F. Silverberg, G.F. Smoot,

and D.T. Wilkenson. Cosmic microwave background dipole spectrum measured by the COBE FIRAS instrument. *The Astrophysical Journal*, 420:445, 1994.

[29] G. Hinshaw, D.N. Spergel, L. Verde, R.S. Hill, S.S. Meyer, C. Barnes, C.L. Bennett, M. Halpern, N. Jarosik, A. Kogut, E. Komatsu, M. Limon, L. Page, G.S. Tucker, J.L. Weiland, E. Wollack, and E.L. Wright. First year Wilkinson microwave anisotropy probe (WMAP) observations : The angular power spectrum. *Supplement to the Astrophysical Journal*, 148:135, 2003.

[30] R.A. Sunyaev and Y.B. Zel'Dovich. Small-scale fluctuations of relic radiation. *Astrophysics and Space Science*, 7:3, 1970.

[31] R.A. Sunyaev and Y.B. Zel'Dovich. The observation of relic radiation as a test of the nature of X-ray radiation from the clusters of galaxies. *Comments on Astrophysics*, 4:173, 1972.

[32] P. Fosalba, E. Gaztañaga, and F.J. Castander. Detection of the integrated Sachs-Wolfe and Sunyaev-Zel'Dovich effects from the cosmic microwave background-galaxy correlation. *The Astrophysical Journal*, 597:L89, 2003.

[33] K.M. Huffenberger, U. Seljak, and A. Makarov. Sunyaev-Zeldovich effect in WMAP and its effect on cosmological parameters. astro-ph/0404545, 2004.

[34] J.R. Bond, C.R. Contaldi, U.L. Pen, D. Pogosyan, S. Prunet, M.I Ruetalo, J.W. Wadsley, P. Zhang, B.S. Mason, S.T. Myers, T.J. Pearson, A.C.S. Readhead, J.L. Seivers, and P.S. Udomprasert. The Sunyaev-Zel'Dovich effect in CMB-calibrated theories applied to he Cosmic Background Imager anisotropy power at ℓ ¿ 2000. astro-ph/0205386 v1, 2002.

[35] B.S. Mason, T.J. Pearson, A.C.S. Readhead, M.C. Shepherd, J. Sievers, P.S. Udomprasert, J.K. Cartwright, A.J. Farmer, S. Padin, S.T. Meyers, J.R. Bond, C.R. Contaldi, U. Pen, S. Prunet, D. Pogosyan, J.E. Carlstrom, J. Kovac, E.M. Leitch, C. Pryke, N.W. Halverson, W.L. Holzapfel, P. Altamirano, L. Bronfman, S. Casassus, and J. May. The anisotropy of the microwave background to $\ell = 3500$: deep field observations with the cosmic background imager. *The Astrophysical Journal*, 591:540, 2003.

[36] E. Komatsu and U. Seljak. The Sunyaev-Zel'dovich angular power spectrum as a probe of cosmological parameters. *Monthly Notices of the Royal Astronomical Society*, 336:1256, 2002.

[37] N. Aghanim, K.M. Gorski, and J.-L. Puget. How accurately can the SZ effect measure peculiar velocities and bulk flows? *Astronomy and Astrophysics*, 374:1, 2001.

[38] A. Diaferio, S. Borgani, L. Moscardini, G. Murante, K. Dolag, V. Springel, G. Tormen, L. Tornatore, and P. Tozzi. Measuring cluster peculiar velocities

with the Sunyaev-Zeldovich effects: scaling relations and systematics. astro-ph/0405365, 2004.

[39] J.M. Bardeen, J.R. Bond, N. Kaiser, and A.S. Szalay. The statistics of peaks of Gaussian random fields. *The Astrophysical Journal*, 304:15, 1986.

[40] C.-P. Ma. Analytical approximation to the nonlinear power spectrum of gravitational clustering. *The Astrophysical Journal*, 508:L5, 1998.

[41] C.-P. Ma and J.N. Fry. Deriving the nonlinear cosmological power spectrum and bispectrum from analytic dark matter halo profiles and mass functions. *The Astrophysical Journal*, 543:503, 2000.

[42] P. Zhang, U.-L. Pen, and H. Trac. Precision era of the kinetic Sunyae-Zeldovich effect: simulations, analytical models and observations and the power to constrain reionization. astro-ph/0304534v6, 2003.

[43] Y.P. Jing and Y. Suto. The density profiles of the dark matter halos are not universal. *The Astrophysical Journal*, 529:L69, 2000.

[44] Y.P. Jing. Accurate fitting formula for the two-point correlation function of dark matter halos. *The Astrophysical Journal*, 503:L9, 1998.

[45] C.-P. Ma and J.N. Fry. The nonlinear kinetic Sunyaev-Zeldovich effect. *Physical Review Letters*, 88:211301, 2002.

[46] N. Kaiser. Weak graviational lensing of distant galaxies. *The Astrophysical Journal*, 388:272, 1992.

[47] D.N. Limber. The analysis of counts of the extragalactic nebulae in terms of a fluctuating density field. *The Astrophysical Journal*, 119:655, 1954.

[48] A. Jaffe and M. Kamionkowski. Calculation of the Ostriker-Vishniac effect in cold dark matter models. *Physical Review D*, 58:0403001, 1998.

[49] N. Aghanim, F.X. Desert, J.L. Puget, and R. Gispert. Ionization by early quasars and cosmic microwave background anisotropies. *Astronomy and Astrophysics*, 311:1, 1996.

[50] M.G. Santos, A. Cooray, Z. Haiman, L. Knox, and C.-P. Ma. Small-scale Cosmic Microwave Background temperature and polarization anisotropies due to patchy reionization. *The Astrophysical Journal*, 598:756, 2003.

[51] A. Cooray and X. Chen. Kinetic Sunyaev-Zel'Dovich effect from halo rotation. *The Astrophysical Journal*, 573:43, 2002.

[52] J.S. Bullock, A. Dekel, T.S. Kolatt, A.V. Kravtsov, A.A. Klypin, C. Porciani, and J.R. Primack. A universal angular momentum profile for galactic halos. *The Astrophysical Journal*, 555:240, 2001.

[53] E.L. Łokas and Y. Hoffman. Formation of cuspy density profiles: a generic feature of collisionless gravitational collapse. *The Astrophysical Journal*, 542:L139, 2000.

[54] W.H. Press, S.A. Teukolsky, W.T. Vetterling, and B.P. Flannery. *Numerical Recipes in C.* Cambridge University Press, Cambridge, MA, second edition, 1993.

BIOGRAPHICAL SKETCH

James Cooney was born in 1975 in Silver Spring, Maryland. There he attended Paint Branch High School, from which he graduated in 1993. He then went to get his undergraduate education at St. Mary's College of Maryland, from which he received a Bachelor of Arts degree in physics in 1997. He then headed south to attend graduate school at the University of Florida. His research has centered around large-scale structure in general, and peculiar velocities in perturbation theory and non-linear theory in specific. Along the way he received his Master of Science in Teaching in 2000.

I certify that I have read this study and that in my opinion it conforms to acceptable standards of scholarly presentation and is fully adequate, in scope and quality, as a dissertation for the degree of Doctor of Philosophy.

James N. Fry, Chair
Professor of Physics

I certify that I have read this study and that in my opinion it conforms to acceptable standards of scholarly presentation and is fully adequate, in scope and quality, as a dissertation for the degree of Doctor of Philosophy.

Steven Detweiler
Professor of Physics

I certify that I have read this study and that in my opinion it conforms to acceptable standards of scholarly presentation and is fully adequate, in scope and quality, as a dissertation for the degree of Doctor of Philosophy.

Bernard Whiting
Associate Professor of Physics

I certify that I have read this study and that in my opinion it conforms to acceptable standards of scholarly presentation and is fully adequate, in scope and quality, as a dissertation for the degree of Doctor of Philosophy.

Peter Hirschfeld
Professor of Physics

I certify that I have read this study and that in my opinion it conforms to acceptable standards of scholarly presentation and is fully adequate, in scope and quality, as a dissertation for the degree of Doctor of Philosophy.

Arthur Hebard
Professor of Physics

I certify that I have read this study and that in my opinion it conforms to acceptable standards of scholarly presentation and is fully adequate, in scope and quality, as a dissertation for the degree of Doctor of Philosophy.

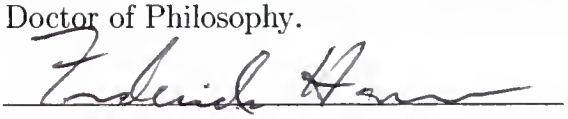

Frederick Hamann
Associate Professor of Astronomy

This dissertation was submitted to the Graduate Faculty of the Department of Physics in the College of Liberal Arts and Sciences and to the Graduate School and was accepted as partial fulfillment of the requirements for the degree of Doctor of Philosophy.

August 2004

Dean, Graduate School

LD
1780
2004
.C775

UNIVERSITY OF FLORIDA
3 1262 08554 2537